9-16-2014 12:00 AM

Thermal Convection of Non-Fourier Fluids

Rahim Mohammadhasani Khorasany, *The University of Western Ontario*

Supervisor: Roger E. Khayat, *The University of Western Ontario*

A thesis submitted in partial fulfillment of the requirements for the Master of Science degree in Mechanical and Materials Engineering

THERMAL CONVECTION OF NON-FOURIER FLUIDS

(Thesis format: Integrated Article)

by

Rahim Mohamadhasani Khorasany

Graduate Program in Engineering Science
Department of Mechanical and Materials Engineering

A thesis submitted in partial fulfillment
of the requirements for the degree of
Master of Science

The School of Graduate and Postdoctoral Studies
The University of Western Ontario
London, Ontario, Canada

Abstract

The natural convection of non-Fourier fluids of the dual-phase-lagging (DPL) type is examined. These fluids possess a relaxation time and a retardation time, reflecting the delay in the response of the heat flux and the temperature gradient with respect to one another. DPL fluids span a wide range of applications, including low-temperature liquids, fluids subjected to fast heat transfer processes, and nanofluids (NFs), for which both the relaxation and retardation times are expressed in terms of nanoparticle concentration and solution properties. Both stationary and oscillatory convection become equally probable as the relaxation time increases. A nonlinear spectral approach is also used to model the post-critical convective state for thermo-gravitational instability in a non-Fourier fluid of the single-phase-lagging (SPL) type heated from below. The Spectral approach reveals the number and type of required modes. It is found that the Cattaneo number increases the Nusselt number compared to a Fourier fluid.

Keywords

Non-Fourier, Single-phase-lagging (SPL), Dual-phase-lagging (DPL), Nanofluids, Rayleigh-Bénard convection, Nonlinear spectral solution, perturbation expansion.

To my wife and my parents

for their endless love, encouragement and support.

Acknowledgments

It is a pleasure to thank the many people who made this thesis possible. It is difficult to overstate my gratitude to my supervisor, Dr. Roger E. Khayat. The completion of this dissertation would not have been possible without his incomparable assistance and invaluable guidance.

I would also like to thank all of my colleagues (past and present), Dr. Bashar Albaalbaki, Mohammad Niknami and Daniel Stranges for their friendship, cooperation and helping attitude.

Words are not enough to express my gratitude towards my wife, Motahareh Z. Mehrizi. Without her unconditional love, encouragement, tremendous patience and understanding, I would not have been able to accomplish my goals.

Lastly, and most importantly, I wish to thank my parents. Their love provided my inspiration and was my driving force. I owe them everything and wish I could show them just how much I love and appreciate them.

Table of Contents

List of Figures

List of Abbreviations Nomenclature, Symbols, Superscripts and Subscripts

Abbreviations

DPL	Dual-Phase-Lag
SPL	Single-Phase-Lag
NPs	Nanoparticles
NFs	Nanofluids
CV	Cattaneo-Vernotte
RBC	Rayleigh-Bénard Convection
Nu	Nusselt Number

Nomenclature

$a_v =$	interfacial area per unit volume
$C =$	Cattaneo number
$c_p =$	specific heat
$d =$	diameter
$D =$	length scale(distance between plates)
$E =$	Elasticity number

$\boldsymbol{e}_z$ =	unit vector in the z direction
g =	gravity acceleration
j =	$\nabla \cdot \mathbf{q}$
K=	thermal conductivity
$k_{x=}$	wavenumber in x direction
$k_{y=}$	wavenumber in y direction
n=	mode number
P =	pressure
p =	dimensionless pressure deviations from the base state
Pr=	Prandtl number
$\boldsymbol{Q}$=	heat flux vector
$\boldsymbol{q}$=	dimensionless heat flux vector
qz	heat flux in z direction
Ra=	Rayleigh number
S=	dimensionless retardation time
s=	time evolution
T=	temperature

τ_Q = relaxation time

τ_T = retardation time

$\boldsymbol{v}(u, w)$= dimensionless velocity vector

v_i = perturbation velocity

$\boldsymbol{V}$ = velocity vector

Greek Symbols

∇ = Gradient operator

Δ = Laplacian operator

ρ = density of fluid (kg/m^3)

ρ_0 = density of fluid at temperature T_0 (kg/m^3)

μ = viscosity

θ = dimensionless temperature deviations from the base state

ψ = dimensionless stream function

κ = thermal diffusivity

ω= frequency

ϕ = nanoparticles concentration

$\delta_{=}$ mean interaction length

$\alpha_{T=}$ volume expansion coefficient

Superscripts and Subscripts

$B=$ base fluid

$i=$ intersection

$m=$ minimum

$H=$ threshold

$c=$ critical

$F=$ Fourier

$z=$ partial differentiation wrt z

$t=$ partial differentiation wrt t

$NP=$ NanoParticle

$NF=$ NanoFluid

Chapter 1

1.1 Non-Fourier characteristic

Fourier's law is the most common equation to study the conduction heat transfer, which states that the rate of heat transfer through a medium is proportional to the negative temperature gradient across the medium. Fourier's law assumes that when a thermal disturbance is applied to an object, the perturbation is felt immediately at all points of the object accordingly. Sometimes Fourier's law is not accurate enough and another equation is needed to study conduction heat transfer [1]. Peshkov [1] was the first one who found the second sound wave in superfluid helium (He II) at low temperatures ($T < 2.2$ K) experimentally. Cattaneo [2] and Vernotte [3] proposed Cattaneo-Vernotte (C-V) equation including a transient term multiplied by the thermal relaxation time of the subject. In most of materials, thermal relaxation time is negligible and Cattaneo equation returns back to the Fourier model. Also, there are some conditions and materials in which the relaxation time is considerable and should be attended such as non-homogeneous medium [2]–[4], high speed electronic devices [4], ultrashort laser pulses [4], [5], skin burns[6], processed meat [7], heat transfer in stars[8], , drying sand [9] heat transport in a nuclear fuel rod in a light water reactor [10] and microscale" applications[3]. Note that beside the relaxation time, the rate of heating could also cause the transient term and non-Fourier effect to become significant. For example, some thermal processes like laser pulse heating, generates a sizeable amount of energy in a short time on the scale of femto- or 10^{-15} seconds [11]. Non-Fourier effects have been studied using numerical [2], [12]–[22] and analytical [23], [24] methods in a wide variety of geometries such as cylindrical [25], spherical [26], slabs [27], crack tip [28] and fins geometry [29].

Different models have been used to describe the non-Fourier heat transfer. Single-Phase-Lag model (SPL) suggests that materials have only a relaxation time exposing the delay in the response of the heat flux in the Christov's study [30]. Recently, Khayat and co-workers used the extended Cattaneo-Vernotte equation to study the natural convection in non-Fourier fluids of single phase-lagging type [31], [32]. The present study however, focuses on the natural convection in non-Fourier fluids using dual phase-lagging model. Despite being more accurate than Fourier's heat transfer, SPL models could not explain

some heat transfer processes. Dual-Phase-Lag (DPL) model offers presence of relaxation and retardation times in materials exposing the delay in the response of the heat flux and the temperature gradient, respecitvely. For example, to analyze the non-Fourier heat transfer process in skin tissue, Xu et al. [33] used the Dual-Phase-Lag model. Vadasz [34] represents a specific case of Dual-Phase-Lagging heat conduction as,

$$\mathrm{Q}\left(\mathrm{r}, t+\tau_q\right)=-k \nabla T\left(\mathrm{r}, t+\tau_T\right) \tag{1.1.1b}$$

where τ_q is relaxation time of heat flux and τ_T is the retardation time of temperature gradient. The retardation time, τ_T , is interpreted as being induced by micro-structural interactions such as phonon-electron interaction or phonon scattering, and is called the phase-lag of the temperature gradient. Vadasz [34] and Quaresma [35] found that the correlation between the heat flux and temperature gradient is not instantaneous but quite affected by the two time lags, a temperature gradient time lag and a heat flux time lag. They also elaborated an estimated equivalence between Fourier heat conduction in porous media and dual-phase-lagging heat conduction not including the coupled thermal conductivity which has been attended by Wang and Wei [36]. Vadasz [34] proposed that the heat conduction is not valid at the macro-system level when nano-elements are suspended in a fluid. Donzelli [37] observed transient oscillatory convection when a homogeneous suspension of nanofluids was heated suddenly from below in the Rayleigh-Benard convection.

Nanofluids are suspensions of solid nanoparticles (NPs), with normally at least one of their principal dimensions in the order of 1–100 nm, in a base fluid such as water or ethylene glycol. The NPs could be the oxides of aluminum and silicon, as well as metals such as copper and gold [38]–[40]. In recent years, nanofluids received significant attention because of the significant enhancement in their thermophysical properties such as thermal conductivity, thermal diffusivity, viscosity and convective heat transfer coefficients compared to those of base fluids [41]–[45]. A small percent of nanoparticles causes a major increase in the effective thermal conductivity of nanofluids, which rises with increasing concentration of nanoparticles. For example, a small amount of nanoparticles dispersed in ethylene glycol or oil can increase their inherently thermal conductivity by 40% [38], [46]–[48]. Vadasz [34] and Quaresma [35] have studied the

heat conduction mechanism in nanofluid suspensions for transient processes and found that the relationship between the heat flux and temperature gradient is not instantaneous but rather affected by two time lags, a heat flux time lag and a temperature gradient time lag. They developed an approximate equivalence between Fourier heat conduction in porous media and dual-phase-lagging heat conduction not considering the coupled thermal conductivity which has been attended by Wang and Wei [36]. The connection between the two-phase model and non-Fourier effect was also recognized in other systems. See, for instance, Donnelly [49] on the two-fluid theory and second sound in liquid helium.

Nanofluids are non-Fourier fluids with a wide range of applications. Having enhanced properties as thermal conductivity for example, nanofluids could be employed in various engineering applications such as medical field, automotive industry, computers and power plant cooling systems.

Through an experimental examination, Das et al. [52] observed thermal conductivity enhancement of nanofluids consisting of CuO and Al_2O_3 nanoparticles and recommend that nanofluids could operate as cooling fluids for devices. Han et al. [53] observed considerable increase in the nanofluids effective specific heat and thermal conductivity using melting-freezing phase transition of the Indium particles in nanofluids. Donzelli et al. [37] observed bi-stable heat transfer while studding a specific class of nanofluids and suggested that they can be employed as a smart material serving as a heat valve controlling the heat flow rate.

1.2 Motivation

Previous studies have reported some unusual behaviours in the heat transfer of some fluids such as nanofluids and superfluid helium and used different approaches to explain observed behaviours in those fluids. Buongiorno [46] argued that thermophoresis and Brownian motion as the only significant factors that could suitably describe the higher heat transfer capabilities of nanofluids. Tzou [54] by using the two-phase flow, suggests the possibility of oscillatory convection at instability, depending on the imposed boundary conditions. In fact, the adoption and nature of the boundary conditions for the

concentration of NPs is one of the major drawbacks of the two-phase approach for NFs. These conditions are unrealistic, and lead to dramatically different stability pictures, depending on their relative values. In reality, NFs are quite homogeneous solutions. Indeed, if the concentrations at the upper and lower surfaces are taken equal, the two-phase model predicts that the effect of the NPs on the instability is lost, despite the presence of Brownian motion and thermophoretic effects [55].

There are some studies for conduction state of nanofluids based on non-Fourier effect but to our knowledge, there is no existing study on the effect of non-Fourier heat transfer for nanofluids in the convection state. Behaviour of non-Fourier fluids (such as nanofluids) must be better understood before they can be safely employed. The aim of this work is to study this problem mathematically and show that one can model and simulate the behavior of non-Fourier fluids.

1.3 Objective

The objectives of the present study are to:

1- Investigate the effect of non-Fourier characteristics in the stability of non-Fourier fluids in the Rayleigh Bernard Convection.

2- Clarify the unsusal behaviors of nanofluids and establish the explanation using non-Fourier equations.

3- Model the post-critical convective state for thermo-gravitational instability in a non-Fourier fluid of the single-phase-lagging (SPL) type heated from below using a nonlinear spectral approach.

In this study, a different approach is adopted to study the heat transfer in non-Fourier fluids especially nanofluids, by considering the fluid as a homogeneous solution, and accounting for the thermal relaxation time resulting from the non-Fourier characteristic.

1.4 Thesis layout

First chapter provides an introduction to the non-Fourier fluids and a short literature review on the previous works and the models that have been used. The limitations of these models are also provided. Then the motivation and the objective of the present study are described.

In the second chapter, natural convection of non-Fourier fluids of the dual-phase-lagging (DPL) type is examined. Linear stability analysis indicates that, in contrast to ordinary fluids, a DPL fluid can lose its conductive mode to stationary or oscillatory convection. As Cattaneo number related to the non-Fourier fluid increases and reaches a critical value, both stationary and oscillatory convection become equally probable, confirming the existence of the bistable mode observed in experiment [37].

In the third chapter, a spectral approach is used to treat nonlinear convection which is not based on arbitrary mode selection. It has been shown that the leading-order contribution is essentially dominant for temperature field and stream function which usually are ignored in the other models.

Fourth chapter summarizes the conclusions of each chapter and presents an understanding of the heat transfer in non-Fourier fluids and lists some future recommendations.

1.5 References

[1] V. Peshkov, “Second sound in helium II,” *J. Phys. 8*, p. 381, 1944.

[2] P. Duhamel, “A new finite integral transform pair for hyperbolic conduction problems in heterogeneous media,” *Int. J. Heat Mass Transf.*, vol. 44, no. 17, pp. 3307–3320, Sep. 2001.

[3] P. J. Antaki, “Analysis of hyperbolic heat conduction in a semi-infinite slab with surface convection,” *Int. J. Heat Mass Transf.*, vol. 40, no. 13, pp. 3247–3250, Sep. 1997.

[4] P.-T. Hsu and Y.-H. Chu, “An inverse non-Fourier heat conduction problem approach for estimating the boundary condition in electronic device,” *Appl. Math. Model.*, vol. 28, no. 7, pp. 639–652, Jul. 2004.

[5] F. Jiang, “Non-Fourier heat conduction phenomena in porous material heated by microsecond laser pulse,” *Microscale Thermophys. Eng.*, vol. 6, no. 4, pp. 331–346, Jan. 2003.

[6] W. Dai, H. Wang, P. M. Jordan, R. E. Mickens, and A. Bejan, “A mathematical model for skin burn injury induced by radiation heating,” *Int. J. Heat Mass Transf.*, vol. 51, no. 23–24, pp. 5497–5510, Nov. 2008.

[7] K. Mitra, S. Kumar, A. Vedevarz, and M. K. Moallemi, “Experimental Evidence of Hyperbolic Heat Conduction in Processed Meat,” *J. Heat Transfer*, vol. 117, no. 3, p. 568, Aug. 1995.

[8] L. Herrera and N. Falcón, “Heat waves and thermohaline instability in a fluid,” *Phys. Lett. A*, vol. 201, no. 1, pp. 33–37, May 1995.

[9] R. J. Meyer, “Ultrasonic drying of saturated porous solids via second sound.” 30-Oct-2002.

[10] G. Espinosa-Paredes and E.-G. Espinosa-Martínez, “Fuel rod model based on Non-Fourier heat conduction equation,” *Ann. Nucl. Energy*, vol. 36, no. 5, pp. 680–693, May 2009.

[11] R. R. Letfullin, T. F. George, G. C. Duree, and B. M. Bollinger, “Ultrashort Laser Pulse Heating of Nanoparticles: Comparison of Theoretical Approaches,” *Adv. Opt. Technol.*, vol. 2008, pp. 1–8, 2008.

[12] K.-C. Liu and H.-T. Chen, “Analysis for the dual-phase-lag bio-heat transfer during magnetic hyperthermia treatment,” *Int. J. Heat Mass Transf.*, vol. 52, no. 5–6, pp. 1185–1192, Feb. 2009.

[13] H. Zhang, S. Zhang, X. Guo, and J. Bi, “Multiple spatial and temporal scales method for numerical simulation of non-classical heat conduction problems: one dimensional case,” *Int. J. Solids Struct.*, vol. 42, no. 3–4, pp. 877–899, Feb. 2005.

[14] C.-C. Wang, “Direct and inverse solutions with non-Fourier effect on the irregular shape,” *Int. J. Heat Mass Transf.*, vol. 53, no. 13–14, pp. 2685–2693, Jun. 2010.

[15] Y. Chou and R.-J. Yang, “Application of CESE method to simulate non-Fourier heat conduction in finite medium with pulse surface heating,” *Int. J. Heat Mass Transf.*, vol. 51, no. 13–14, pp. 3525–3534, Jul. 2008.

[16] W. Wu and X. Li, “Application of the time discontinuous Galerkin finite element method to heat wave simulation,” *Int. J. Heat Mass Transf.*, vol. 49, no. 9–10, pp. 1679–1684, May 2006.

[17] T.-M. Chen, “A hybrid Green’s function method for the hyperbolic heat conduction problems,” *Int. J. Heat Mass Transf.*, vol. 52, no. 19–20, pp. 4273–4278, Sep. 2009.

[18] C. Han-Taw and L. Jae-Yuh, “Analysis of two-dimensional hyperbolic heat conduction problems,” *Int. J. Heat Mass Transf.*, vol. 37, no. 1, pp. 153–164, Jan. 1994.

[19] C. Han-Taw and L. Jae-Yuh, “Numerical analysis for hyperbolic heat conduction,” *Int. J. Heat Mass Transf.*, vol. 36, no. 11, pp. 2891–2898, Jul. 1993.

[20] Q.-M. Fan and W.-Q. Lu, “A new numerical method to simulate the non-Fourier heat conduction in a single-phase medium,” *Int. J. Heat Mass Transf.*, vol. 45, no. 13, pp. 2815–2821, Jun. 2002.

[21] J. Ghazanfarian and Z. Shomali, “Investigation of dual-phase-lag heat conduction model in a nanoscale metal-oxide-semiconductor field-effect transistor,” *Int. J. Heat Mass Transf.*, vol. 55, no. 21–22, pp. 6231–6237, Oct. 2012.

[22] Y. Chou and R.-J. Yang, “Two-dimensional Dual-Phase-Lag thermal behavior in single-/multi-layer structures using CESE method,” *Int. J. Heat Mass Transf.*, vol. 52, no. 1–2, pp. 239–249, Jan. 2009.

[23] T. T. Lam and E. Fong, “Application of solution structure theorem to non-Fourier heat conduction problems: Analytical approach,” *Int. J. Heat Mass Transf.*, vol. 54, no. 23–24, pp. 4796–4806, Nov. 2011.

[24] D. W. Tang and N. Araki, “Non-fourier heat conduction in a finite medium under periodic surface thermal disturbance,” *Int. J. Heat Mass Transf.*, vol. 39, no. 8, pp. 1585–1590, May 1996.

[25] S. C. Mishra and H. Sahai, “Analyses of non-Fourier heat conduction in 1-D cylindrical and spherical geometry – An application of the lattice Boltzmann method,” *Int. J. Heat Mass Transf.*, vol. 55, no. 23–24, pp. 7015–7023, Nov. 2012.

[26] S. C. Mishra and A. Stephen, “Combined mode conduction and radiation heat transfer in a spherical geometry with non-Fourier effect,” *Int. J. Heat Mass Transf.*, vol. 54, no. 13–14, pp. 2975–2989, Jun. 2011.

[27] P. J. Antaki, “Solution for non-Fourier dual phase lag heat conduction in a semiinfinite slab with surface heat flux,” *Int. J. Heat Mass Transf.*, vol. 41, no. 14, pp. 2253–2258, Jul. 1998.

[28] B. L. Wang and J. C. Han, “A crack in a finite medium under transient non-Fourier heat conduction,” *Int. J. Heat Mass Transf.*, vol. 55, no. 17–18, pp. 4631–4637, Aug. 2012.

[29] C.-H. Huang and H.-H. Wu, “An iterative regularization method in estimating the base temperature for non-Fourier fins,” *Int. J. Heat Mass Transf.*, vol. 49, no. 25–26, pp. 4893–4902, Dec. 2006.

[30] C. I. Christov, “On frame indifferent formulation of the Maxwell–Cattaneo model of finite-speed heat conduction,” *Mech. Res. Commun.*, vol. 36, no. 4, pp. 481–486, Jun. 2009.

[31] D. F. Stranges, R. E. Khayat, and B. Albaalbaki, “Thermal convection of non-Fourier fluids. Linear stability,” *Int. J. Therm. Sci.*, vol. 74, pp. 14–23, Dec. 2013.

[32] M. Niknami and R. E.khayat, “Energy growth of disturbances in a non-Fourier fluid,” *Int. J. Heat Mass Transf.*, vol. 67, pp. 613–626, Dec. 2013.

[33] F. Xu, T. Lu, and K. A. Seffen, “Dual-Phase-Lag Model of Skin Bioheat Transfer,” in *2008 International Conference on BioMedical Engineering and Informatics*, 2008, vol. 1, pp. 505–511.

[34] P. Vadasz, “Heat Conduction in Nanofluid Suspensions,” *J. Heat Transfer*, vol. 128, no. 5, p. 465, May 2006.

[35] J. N. N. Quaresma, E. N. Macêdo, H. M. da Fonseca, H. R. B. Orlande, and R. M. Cotta, “An Analysis of Heat Conduction Models for Nanofluids,” *Heat Transf. Eng.*, vol. 31, no. 14, pp. 1125–1136, Dec. 2010.

[36] L. Wang and X. Wei, “Equivalence between dual-phase-lagging and two-phase-system heat conduction processes,” *Int. J. Heat Mass Transf.*, vol. 51, no. 7–8, pp. 1751–1756, Apr. 2008.

[37] G. Donzelli, R. Cerbino, and A. Vailati, “Bistable Heat Transfer in a Nanofluid,” *Phys. Rev. Lett.*, vol. 102, no. 10, p. 104503, Mar. 2009.

[38] L. W. et al. Y. Ding, H. Chen, “Heat Transfer Intensification Using Nanofluids,” *J. Part. Powder*, vol. 25, pp. 23–36, 2007.

[39] J. Buongiorno, “Convective Transport in Nanofluids,” *J. Heat Transfer*, vol. 128, no. 3, p. 240, Mar. 2006.

[40] S. Samouhos and G. McKinley, “Carbon Nanotube–Magnetite Composites, With Applications to Developing Unique Magnetorheological Fluids,” *J. Fluids Eng.*, vol. 129, no. 4, p. 429, Apr. 2007.

[41] T. Tyler, O. Shenderova, G. Cunningham, J. Walsh, J. Drobnik, and G. McGuire, “Thermal transport properties of diamond-based nanofluids and nanocomposites,” *Diam. Relat. Mater.*, vol. 15, no. 11–12, pp. 2078–2081, Nov. 2006.

[42] S. K. Das, S. U. S. Choi, and H. E. Patel, “Heat Transfer in Nanofluids—A Review,” *Heat Transf. Eng.*, vol. 27, no. 10, pp. 3–19, Dec. 2006.

[43] W. Yu, D. M. France, J. L. Routbort, and S. U. S. Choi, “Review and Comparison of Nanofluid Thermal Conductivity and Heat Transfer Enhancements,” *Heat Transf. Eng.*, vol. 29, no. 5, pp. 432–460, May 2008.

[44] S. U. S. Choi, “Nanofluids: From Vision to Reality Through Research,” *J. Heat Transfer*, vol. 131, no. 3, p. 033106, Mar. 2009.

[45] M.-S. Liu, M. Ching-Cheng Lin, I.-T. Huang, and C.-C. Wang, “Enhancement of thermal conductivity with carbon nanotube for nanofluids,” *Int. Commun. Heat Mass Transf.*, vol. 32, no. 9, pp. 1202–1210, Oct. 2005.

[46] J. Buongiorno, “Convective Transport in Nanofluids,” *J. Heat Transfer*, vol. 128, no. 3, pp. 240–250, 2006.

[47] J. Garg, B. Poudel, M. Chiesa, J. B. Gordon, J. J. Ma, J. B. Wang, Z. F. Ren, Y. T. Kang, H. Ohtani, J. Nanda, G. H. McKinley, and G. Chen, “Enhanced thermal conductivity and viscosity of copper nanoparticles in ethylene glycol nanofluid,” *J. Appl. Phys.*, vol. 103, no. 7, p. 074301, Apr. 2008.

[48] P. Vadasz, “Heat transfer augmentation in nanofluids via nanofins.,” *Nanoscale Res. Lett.*, vol. 6, no. 1, p. 154, Jan. 2011.

[49] R. J. Donnelly, “The two-fluid theory and second sound in liquid helium,” *Phys. Today*, vol. 62, no. 10, p. 34, Oct. 2009.

[50] D. Y. Tzou and K. S. Chiu, “Temperature-dependent thermal lagging in ultrafast laser heating,” *Int. J. Heat Mass Transf.*, vol. 44, no. 9, pp. 1725–1734, May 2001.

[51] R. Quintanilla and R. Racke, “A note on stability in dual-phase-lag heat conduction,” *Int. J. Heat Mass Transf.*, vol. 49, no. 7–8, pp. 1209–1213, Apr. 2006.

[52] S. K. Das, N. Putra, P. Thiesen, and W. Roetzel, “Temperature Dependence of Thermal Conductivity Enhancement for Nanofluids,” *J. Heat Transfer*, vol. 125, no. 4, p. 567, Aug. 2003.

[53] Z. H. Han, F. Y. Cao, and B. Yang, “Synthesis and thermal characterization of phase-changeable indium/polyalphaolefin nanofluids,” *Appl. Phys. Lett.*, vol. 92, no. 24, p. 243104, Jun. 2008.

[54] D. Y. Tzou, “Instability of Nanofluids in Natural Convection,” *J. Heat Transfer*, vol. 130, no. 7, p. 072401, Jul. 2008.

[55] D. A. Nield and A. V. Kuznetsov, “The onset of convection in a horizontal nanofluid layer of finite depth,” *Eur. J. Mech. - B/Fluids*, vol. 29, no. 3, pp. 217–223, May 2010.

Chapter 2

2 Thermal convection of dual-phase-lagging non-Fourier fluids. Linear stability and application to nanofluids

2.1 Introduction

In general, when a thermal disturbance applies to an object, the perturbation effects immediately at all points of the object where the temperature diffusion is described by Fourier's law and gives a parabolic equation. By Fourier's law, the flow rate of heat energy through a surface is proportional to the negative temperature gradient across the surface. Unlimited speed of heat propagation is assumed in Fourier's law as a result Fourier's law is not accurate enough and sometimes another equation is needed to study heat transfer [1] and [2]. Cattaneo [3] and Vernotte [4] proposed Cattaneo-Vernotte (C-V) equation including a transient term multiplied by the thermal relaxation time of the subject. The thermal relaxation time is related to the average communication time among the collisions of electrons and phonons[5], and theoretically has been estimated for metals, semiconductors and superconductors to be in the order of microseconds (10^{-6} s) to picoseconds (10^{-12} s)[6]–[9]. The lagging behavior in the transient process is caused by the infinite time required for the substractural interaction to occur. These interactions may take place on the order of several seconds (such as delayed response induced by the low-conducting pores in sand media) to nanoseconds (the delayed respond caused by inert behavior of molecules at low temperatures) to picoseconds (the delayed response due to phonon scattering or phonon-electron interaction)[10]. It is important to realize that not only relaxation times but also the rate of heating could make the transient term considerable. For example laser pulse heating makes a significant amount of energy over a small time. There are some applications where the duration of the laser pulse can be measured on the scale of femto- or 10^{-15} seconds [11]. Limited literature is available on non-Fourier convection, and most of it concerns only to thermal instability [12]–[14]. Recently, Khayat and co-workers examined the natural convection of non-Fourier fluids of the single phase-lagging type, using the extended Cattaneo-Vernotte equation [15], [16]. They showed that the neutral stability curve contains a Fourier branch and an

oscillatory branch as well as the possibility of existence of a bistable mode, even for small relaxation time. They also showed that for high enough Cattaneo number, only oscillatory convection is predicted, and the critical Rayleigh number decreases with Cattaneo number. For large Cattaneo number, oscillatory convection becomes increasingly the mode of preference. Nanofluids are a base fluid, consisting of solid nanoparticles, with sizes normally on the order of 1–100 nm. Antaki [17] proposed that non-homogeneous structures apparently induce waves by delaying the response between heat flux and temperature gradient. Vadsaz [18] suggested that Fourier's law is not valid at the macro-system level when nano-elements are suspended in the fluid. As a non-homogeneous material with nano-elements, nanofluids have been studied widely as a non-Fourier substance.

Experiments confirmed that the CV constitutive relation produces a more precise forecast than the classical Fourier law but a number of its predictions disagree with experimental results [10], [19]. A complete study illustrates that the Cattaneo-Vernotte constitutive relation takes into consideration the fast-transient effects only, but not the micro-structural interactions. Both of these effects can be reasonably represented by the dual-phase-lag between q and ∇T. In the other hand, Energy equation at a general position **r** and time t during the transient process may be written as,

$$-\nabla \cdot \mathbf{Q}(\mathbf{r},t) + F(\mathbf{r},t) = \rho c_p \frac{\partial T}{\partial t}(\mathbf{r},t) \tag{2.1.1}$$

where **Q** being the heat flux, T the temperature, ρc_p the volumetric heat capacity, F the volumetric heat source. Although allowing for a delayed response between the heat flux vector and the temperature gradient, evidently, the Cattaneo-Vernotte wave model still assumes an immediate response between the temperature gradient and the energy transport this response occurs right after a temperature gradient is established across a material volume; in other words, the Cattaneo-Vernotte wave model assumes an instantaneous heat flow, the temperature gradient is always the cause for heat transfer, while the heat flux is always the effect. The small scales in both space and time challenge the concept of Fourier model (thermal diffusion) and thermal relaxation (Cattaneo-Vernotte wave model) when used alone for describing the heat transport process [10].

The most commonly used base fluids are water and organic fluids such as ethanol and ethylene glycol. The materials that have been utilized as NPs include oxides of aluminum and silicon, as well as metals such as copper and gold. Diamonds and nanotubes have also been widely experimented with [20], [21]. This makes NFs extremely valuable, especially in processes where cooling is of primary concern, and thus there is an increasing focus on the convective properties of NFs in the literature. The presence of flow is expected to lead to complex and rich physical behaviour[7]. One advantage that a fluid containing NPs has over its milliparticle and microparticle counterparts is the small size of the NPs, which may be on the same order of magnitude as the molecules in the base fluid. This allows the solution to exist in a very stable manner without the occurrence of gravitational settling or particle agglomeration [20], [22], [23]. If the fluid in a cooling process has improved thermal properties, then the workload of other driving components in the system can be reduced. Better thermal conductivity and heat transfer coefficients would allow systems involving microelectronics to run with increased power, while still maintaining appropriate operating temperatures, furthering the processing capabilities. The potential positive impact of NFs in many applications is very promising.

Earlier attempts to examine NFs were based on modelling the overall change in the thermophysical properties, such as thermal conductivity and viscosity of the NF, as a result of the addition of NPs [24]. More recently, extensive efforts have been devoted to understand heat transfer enhancement during conduction [22]. Relative to conduction, the convection of NFs has received little attention. So far, emphasis has been on forced convection (see, for instance, [22], [25];), and not so much on natural convection, despite the rich dynamics expected for a NF. Buongiorno [20] examined several potential factors that could be responsible for the observed heat transfer enhancement in forced convection, namely, the mechanisms behind slip (the difference between the absolute velocity of a NP and the velocity of the base fluid). The potential mechanisms for slip include inertia, gravity settling, diffusiophoresis, the Magnus effect, fluid drainage, Brownian diffusion and thermophoresis. However, Brownian motion and thermophoresis seem to be the only significant factors that could properly explain the unexpected heat transfer capabilities of NFs observed in experiment [20]. The Brownian motion, in this case, is the induced random drifting caused by the collisions of NPs with the molecules in

the base fluid, whereas thermophoresis is a diffusive effect that causes particles to move as a result of a temperature gradient within the fluid.

As to natural convection, Tzou [26] carried out the linear thermal stability of Rayleigh-Benard convection using a two-phase system approach, incorporating the effects of Brownian motion and thermophoresis. Tzou [26] showed that adding NPs to the base fluid increases the ability of the fluid to transfer heat by promoting the onset of convection, at a Rayleigh number lower by one or two orders of magnitude when compared to the base fluid. A similar stability analysis was carried out later by Nield [23], confirming Tzou's findings and suggesting the possibility of oscillatory convection at instability, depending on the boundary conditions imposed. In fact, the adoption and nature of the boundary conditions for the concentration of NPs is one of the major drawbacks of the two-phase approach for NFs. So far, only Dirichlet conditions, specifying the unequal NP concentrations at the top and bottom boundaries, have been used. These conditions are not only impractical to control, but are unrealistic, and lead to dramatically different stability pictures, depending on their relative values. In reality, NFs are quite homogeneous solutions. Indeed, if the concentrations at the upper and lower surfaces are taken equal, the two-phase model predicts that the effect of the NPs on the instability is lost, despite the presence of Brownian motion and thermophoretic effects [23]. Consequently, the NF behaves as if it were solely the base fluid with different fluid properties. This prediction seems to contradict experiment. In fact, in their experiment on the thermal convection of a NF solution of copolymer NPs in water, Donzelli [1] observed oscillatory convection for uniformly distributed NPs. One possible explanation for the discrepancy between the two-phase model and experiment is that a small temperature difference at criticality may not be sufficient to cause a significant concentration gradient resulting from thermophoresis. This issue will be revisited in section 2.4. Generally, however, the two-phase model suggests the existence of stationary and oscillatory convection, depending on flow and fluid parameters [23], [27].

In this study, an alternative approach to the two-phase model is adopted to examine the heat transfer in a NF, and non-Fourier fluids in general, by considering the fluid as a homogeneous solution, and accounting for the finite thermal relaxation time resulting

from the addition of NPs to the base fluid. This is a similar approach to that used in modelling viscoelastic fluids with colloidal and particle suspensions: the addition of the polymer to a base solvent leads to a finite relaxation time of the stress [28]. The non-Fourier character of NFs has also been recognized in the literature[26], [29], [30]. [29] established the equivalence between the conduction of a two-phase Fourier solution and that of a homogeneous dual-phase-lagging (DPL) fluid. The resulting DPL constitutive equation for heat conduction is of the non-Fourier type, relating the temperature gradient to the heat flux with lagging relaxation and retardation times. Also, the equivalence between the conduction of a two-phase Fourier solution and conduction of a homogeneous dual-phase-lagging has been made in other research. Vadasz [18] and Quaresma [31] has studied the heat conduction mechanism in nanofluid suspensions for transient processes and found that the relationship between the heat flux and temperature gradient is not instantaneous but rather affected by two time lags, a heat flux time lag and a temperature gradient time lag. They developed an approximate equivalence between Fourier heat conduction in porous media and dual-phase-lagging heat conduction not considering the coupled thermal conductivity which has been attended by Wang and Wei [29]. The connection between the two-phase model and non-Fourier effect was also recognized in other systems. See, for instance, Donnelly [32] on the two-fluid theory and second sound in liquid helium. The equivalence between the two-phase and DPL configurations is fundamentally significant, as it offers an alternative approach to the traditional two-phase formulations, where possible advantages of the DPL approach include: easier implementation of measureable/controllable initial and boundary conditions in heat flux and temperature, reduction in the number of fluid parameters, more manageable analytical steady solution for the base state, and a wider range of applications including the non-Fourier heat transfer of single-phase-lagging (SPL) fluids for fast heating processes. The DPL approach will be the premise of the current work, and will be revisited in section 2.2, to include convective effects, generalizing the existing SPL model [33], [34]. Although the DPL formulation and current analysis apply to a variety of phenomena[35], [36] , the emphasis in this work will be on the convection of NFs. The formulation is then applied to the thermal convection of a DPL fluid (section

2.3) and its linear stability (section 2.4). Discussion and results will be covered in section 2.5. Finally, concluding remarks are given in section 2.6.

2.2 Non-Fourier character of nanofluids

It is envisaged at both the theoretical [10], [29], [37] and the experimental [30] levels that non-Fourier effects as being behind heat transfer enhancement in NFs, resulting from the addition of NPs to the base fluid. As mentioned above,[29] established the equivalence between DPL and two-phase systems for heat conduction of NFs, by assuming each of the base solvent and NP phases to obey Fourier's law. Following [38] and accounting for interfacial interaction, the energy equation in each phase is then integrated over a representative volume element, yielding averaged coupled equations in terms of an effective thermal conductivity tensor, the NP concentration, □, the film heat transfer coefficient, h, the interfacial area per unit volume, a_V, and the base fluid and NP properties. The two averaged equations are then combined to obtain an equation for heat conduction of the NF, of the DPL type (as opposed to the SPL Maxwell-Cattaneo equation), involving both a relaxation time and a retardation time, which can be expressed in terms of the properties of the original two-phase system (see below). The DPL model for heat conduction is now generalized for thermal convection.

Following the formulation for viscoelastic constitutive equations for polymeric solutions [28], consider a NF solution of thermal conductivity K, comprising a solvent Fourier fluid of thermal conductivity K_F and a solute of NPs of thermal conductivity K_{NP}. The addition of NPs causes a change (normally increase) in the thermal conductivity of the solvent given by

$$K' = K - K_F \tag{2.2.1}$$

In this case, the heat flux of the solution may be written as a superposition of Fourier and non-Fourier contributions:

$$\mathbf{Q} = \mathbf{Q}_F + \mathbf{Q}', \qquad \mathbf{Q}_F = -K_F \nabla T \tag{2.2.2}$$

The Maxwell-Cattaneo equation for heat conduction [39] is the most commonly used constitutive equation for $\mathbf{Q}'$. Christov [33] reformulated and rendered objective for a moving fluid, Khayat [34] revisited later. The resulting equation is simply reproduced here:

$$\tau_Q \frac{\delta \mathbf{Q}'}{\delta t} + \mathbf{Q}' = -K' \nabla T \tag{2.2.3}$$

where τ_Q is the relaxation time, and the Jaumann or Li type derivative is given by

$$\frac{\delta(\ )}{\delta t} \equiv \frac{\partial(\ )}{\partial t} + \mathbf{V} \cdot \nabla(\ ) - (\ ) \cdot \nabla \mathbf{V} - (\ ) \nabla \cdot \mathbf{V} \tag{2.2.4}$$

In this case, the constitutive equation for the solution heat flux is obtained from (2.2.2) and (2.2.3) to read

$$\tau_Q \frac{\delta \mathbf{Q}}{\delta t} + \mathbf{Q} = -K \nabla T - \tau_Q K_F \frac{\delta \nabla T}{\delta t} = -K \left(\nabla T + \tau_T \frac{\delta \nabla T}{\delta t} \right) \tag{2.2.5}$$

where

$$\tau_T = \tau_Q \frac{K_F}{k} \equiv \tau_Q \gamma \tag{2.2.6}$$

is the retardation time, expressed as the product of the relaxation time and γ, the thermal conductivity ratio of the solvent to that of the NF solution. Relation (2.2.6) is the same as that relating the relaxation and retardation times in terms of the solvent-to-solution viscosity ratio of purely elastic (non-shear thinning) Boger fluids (see, for instance, Park

and Lee 1996 in the context of thermal convection). For pure heat conduction, equation (2.2.5) reduces to the dual-phase-lagging model [19], [29]:

$$\tau_Q \frac{\partial \mathbf{Q}}{\partial t} + \mathbf{Q} = -K\left(\nabla T + \tau_T \frac{\partial \nabla T}{\partial t}\right) \tag{2.2.7}$$

It is not difficult to see that this equation relates the temperature gradient at a material point **x** and time $t + \tau_T$ to the heat flux vector at the same point at time $t + \tau_Q$ for a medium of thermal conductivity k. The relation reads:

$$\mathbf{Q}\left(\mathbf{x}, t + \tau_Q\right) = -K\nabla T\left(\mathbf{x}, t + \tau_T\right) \tag{2.2.8}$$

Both of the phase-lags are treated as intrinsic thermal or structural properties of the material. When $\tau_T = 0$, this relation diminishes to the Cattaneo-Vernotte relation. For a NF, it is generally observed that the thermal conductivity increases relative to that of the base fluid. In this case, expression (2.6) suggests that the retardation time should be smaller than the relaxation time for a NF. Thus, it will be assumed that

$$\tau_T < \tau_Q \tag{2.2.9}$$

The inequality is in agreement with the observation made by Wang and Wei [29] but in disagreement with [18] and [31] finding because they have not considered the coupled thermal conductivity. The coupled thermal conductivity is not negligible especially in low concentration of NPs (see Figure 2-2). Wang and Wei [29] showed that the relaxation and retardation times can be related to the properties of the two-phase system, of the Fourier solvent phase (F) and nanoparticle phase (NP), with corresponding concentrations $1 - \phi$ and ϕ, respectively. The relations are rewritten here as:

$$\tau_Q = \frac{\phi(\rho c)_{NP}(1-\phi)(\rho c)_F}{h a_v\left[\phi(\rho c)_{NP} + (1-\phi)(\rho c)_F\right]},\ \tau_T = \frac{\phi(\rho c)_{NP} K_F + (1-\phi)(\rho c)_F K_{NP}}{h a_v\left(K_{NP} + K_F + 2K_{NP/F}\right)} \qquad (2.2.10)$$

Here ρ, c and K are the density, specific heat and thermal conductivity of each phase, respectively, and $K_{NP/F}$ is a coupling term arising from the averaging process [29], [38]. Recall that h is the film heat transfer coefficient, and $a_v = \frac{2}{\delta_F + \delta_{NP}}$ is the interfacial area per unit volume, where δ_F and δ_{NP} are mean interaction length in the base fluid and NP phase, which in the present case, are identified as the mean inter-particle distance and particle diameter, d_{NP}, respectively. Thus, the relaxation time can be explicitly determined in terms of NP concentration from (2.2.10) once a_v is evaluated. The interfacial area per unit volume may be estimated as is customarily done in condensed matter physics, by recalling the radius of a sphere of solvent whose volume is equal to the mean volume per NP, the Wigner-Seitz radius, r_s (see, for instance, page 123 in [41]. In a 3-D system with N particles in a volume B, the radius is defined by $\frac{4}{3}\pi r_s^3 = \frac{B}{N} \equiv \frac{1}{n}$, where n is the particle density. Thus, noting that $n = \frac{6\phi}{\pi d_{NP}^3}$, then $\delta_F = \frac{d_{NP}}{2\phi^{1/3}}$ and $\delta_{NP} = d_{NP}$. In this case,

$$a_v = \frac{4\phi^{1/3}}{d_{NP}\left(2\phi^{1/3} + 1\right)} \qquad (2.2.11)$$

Note that, typically, for a NF, the interaction lengths are of the same order of magnitude. The retardation time is determined from (2.2.6) once the thermal conductivity of the NF is estimated. Generally, the retardation increases with NP concentration and vanishes in the absence of NP (see below). In this case, $\tau_Q, \tau_T \to 0$ as $\phi \to 0$, and the Fourier limit is

recovered as expected. Interestingly, $k_{NP/F}$ can be estimated by combining (2.2.6) and (2.2.10). The retardation time can be estimated from (2.2.6) once the thermal conductivity of the NF is known and the relaxation time is evaluated from (2.2.10). Here, the dependence of the thermal conductivity on NP concentration for Al2O3, TiO2 and CuO are determined following [20],[24] and [42] respectively:

$$\frac{K}{K_F} = 1 + 7.47\phi \qquad \text{(Al2O3)}$$

$$\frac{K}{K_F} = 1 + 2.92\phi - 11.99\phi^2 \qquad \text{(TiO2)} \qquad \text{(2.2.12 a, b and c)}$$

$$\frac{K}{K_F} = \frac{K_{NP} + 2K_F + 2\left(K_{NP} - K_F\right) + 1.33\phi}{K_{NP} + 2K_F - \left(K_{NP} - K_F\right) + 1.33\phi}. \qquad \text{(CuO)}$$

Obviously, thermal conductivity of NPs affects the relaxation and retardation times. Figure 2-1 illustrates the dependence of the relaxation (Figure 2-1a) and the retardation times (Figure 2-1b) on NP concentration. In this case, the NF solution comprises water, as a base (Fourier) fluid solvent, and Al_2O_3, TiO_2 and CuO, as solute NPs. Figure 2-1 illustrates that Al_2O_3 has the highest relaxation and retardation time. The main reason is higher thermal conductivity of Al_2O_3 compare to the other NPs. Surprisingly, Figure 2-1 shows that despite of lower thermal conductivity of TiO_2 compare to CuO, TiO_2 has higher relaxation and retardation times than CuO. It rises from dependence of time and phase lags on specific heat and density of NPs. In the other word, time and phase lags intensively increase with specific heat and density of NPs. In Figure1, Al_2O_3 has a higher relaxation and retardation times because of its higher specific heat and density (and thermal conductivity). Obviously the ability to store the heat of NPs is a considerable parameter for induced time and phase lags and it is even more important than thermal conductivity. Note that the ρc term of Al_2O_3, CuO and TiO_2 are 3.5×10^6, 2.4×10^6 and 2.9×10^6 respectively. Both times or phase lags increase with concentration, with the retardation time remaining always lower than the relaxation time ($\gamma < 1$). The inset

displays an essentially power-law growth for both times, particularly at low concentration: $\tau_Q, \tau_T \sim \phi^{3.5}$. Using (2.6), (2.10) and (2.12) one obtains

$$K_{NP/F} = \left(\frac{K}{K_F} - 1\right)\left(K_{NP} + K_F\right) + \left(\frac{(1-\phi)(\rho c)_F}{\phi(\rho c)_{NP}}\right)\frac{K}{K_F}K_{NP} + \left(\frac{\phi(\rho c)_{NP}}{(1-\phi)(\rho c)_F}\right)K \quad (2.2.13)$$

The influence of the NP concentration on the coupled thermal conductivity for Al_2O_3, TiO_2 and CuO in the water is illustrated in Figure 2-2. From (2.2.13), definitely, conductivity of NPs is the most important parameter in the coupled thermal conductivity and as Figure 2-2 illustrates, it increases by thermal conductivity of NPs. Note that thermal conductivity of Al_2O_3, CuO and TiO_2 are 40, 20 and 11.7 watts per meter Kelvin respectively. The coupled thermal conductivity is high at low NP concentration, decreases monotonically with NP concentration and eventually vanishes. It means that the thermal resistance, which grows with the NP concentration, should be considered especially at higher NP concentrations.

Finally, and as mentioned above, a dimensionless relaxation time is given by the Cattaneo number: $C = \frac{\tau_Q \kappa}{D^2}$, which will be formally introduced in the next section, and should be compared with the elasticity number, $E = \frac{\tau\kappa}{D^2}$, for a polymeric solution with relaxation time, τ for stress, Thus, both C and E are the ratios of a relaxation time over a thermal diffusion time. For a NF solution of water and TiO_2 NPs, the relaxation time is obtained as per the procedure in section 2.2. In this case, $\tau_Q = 2.05\times10^{-4}$ s for NP concentration of 7%, and can lead to a non-negligible Cattaneo number for a moderately small gap: C = 0.003 for D = 0.1 mm. The corresponding retardation time is $\tau_T = 1.775\times10^{-4}$ s.

(a)

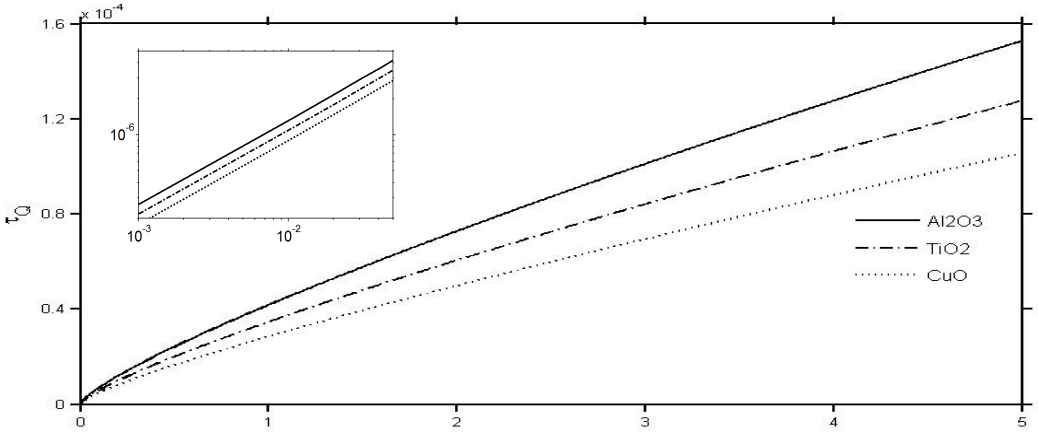

(b)

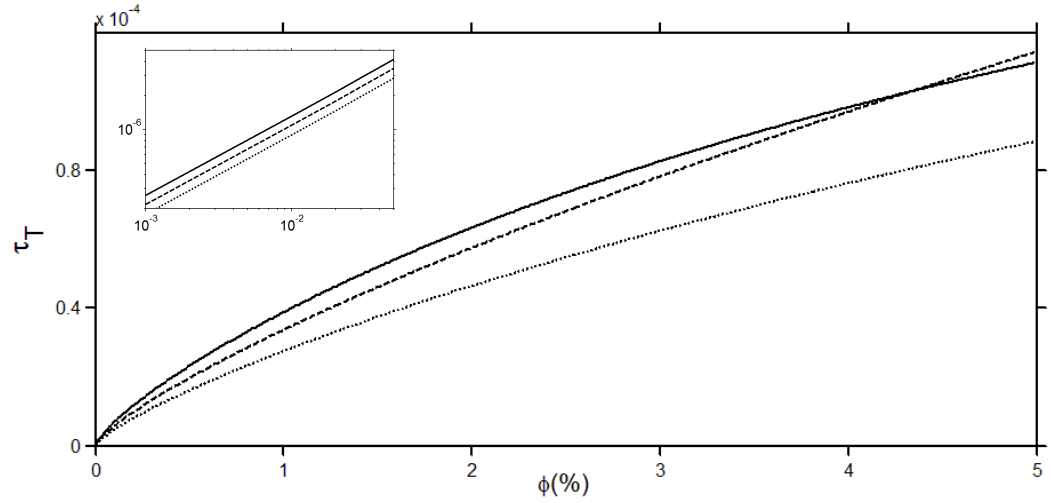

Figure 2-1: *Influence of the NP concentration on (a) the relaxation and (b) retardation times for Al2O3, TiO2 and CuO.*

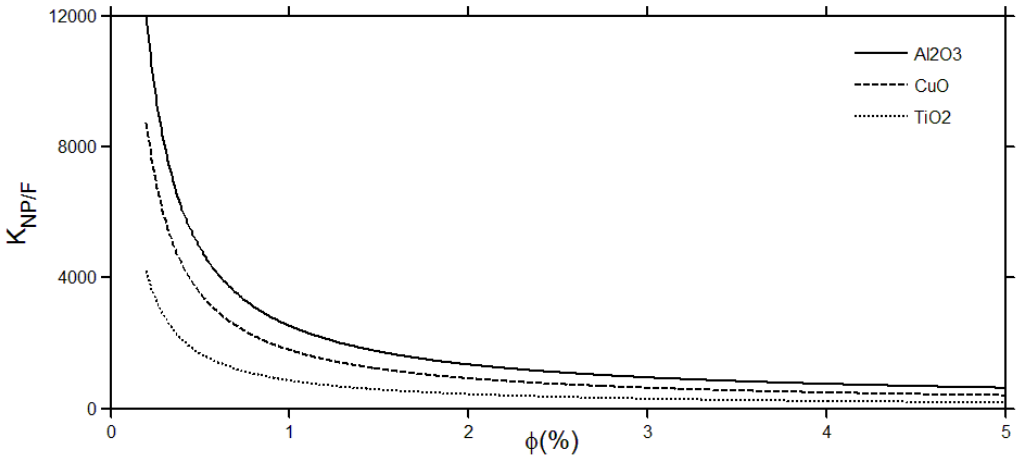

Figure 2-2: *Dependence of the coupled thermal conductivity on NP concentration for Al2O3, TiO2 and CuO in the water.*

2.3 Governing equations and boundary conditions

Consider a thin layer of a Newtonian non-Fourier liquid confined between the (X, Z) planes at $Z = 0$ and the planes, maintained at fixed temperatures $T_0 + \delta T$ and T_0, respectively. The fluid layer is assumed to be of infinite horizontal extent. Convection emerges when the buoyancy effect exceeds a critical threshold relative to the viscous effect. The gravity acceleration vector is given by $\mathbf{g} = -g\mathbf{e}_z$, where $\mathbf{e}_z$ is the unit vector in the Z direction. The fluid density, ρ, is assumed to depend on the temperature, T, following

$$\rho = \rho_0 \left[1 - \alpha_T \left(T - T_0\right)\right] \tag{2.3.1}$$

where α_T is the coefficient of volume expansion and ρ_0 is the mass density of the fluid at T_0. The fluid is assumed to be incompressible, of specific heat at constant pressure C_p, thermal conductivity K and viscosity μ. In this case, the general governing equations for a non-Fourier fluid comprise the conservation of mass, linear momentum and energy, as well as the constitutive equation for the heat flux. In this case, the conservation equations are given by

$$\nabla \cdot \mathbf{V} = 0 \tag{2.3.2}$$

$$\rho_0 \left(\mathbf{V}_t + \mathbf{V} \cdot \nabla \mathbf{V} \right) = -\nabla P - \rho g \mathbf{e_z} + \mu \Delta \mathbf{V} \tag{2.3.3}$$

$$\rho_0 c_p \left(T_t + \mathbf{V} \cdot \nabla T \right) = -\nabla \cdot \mathbf{Q} \tag{2.3.4}$$

where ∇ and Δ are the gradient and Laplacian operators, respectively, and a subscript denotes partial differentiation. Here **V =** (U, W) is the velocity vector, P is the pressure, T is the temperature and **Q** is the heat flux vector. Note that the Boussinesq approximation, which states that the effect of compressibility is negligible everywhere in the conservation equations except in the buoyancy term, is assumed to hold. In this work, the heat flux is assumed to be governed by dual-phase-lagging equation (2.2.5), explicitly re-written here as

$$\tau_Q \left(\mathbf{Q}_t + \mathbf{V} \cdot \nabla \mathbf{Q} - \mathbf{Q} \cdot \nabla \mathbf{V} \right) = -\mathbf{Q} - K \left[\nabla T + \tau_T \left(\nabla T_t + \mathbf{V} \cdot \nabla \nabla T - \nabla T \cdot \nabla \mathbf{V} \right) \right] \tag{2.3.5}$$

where τ_Q and τ_T are the relaxation and retardation times, respectively. It is also possible to generate a generalized energy equation. Indeed, upon taking the divergence of (2.3.4), noting the identity $\nabla \cdot \left(\mathbf{a} \cdot \nabla \mathbf{b} \right) = \nabla \mathbf{a} : \nabla \mathbf{b} + \mathbf{a} \cdot \nabla \left(\nabla \cdot \mathbf{b} \right)$, **a** and **b** being two general vectors, and using (3.5), one obtains

$$\begin{aligned} &\tau_Q \left[T_{tt} + 2\mathbf{V} \cdot \nabla T_t + \mathbf{V}_t \cdot \nabla T + \mathbf{V} \cdot \nabla \left(\mathbf{V} \cdot \nabla T \right) \right] \\ &\quad + T_t + \mathbf{V} \cdot \nabla T = \kappa \left[\nabla^2 T + \tau_T \left(\nabla^2 T_t + \mathbf{V} \cdot \nabla \nabla^2 T \right) \right], \end{aligned} \tag{2.3.6}$$

where $\kappa = \dfrac{K}{\rho_0 c_p}$ is the thermal diffusivity. The boundary conditions at the lower and upper surfaces are taken to correspond to free-free conditions. In this case

$$\begin{aligned}
&\mathbf{V}\left(X,Z=0,t\right)\cdot\mathbf{e}_Z=\mathbf{V}\left(X,Z=D,t\right)\cdot\mathbf{e}_Z=0,\\
&\mathbf{V}_{ZZ}\left(X,Z=0,t\right)\cdot\mathbf{e}_Z=\mathbf{V}_{ZZ}\left(X,Z=D,t\right)\cdot\mathbf{e}_Z=0,\\
&T\left(X,Z=0,t\right)=T_0+\delta T,\qquad T\left(X,Z=D,t\right)=T_0.
\end{aligned}\tag{2.3.7}$$

Other boundary conditions could be adopted, such as the rigid-rigid or rigid-free conditions. However, the free-free conditions are convenient and most commonly used in the literature. Moreover, no qualitative change in behaviour is expected if one set of boundary conditions is used over another [43]. In fact, [44] confirmed this consistency in behaviour for rotating flow as well.

The base state corresponds to stationary heat conduction, which remains the same as for a Fourier fluid since both transient and upper convective terms in (3.5) vanish in this case. Consequently, the temperature, pressure gradient and heat flux for the conductive state are given by

$$\begin{aligned}
&T_B=-\left(Z/D\right)\delta T+T_0+\delta T\\
&dP_B/dZ=-\rho_0\left[1-\alpha_T\delta T\left(1-Z/D\right)\right]g\\
&\mathbf{Q}_B=\left(0,K\frac{\delta T}{D}\right)
\end{aligned}\tag{2.3.8}$$

respectively. The problem is conveniently cast in dimensionless form by taking the length, time and velocity scales as D, $\frac{D^2}{\kappa}$ and $\frac{\kappa}{D}$, respectively. Let $p=\frac{D^2}{\kappa\mu}\left(P-P_B\right)$ and $\theta=\frac{T-T_B}{\delta T}$ be the dimensionless pressure and temperature deviations from the base (conductive) state. In this case, the dimensionless equations are given by

$$\nabla\cdot\mathbf{v}=0 \tag{2.3.9}$$

$$Pr^{-1}\left(\mathbf{v}_t+\mathbf{v}\cdot\nabla\mathbf{v}\right)=-\nabla p+Ra\theta\mathbf{e}_Z+\Delta\mathbf{v} \tag{2.3.10}$$

$$\theta_t + \mathbf{v}\cdot\nabla\theta = -j + w \tag{2.3.11}$$

$$C\left(\mathbf{q}_t - \mathbf{v}_z + \mathbf{v}\cdot\nabla\mathbf{q} - \mathbf{q}\cdot\nabla\mathbf{v}\right) = -\mathbf{q} - \nabla\theta - S\left(\nabla\theta_t + \mathbf{v}_z + \mathbf{v}\cdot\nabla\nabla\theta - \nabla\theta\cdot\nabla\mathbf{v}\right) \tag{2.3.12}$$

where **v**(u, w) and **q** are the dimensionless velocity and heat flux vectors, respectively. Here $j = \nabla\cdot\mathbf{q}$. It is interesting to note the presence of four linear terms of non-Fourier origin in equation (2.3.12), namely the transient terms and the velocity gradient in the z direction. This contrasts with the convection of viscoelastic fluids where the transient terms are the only linear terms that survive in the stress equations (see [45]). This is an important point that will be explored further in section 2.4. Equation (2.3.6) takes the form:

$$\begin{aligned} &C\left[\theta_{tt} + 2\mathbf{v}\cdot\nabla\theta_t + \mathbf{v}_t\cdot\nabla\theta - w_t + \mathbf{v}\cdot\nabla\left(\mathbf{v}\cdot\nabla\theta\right)\right] \\ &\quad + \theta_t + \mathbf{v}\cdot\nabla\theta - w = \nabla^2\theta + S\left(\nabla^2\theta_t + \mathbf{v}\cdot\nabla\nabla^2\theta\right). \end{aligned} \tag{2.3.13}$$

The following non-dimensional groups have been introduced, namely, the Prandtl number, the Cattaneo number, the Rayleigh number and dimensionless retardation time, respectively, given by

$$Pr = \frac{\nu}{\kappa}, \qquad C = \frac{\tau_Q\kappa}{D^2}, \qquad Ra = \frac{\delta T\alpha_T g D^3}{\nu\kappa}, \qquad S = \frac{\tau_T\kappa}{D^2} \tag{2.3.14}$$

From the discussion in section 2.2, C and S are not entirely unrelated. In fact, they are both related directly to the NP concentration. Since $S = \frac{k_F}{k}C$, S must always be smaller than C for a NF. In this work, although C and S involve other parameters, they will be interpreted as reflecting the effect of NP concentration (see Figure 2-1). Note that

$$S = \gamma C, \qquad \gamma = \frac{k_F}{k} < 1 \tag{2.3.15}$$

The problem can be simplified by casting the constitutive equation for heat flux in terms of the scalar variable j. Thus, upon taking the divergence of equation (2.3.12), and recalling again the identity $\nabla\cdot(\mathbf{a}\cdot\nabla\mathbf{b}) = \nabla\mathbf{a}:\nabla\mathbf{b} + \mathbf{a}\cdot\nabla(\nabla\cdot\mathbf{b})$, one obtains the following constitutive equation for j:

$$C(j_t + \mathbf{v}\cdot\nabla j) + j = -\Delta\theta - S(\Delta\theta_t + \mathbf{v}\cdot\nabla\Delta\theta) \tag{2.3.16}$$

where the continuity equation (2.3.9) is used. The boundary conditions (2.3.7) reduce to

$$\begin{aligned} w(x, z=0, t) &= w(x, z=1, t) \\ &= u_z(x, z=0, t) = u_z(x, z=1, t) \\ &= \theta(x, z=0, t) = \theta(x, z=1, t) = 0, \end{aligned} \tag{2.3.17}$$

which must be used to solve equations (2.3.9), (2.3.10), (2.3.11) and (2.3.16). Finally, the Fourier model is recovered upon setting C = 0 (zero relaxation time) in (2.3.12), (2.3.13) or (2.3.16). Moreover, the Fourier limit is also recovered upon setting γ = 1 (thermal conductivity of the NF solution is the same as that of the base fluid solvent). In this case, $\mathbf{q} = -\nabla\theta$ and $j = -\Delta\theta$ satisfy equations (2.3.12) and (2.3.16), respectively.

2.4 Linear stability analysis

Comparable to a Fourier fluid, the conduction of a non-Fourier fluid is lost to convection once a critical value of the Rayleigh number, $Ra_c(k)$, is exceeded, where k is the wavenumber of the disturbance. However, in contrast to a Fourier fluid, and similar to

a viscoelastic fluid [45], non-Fourier conduction can be lost to steady or oscillatory convection, depending on the flow parameters. The linear stability analysis of the conduction state is similar to the case of a viscoelastic fluid, except that, unlike a viscoelastic fluid, a non-Fourier fluid at rest does further recognize the non-Fourier character, which is reflected by the presence of the additional linear velocity gradient on the two sides of (3.12), in addition to the transient term. The stability of the conduction state is examined to a small (infinitesimal) perturbation of the form

$$\begin{aligned} \mathbf{v}(x,z,t) &= \mathbf{V}(z)e^{st+ikx}, & \theta(x,z,t) &= \Theta(z)e^{st+ikx}, \\ p(x,z,t) &= P(z)e^{st+ikx}, & j(x,z,t) &= J(z)e^{st+ikx}, \end{aligned} \tag{2.4.1}$$

where k is the perturbation wavenumber in the x direction, and s dictates the time evolution of the disturbance. Thus, the conduction/base state is stable (unstable) if the real part of s is negative (positive). Following the standard procedure in linear stability analysis, the z-dependent eigenvector components are governed by

$$\begin{aligned} &ikU + DW = 0, \\ &Pr^{-1}sU = -ikP + \left(D^2 - k^2\right)U, \\ &Pr^{-1}sW = -DP + \left(D^2 - k^2\right)W + Ra\Theta, \\ &s\Theta = -J + W, \\ &(Cs+1)J = -(\gamma Cs+1)\left(D^2 - k^2\right)\Theta, \end{aligned} \tag{2.4.2}$$

where D = d/dz. In this case, taking W = sin(nπz), and eliminating U, P, Θ and J, lead to the following dispersion relation:

$$s^3 + \left(Pr\beta_n + \frac{1}{C} + \gamma\beta_n\right)s^2 + \left(\beta_n\frac{Pr+1}{C} - \frac{k^2 Ra\,Pr}{\beta_n} + \gamma Pr\beta_n^2\right)s + \frac{Pr}{C\beta_n}\left(\beta_n^3 - k^2 Ra\right) = 0 \tag{2.4.3}$$

where $\beta_n = k^2 + n^2\pi^2$, and n is the mode number. In contrast to a Fourier fluid, the presence of the cubic term in (2.4.2) hints to the possibility of stationary or oscillatory convection. Interestingly, the retardation time always appears in the ratio S/C = γ. Thus, the stability picture depends on the relaxation time and thermal conductivity ratio (as well as on Pr and Ra). This is a similar situation to viscoelastic fluids where the retardation time also appears in the form of viscosity ratio [45].

For steady convection, one recovers the same critical Rayleigh number, Ra_c, as a Fourier fluid, namely

$$Ra_c = Ra_{cF} = \frac{\beta_n^3}{k^2} \tag{2.4.4}$$

In this case, the n > 1 neutral curves are all above the n = 1 curve, with Ra_c displaying a minimum, $Ra_m = \frac{27\pi^4}{4}$ at $k_m = \frac{\pi}{\sqrt{2}}$. For oscillatory convection, the corresponding neutral curves are obtained upon setting $s = i\omega$ in (4.3), ω_c being the frequency, and separating real and imaginary parts to give

$$\begin{aligned} Ra_c &= \left[\frac{\left(Pr^2 + 2\gamma Pr + \gamma\right) C\beta_n + Pr + 1}{\beta_n^2 C^2 Pr\left(Pr + \gamma\right)} + \gamma \right] Ra_{cF} \\ \omega_c &= \frac{1}{C}\sqrt{\frac{C Pr \beta_n (1-\gamma) - Pr - 1}{Pr + \gamma}}\,. \end{aligned} \tag{2.4.5}$$

Clearly, oscillatory convection is possible only if

$$\beta_n > \frac{1+\mathrm{Pr}}{\mathrm{Pr}\,C(1-\gamma)} \qquad \text{or} \qquad k > \sqrt{\frac{1+\mathrm{Pr}}{\mathrm{Pr}\,C(1-\gamma)} - n^2\pi^2}\,. \tag{2.4.6}$$

This criterion constrains the range of wavenumber for oscillatory convection. Thus, it is anticipated that each marginal stability curve in the Ra-k plane comprises two distinct branches: a Fourier branch, corresponding to steady convection, for $k < k_i$, and a non-Fourier branch, corresponding to oscillatory convection, for $k > k_i$, where k_i is the wavenumber at which the two branches intersect, and satisfies the relation:

$$k_i = \sqrt{\frac{1+\mathrm{Pr}}{\mathrm{Pr}\,C(1-\gamma)} - n^2\pi^2} \tag{2.4.7}$$

since, at intersection, the frequency vanishes. It is not difficult to verify that substituting (4.6) into (4.5) leads to $\mathrm{Ra}_c(k=k_i) \equiv \mathrm{Ra}_i = \mathrm{Ra}_{cF}(k=k_i)$. Expression (4.7) suggests that a limit, C_∞, of C exists for which $k_i = 0$.

Two limits are worth examining here. Consider first the limit of large Cattaneo number (high NP concentration and relaxation time or the case of a very small gap). In this case, (4.5) reduces to

$$\lim_{C\to\infty} \mathrm{Ra}_c = \gamma \mathrm{Ra}_{cF}, \qquad \lim_{C\to\infty} \omega_c = \sqrt{\frac{\mathrm{Pr}\,\beta_n(1-\gamma)}{C(\gamma+\mathrm{Pr})}} \tag{2.4.8}$$

A couple of interesting observations can be made. First, the oscillation frequency behaves like $\omega_c \sim 1/\sqrt{C}$, suggesting that oscillatory rolls may not be detectable in reality

for large C. Second, the critical Rayleigh number is lower than the Fourier level. Whether this behaviour holds for any C will be examined below. Third, in the absence of retardation, the critical Rayleigh number diminishes like $\mathrm{Ra_c} \sim 1/\mathrm{C}$, suggesting that convection may be spontaneously observed (without a conduction phase), for any temperature differential, for large C. However, real NFs tend to possess non-zero retardation, which leads to a non-zero minimum critical Rayleigh number equal to $\gamma \mathrm{Ra_{cF}}$ for large C, above which convection sets in. In this case, conduction is always present, but its range of temperature differential may decrease significantly with NP concentration. Another limit of interest is the large Pr limit. This is also a limit of practical interest since most NFs possess a relatively large Prandtl number. In this limit, (4.5) reduces to

$$\lim_{\mathrm{Pr}\to\infty} \mathrm{Ra_c} = \left(\frac{1}{\beta_n \mathrm{C}} + \gamma\right)\mathrm{Ra_{cF}}, \qquad \lim_{\mathrm{Pr}\to\infty} \omega_c = \frac{1}{\mathrm{C}}\sqrt{(1-\gamma)\mathrm{C}\beta_n - 1} \tag{2.4.9}$$

In this case, the intersection wavenumber becomes

$$\lim_{\mathrm{Pr}\to\infty} \mathrm{k_i} = \sqrt{\frac{1}{(1-\gamma)\mathrm{C}} - \mathrm{n}^2\pi^2} \tag{2.4.10}$$

In the double limit of large C and Pr, (2.4.9) suggests that oscillatory convection sets in at a Rayleigh number smaller than the Fourier level by a factor γ. Further physical insight of these limits will be gained below when numerical results are reported.

Finally, it is helpful to list the eigenvector components, which will be used later, and take the form:

$$\mathrm{U} = \frac{\mathrm{in}\pi}{\mathrm{k}}\cos(\mathrm{n}\pi\mathrm{z}), \qquad \mathrm{W} = \sin(\mathrm{n}\pi\mathrm{z}), \qquad \mathrm{P} = -\left[\frac{\mathrm{Pr}^{-1}\mathrm{s} + \beta}{\mathrm{k}^2}\right]\mathrm{n}\pi\cos(\mathrm{n}\pi\mathrm{z}),$$

$$\Theta = \left(\frac{Cs+1}{Cs^2 + (\gamma C\beta_n + 1)s + \beta_n} \right) \sin(n\pi z), \qquad J = \left(\frac{\gamma Cs+1}{Cs^2 + (\gamma C + 1)s + \beta_n} \right) \beta_n \sin(n\pi z) \quad (2.4.11)$$

Of particular interest here is the non-Fourier character reflected in the flow and heat transfer. In fact, (2.4.11) clearly reflects the absence of non-Fourier effects at criticality for *stationary* convection. This is easily verified upon setting s = 0, as one recovers the Fourier limit. This is, of course, not the case for oscillatory convection. Consequently, stationary convection of a non-Fourier fluid or a NF is expected to be Fourier in character, near criticality. It is observed that other modes will be present near criticality, which do exhibit a non-Fourier character, but they will be dominated by the critical mode. Of course, as the Rayleigh number increases beyond the critical value, non-Fourier effects become increasingly palpable. Similarly, in the case of a viscoelastic or a non-Newtonian fluid, in general, any convective *steady* state emerging near criticality will not have a significant non-Newtonian character to it given the absence of shearing and elongation rates of the base (conductive) state [45]. However, despite the apparent similarity, there is a significant difference between the current non-Fourier and non-Newtonian loss of conduction to steady convection. For non-Newtonian convection near criticality, the elastic component of the stress remains small given the absence of flow in the pre-critical range of Rayleigh number. More generally, for a non-Newtonian flow, the destabilization of the base to a steady state leads to a Newtonian state at criticality. However, if the base state involves shearing and elongation, as in the case of Taylor-Couette flow, the steady vortex flow, does exhibit non-Newtonian character near criticality [44].

The lack of Fourier character in the stationary convection mentioned above is only apparent, as (4.11) does not reflect the whole situation. At the center of the argument is the relation between the heat flux vector components and the temperature (gradient), which has not been invoked so far in the discussion since j, and not **q**, is needed for the solution of the problem. The replacement of the heat equation (2.3.12) by (2.3.16) leads to significant simplification in the current linear stability (and, eventually, any nonlinear) analysis as the formulation includes the scalar variable, j instead of the vector **q**, reducing

the number of degrees of freedom. Moreover, the upper-convective terms are replaced by a convective term, $\mathbf{v}\cdot\nabla j$. This term does not survive in the linear analysis given the stationary character of the base conductive state. Even the generalized energy equation (2.3.13) illustrates the absence of non-Fourier character upon the onset of stationary convection. However, the heat flux vector does exhibit a non-Fourier contribution at criticality, emerging from the upper-convective terms. Indeed, near criticality, the heat flux in (3.12) reduces to

$$\mathbf{q}= -\nabla\theta + C(\gamma-1)\,\mathbf{v}_z \tag{2.4.12}$$

Although, as deduced upon setting s = 0 in (4.11), the temperature, velocity and pressure do not display any non-Fourier character at criticality, the heat flux does, as (4.12) suggests. This is verified further by substituting for the temperature and velocity from (4.11) into (4.12), to give

$$Q_x = -i\left[\frac{C(\gamma+1)}{sC+1}\frac{n^2\pi^2}{k}+\frac{k(\gamma Cs+1)}{Cs^2+s+\beta_n}\right]\sin(n\pi z) \tag{2.4.13 a, b}$$

$$Q_z = n\pi\left(\frac{\gamma+1}{Cs+1}C-\frac{\gamma Cs+1}{Cs^2+s+\beta_n}\right)\cos(n\pi z)$$

Clearly, the non-Fourier character survives when s = 0. However, given the decoupling from **q**, as equations (2.3.9)-(2.3.11) and (2.3.16) suggest, the flow and temperature fields are not expected to reflect a significant non-Fourier character upon the onset of stationary convection. Of course, this is not the case for the onset of oscillatory convection (see below).

2.5 Results and discussion

In this section, results based on the formulation above are discussed. The case of a SPL fluid with no retardation time is presented first before examining DPL fluids. Conditions for both stationary and oscillatory convection are emphasized. It is helpful to schematically summarize the stability picture and notations used, in anticipation of the ensuing discussion and details. The neutral curves are illustrated in the (Ra_c-k) plane in Figure 2-3 for different non-Fourier levels or, equivalently, different levels of NP concentrations. The Fourier limit is reflected by the C = 0 curve. For a weakly non-Fourier fluid ($C << C_H$) the neutral curve comprises a Fourier branch and an oscillatory branch, intersecting at (Ra_i, k_i). In this case, the minimum critical Rayleigh number is that of the Fourier branch $\left(Ra_{mF} = \frac{27\pi^4}{4}, k_{mF} = \frac{\pi}{\sqrt{2}} \right)$. As C increases, a minimum develops in the oscillatory branch. At $C = C_H$, the minima of the stationary and oscillatory branches reach the same Rayleigh number but different wavenumbers. For a moderately strongly non-Fourier fluid ($C > C_H$), there is only one minimum $\left(Ra_m < Ra_{mF}, k_m > k_{mF} \right)$. Finally, it is well established that the n = 1 mode is the most dangerous mode for a Fourier fluid. Although this is not easy to establish analytically for a DPL fluid, by examining (2.4.5), the n = 1 mode turns out to be the most dangerous mode, for both stationary and oscillatory convection. This is particularly obvious for large C as suggested by (2.4.7), and not difficult to establish for large Pr from (2.4.8). Consequently, only the n = 1 mode will be considered hereafter.

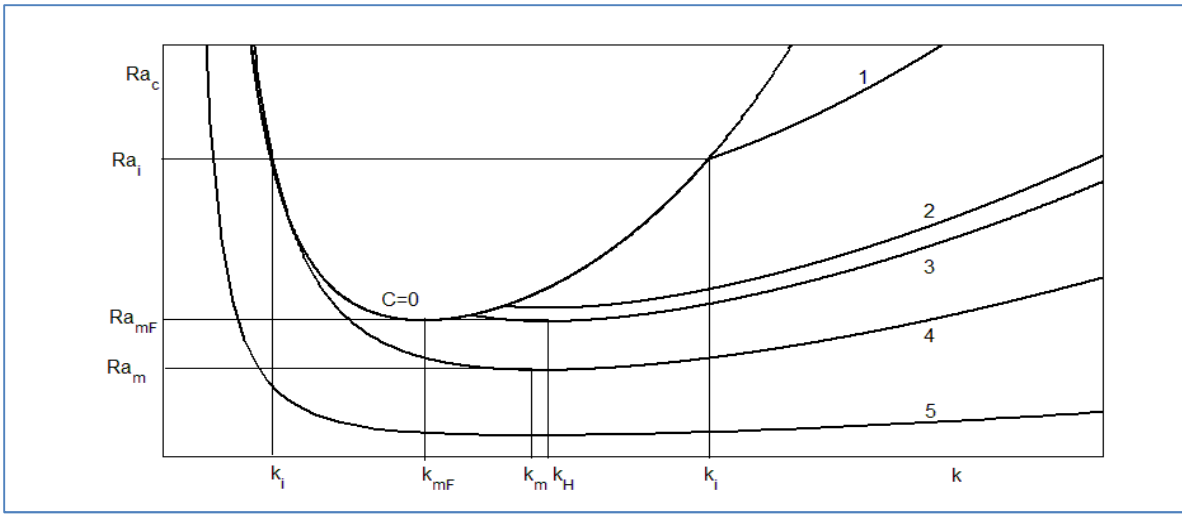

Figure 2-3: *Schematic illustrating notations used in the (Ra-k) plane, showing qualitatively various marginal stability curves and corresponding regimes with respect to the critical Cattaneo number, CH. The curves 1, 2, 3, 4 and 5 correspond to C << CH, C < CH, C = CH, C > CH and C >> CH, respectively.*

2.5.1 Stability of single-phase-lagging fluids

Consider now the case of a SPL fluid, with zero retardation time ($\gamma = 0$). In analogy with viscoelastic fluids, this is equivalent to examining an upper-convected Maxwell fluid (pure polymeric melt). Although somewhat unrealistic as a model for NFs, this limiting case has multiple advantages over a fluid with retardation. It serves as reference case for a fluid with strong non-Fourier character (relaxation time of the same order as the process time), is mathematically more manageable, and can, in the limit, reflect the behaviour of a NF with very high NP concentration. The influence of the Cattaneo number on the overall marginal stability picture is typically illustrated in Figure 2-4, where the marginal stability curves (Figure 2-4a) and corresponding frequency (Figure 2-4b) are plotted against the wavenumber for Pr = 10 and $\gamma = 0$. At the center, is the marginal stability curve for a Fourier fluid, which is recalled to be independent of Pr. For a Fourier fluid, there is an exchange of stability between the pure conduction state and stationary convection for any wavenumber. For relatively small $C > 0$, each non-Fourier curve comprises a stationary branch, also part of the Fourier curve, for $k < k_i$, and an oscillatory convective branch (overstability) for $k > k_i$. The critical Rayleigh number and frequency for the oscillatory branch simplify from (2.4.5) to

$$Ra_c = \frac{\beta C\,Pr^2 + Pr + 1}{\beta^2 C^2\,Pr^2} Ra_{cF}, \qquad \omega_c = \frac{1}{C}\sqrt{\frac{C\,Pr\,\beta - Pr - 1}{Pr}} \tag{2.5.1}$$

Clearly, oscillatory convection is possible only if

$$k > k_i = \sqrt{\frac{1+Pr}{Pr\,C} - \pi^2} \tag{2.5.2}$$

Upon using inequality (2.5.2), it is not difficult to show that the oscillatory branch always lies below the Fourier curve. This is also evident from Figure 2-4a. Thus,

$$\frac{\beta C\,Pr^2 + Pr + 1}{\beta^2 C^2\,Pr^2} < 1, \qquad \text{or} \qquad Ra_c < Ra_{cF} \tag{2.5.3}$$

Inequality (5.2) constrains the range of wavenumbers for oscillatory convection.

(a)

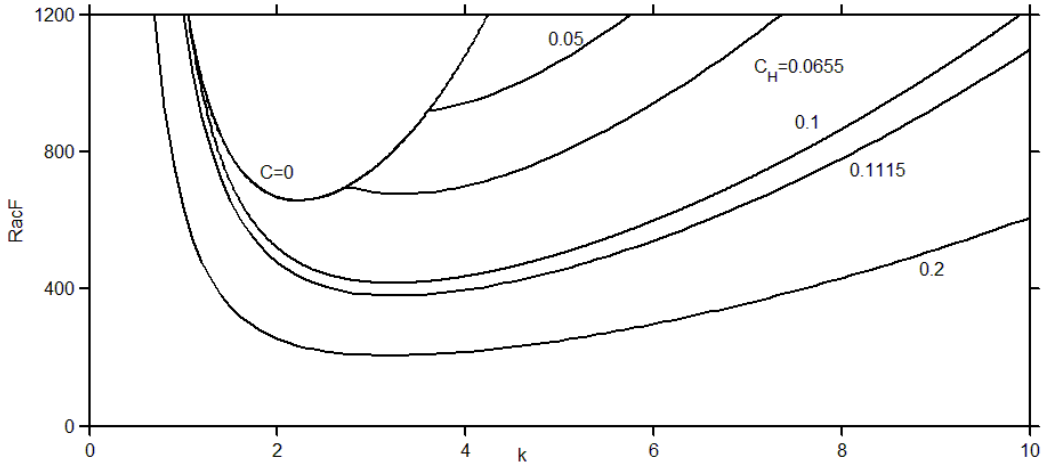

(b)

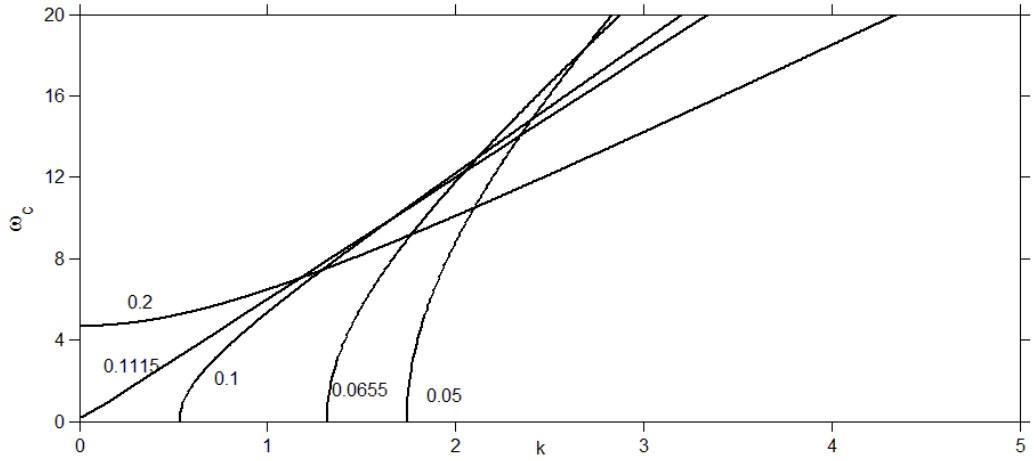

Figure 2-4: *Influence of the Cattaneo number on (a) the marginal stability curves in the Ra-k plane and (b) corresponding oscillation frequency for a single-phase-lagging fluid (Pr = 10 and γ = 0).*

2.5.2 Stability of dual-phase-lagging fluids

Most nanofluids, at least the ones currently used in practice, possess a finite (non-zero) and significant retardation time ($0 < \gamma < 1$). Similar to viscoelastic fluids, where the retardation-to-relaxation time ratio is equal to the solvent-to-solute viscosity ratio, the retardation time for a NF is also smaller than the relaxation time, as its ratio to the relaxation time is equal to the solvent-to-NF thermal conductivity ratio (2.6). This ratio

decreases with NP concentration as reported in Figure 2-1. The presence of the retardation time is expected to reflect the Fourier character of the NF. In this regard, the NF solution is analogous to a Boger (viscoelastic) fluid, obeying the Oldroyd-B constitutive equation [28], [40].

Thus, consider next the stability of a DPL fluid with $\gamma = 0.5$; or a NF of thermal conductivity twice that of the base fluid. The marginal stability curves and corresponding frequencies are displayed in Figures 2-5a and 2-5b, respectively, for Pr = 10. The range of C values [0, 0.3] includes the range [0, 0.2] in Figure 2-4 for reference. Thus, in comparison with a SPL fluid or NF with negligible retardation ($\gamma = 0$), the presence of retardation tends to be stabilizing, resulting in higher critical Rayleigh number and narrower oscillatory range. Interestingly, in contrast to the critical Rayleigh number, the frequency range does not seem to be significantly affected by retardation (compare Figures 2-4b and 2-5b).

(a)

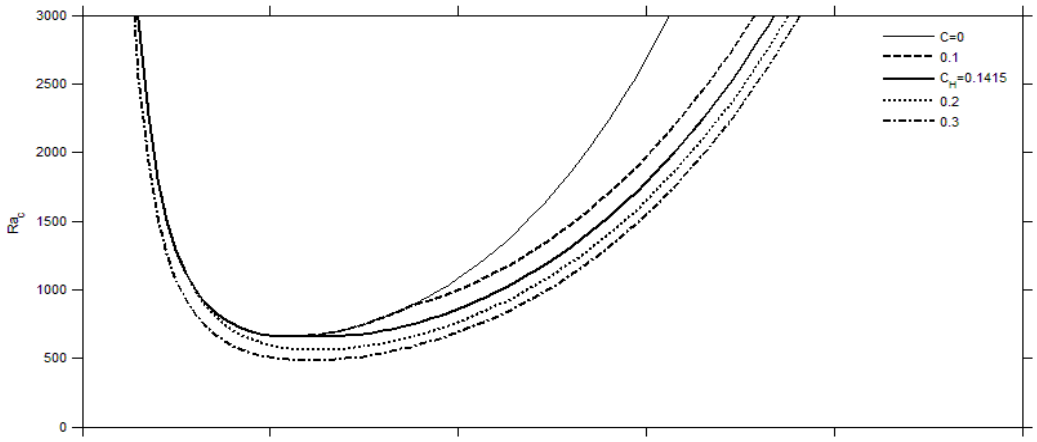

(b)

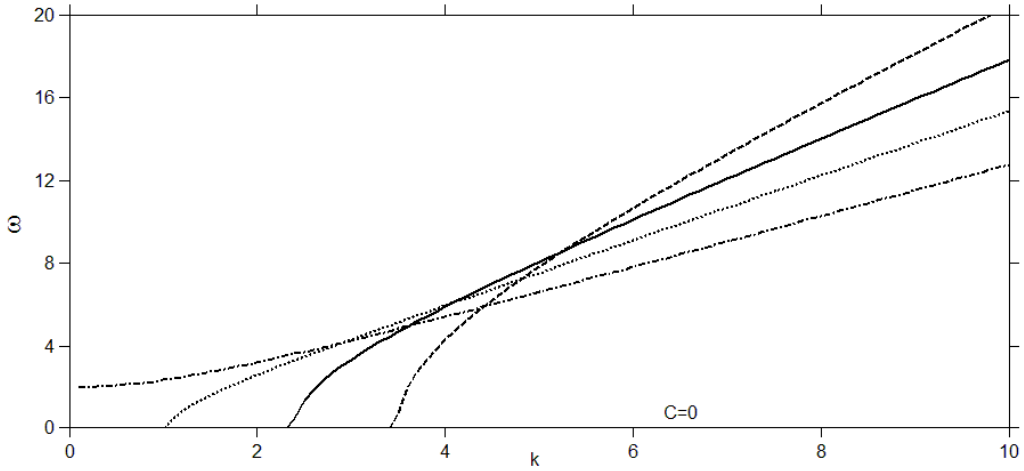

Figure 2-5: *Influence of relaxation time on (a) the marginal stability curves in the Ra-k plane and (b) corresponding oscillation frequency for a dual-phase-lagging fluid (Pr = 10 and γ = 0.5).*

Again, as C increases, the conductive state loses its stability eventually to oscillatory convection at a critical Rayleigh number that decreases with C. The limit in (4.8), as well as Figure 2-5a, reflects a saturation to this decrease, with the Rayleigh number for the oscillatory curve reaching γRa_{cF}. Consequently, for large C (very high NP concentration), in contrast to a SPL fluid, a DPL fluid is expected to always exhibits pure conduction before oscillatory convection.

The influence of retardation is further assessed upon examining the behavior of the Rayleigh number, Ra_i, and corresponding wavenumber, k_i, at the intersection of the oscillatory and stationary branches (see Figure 2-3). Figure 2-6 illustrates the interplay between relaxation and retardation, displaying the dependence of Ra_i (Figure 2-6a) and k_i (Figure 2-6b) on C for Pr = 10 and $\gamma \in [0, 0.75]$. Recall that the case $\gamma = 1$ corresponds to a Fourier fluid, with $Ra_i \to \infty$. The curves in Figure 2-6 are more easily interpreted in conjunction with the marginal stability curves as in Figures 2-4a and 2-5a. Recall from those curves that two intersection points are possible for the same critical Rayleigh number, one for a weakly, and another for a strongly non-Fourier fluid, on the right and left branch of the Fourier curve, respectively. The intersection wavenumber is given by

$$k_i = \sqrt{\beta_i - \pi^2} \tag{2.5.4 a}$$

where $\beta_i = \dfrac{1+\mathrm{Pr}}{\mathrm{Pr}\,C(1-\gamma)}$. The double-valuedness is reflected in Figure 2-6a as well as in the expression of the Rayleigh number at intersection, namely

$$Ra_i = \frac{(1+\mathrm{Pr})\beta_i^2}{1+\mathrm{Pr}-\pi^2\,\mathrm{Pr}\,C(1-\gamma)} \tag{2.5.4 b}$$

(a)

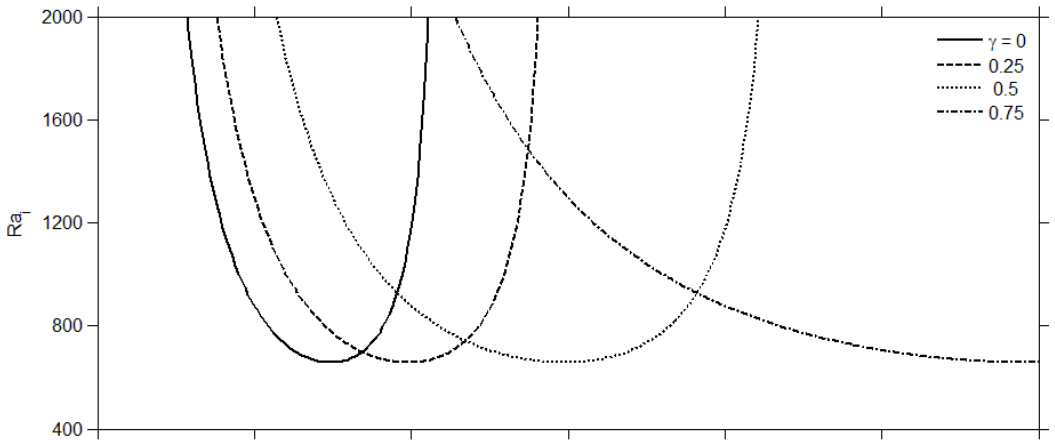

(b)

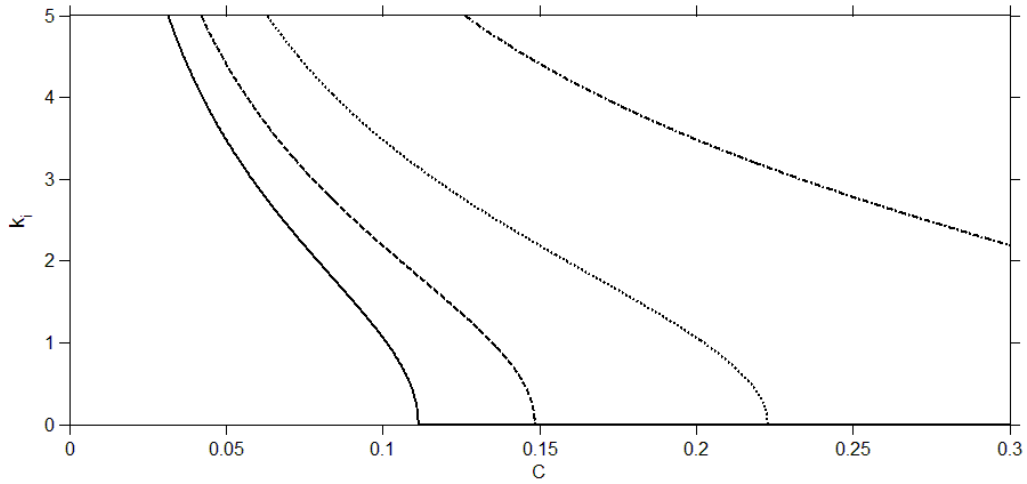

Figure 2-6: *Influence of relaxation and retardation times on (a) the Rayleigh number, Rai, and (b) wavenumber, ki, at the intersection between the steady and oscillatory marginal stability branches (Pr = 10).*

The minimum of Ra_i is the same regardless of the thermal conductivity ratio or the Prandtl number, but occurs at different C values, corresponding to $k_i = \frac{\pi}{\sqrt{2}}$, and given by $C = \frac{2(Pr+1)(1-\gamma)}{3\pi^2 Pr}$. These C values coincide with the intersection of the k_i curves and the $\frac{\pi}{\sqrt{2}}$ line in Figure 2-6b. Figure 2-6a shows a widening of the C range as γ increases. The intersection wavenumber in Figure 2-6b decreases monotonically with C

(or relaxation time), signaling a wider oscillatory range for NFs with higher NP concentration (refer to Figure 2-5a). The decrease is more rapid for small retardation, leading to oscillatory convection over the whole k range at some critical C value. Beyond a level of retardation (here, roughly, $\gamma > 0.6$), there is always a range of small wavenumber for stationary convection.

The marginal stability curves discussed so far only reflect the threshold for the loss of stability of the conduction state, but do not indicate how the stable and unstable states behave with time (monotonically or oscillatorily). This transient behaviour is dictated by the sign of the discriminant in the dispersion cubic relation (4.3). Thus, monotonic or oscillatory behaviour is predicted if the discriminant, $\Delta(\mathrm{Ra}, \mathrm{k}, \mathrm{Pr}, \mathrm{C}, \gamma)$, is positive or negative, respectively.

Figure 2-7 illustrates the stability picture for a non-Fourier fluid with C=0.05, for a SPL fluid ($\gamma = 0$) in Figure 2-7a, and DPL fluid ($\gamma = 0.3$) in Figure 2-7b. The marginal stability curve is shown is solid thick line. Recall that the marginal stability curve has two branches, a stationary or Fourier branch and an oscillatory branch lying to the left ($k < k_i$) and right ($k > k_i$) of the intersection point (Ra_i, k_i), respectively. The curve corresponding to zero discriminant lies below the Fourier branch and above the oscillatory branch since it must pass through the intersection point. In fact this curve is tangent to the Fourier branch at the intersection point. Thus, the dark region between the $\Delta = 0$ curve and the marginal stability curve for $k < k_i$ is a *stationary stable* region (any perturbation from the conduction state is damped monotonically). For k > ki, the cross-hatched region between the two curves is *oscillatory unstable* (any perturbation from the conduction grows oscillatorily). The region below the $\Delta = 0$ curve for k < ki is termed as *oscillatory stable* region (any perturbation from the conduction state decays oscillatorily). Recall that the region below the oscillatory branch of the marginal stability curve (k > ki) is also an oscillatory stable region. Figures 2-7a and 2-7b indicate that the stationary stable (dark) region is larger for a DPL fluid compared to a SPL fluid. This region grows with fluid retardation (as γ increases), eventually invading the whole region below the neutral curve

for a Fourier fluid. The Figures also indicate that the oscillatory unstable (cross-hatched) region diminishes with fluid retardation, and disappears in the Fourier limit.

(a)

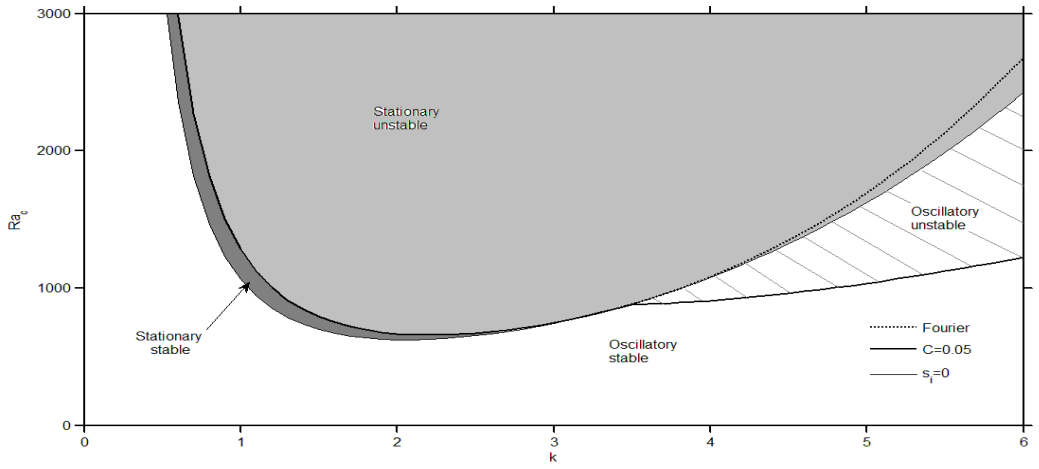

(b)

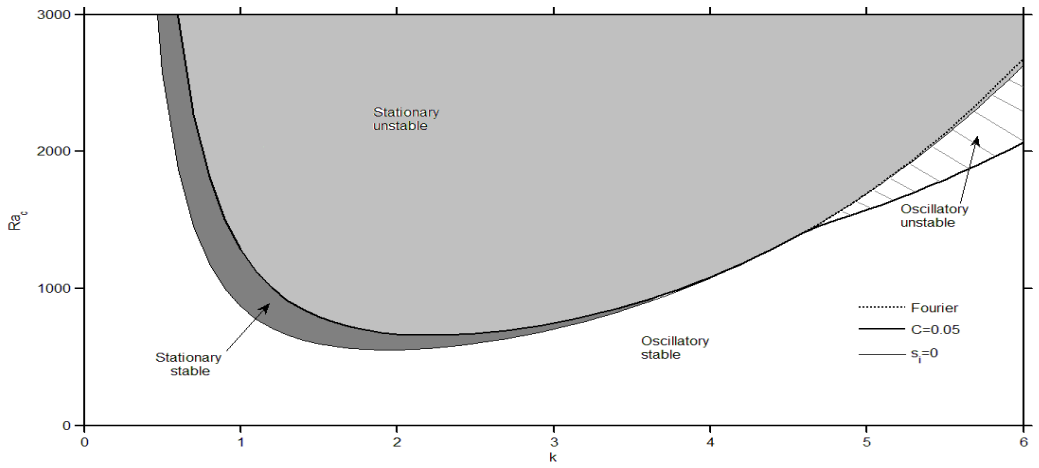

Figure 2-7: *Stationary and oscillatory regions in the marginal stability curve for (a) SPL fluid (C=0.05, γ = 0, Pr=10), (b) DPL fluid (C=0.05, γ = 0.3, Pr=10).*

Figure 2-8 shows the influence of Rayleigh number relaxation time on the temperature perturbation of the critical point for a single-phase-lagging fluid with and Pr = 10. The critical point corresponds to $k = \frac{\pi}{\sqrt{2}}$ and Ra=657 when $C < C_H$. For a Fourier fluid (C = 0), Figure 2-8a indicates a linear increase in the effective root with respect to the Rayleigh number. As the Cattaneo number increases, this quasi-linear increase does not persist. Recall that $s_0 = 0$ at the neutral point. Unlike the Fourier case, a break-point is

observed in the effective root curves for the non-Fourier ($C \neq 0$) fluids. At this point, a discontinuity is observed in the slope with respect to Ra. The break-point signals a mode change for the non-Fourier fluid and shows a transition from oscillatory mode (lower Rayleigh number) to the stationary mode (higher Rayleigh number). Thus, the transition does not occur in the case of a Fourier fluid, and the stability mode is always stationary. As the Cattaneo number exceeds C_H (0.0655 for =0), the critical wave number increases and the critical Rayleigh number decreases, which is confirmed from Figure 2-8. By increasing the Cattaneo number, the onset of convection occurs at a lower Rayleigh number (or temperature difference). At high Rayleigh numbers (> 900 in Figure 2-8a), there is a monotonic increase in the effective root with respect to C. There is no clear trend, however, for smaller Ra. When the mode of the non-Fourier fluid turn from oscillatory to monotonic at the break-point, the slope of the curves increases sharply, reflecting a strong tendency toward instability. The break-point occurs at higher Rayleigh number for a fluid with higher Cattaneo number. Figure 2-8b shows the marginal stability and oscillatory curves for a nanofluid with C=0.05 and $\gamma = 0.3$. The presence of retardation broadens the stationary stable zone when $k < k_i$. It means that at wave numbers smaller than k_i, perturbations are damped monotonically (refer to Figure 2-7).

(a)

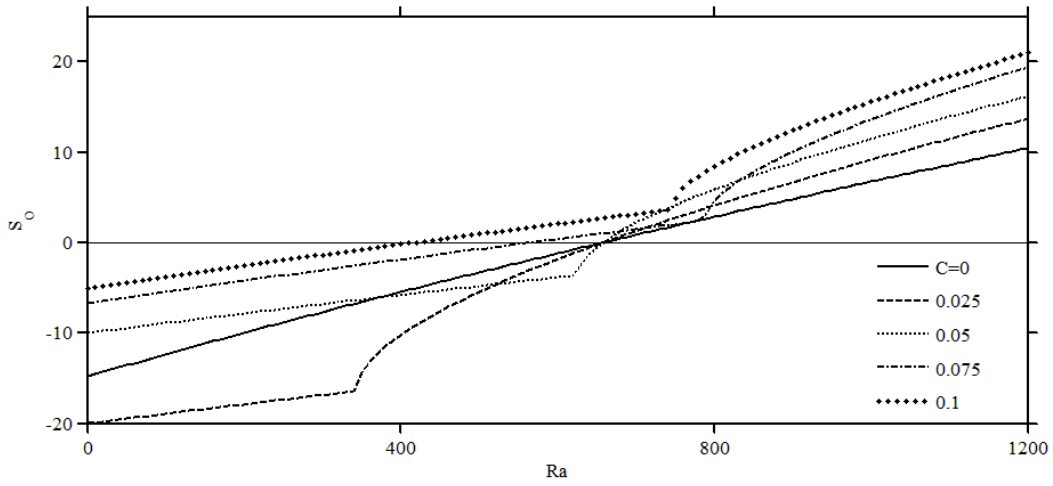

(b)

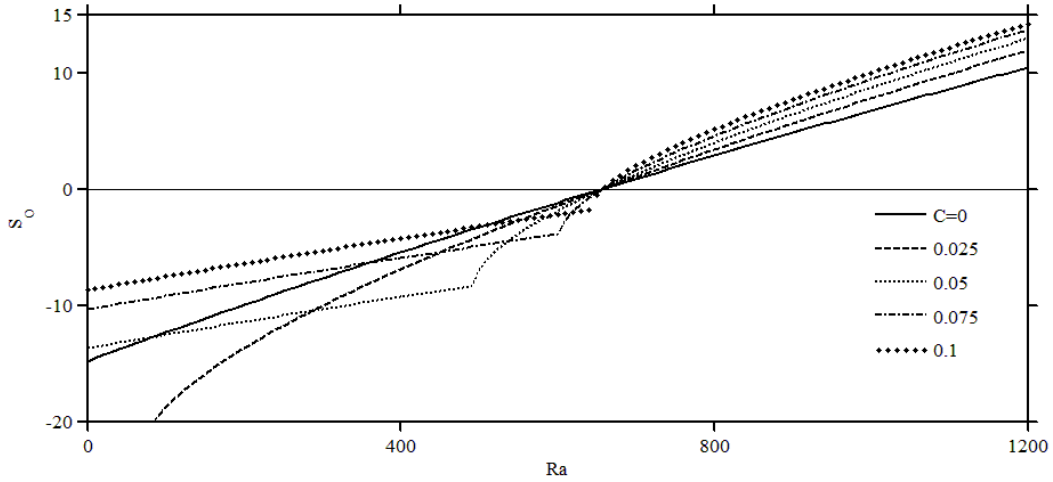

Figure 2-8: *Influence of relaxation time on the effective (or biggest) root of dispersion relation (a) $\gamma = 0$ and (b) $\gamma = 0.5$ ($Pr = 10$).*

2.5.3 Overstability threshold for dual-phase-lagging fluids

The emergence of oscillatory convection is an important phenomenon for non-Fourier fluids and NFs. In their experimental study, [1] observed that above a certain Rayleigh number, "the Nusselt number has a bistable behaviour: an upper permanent oscillatory convection branch and a lower conduction branch separated by a forbidden gap. The selection of the branch is attained by changing the initial concentration profile. Whenever the initial concentration of NP is homogeneous the system bifurcates into the

upper branch, while in the presence of a fully developed concentration profile the lower branch is selected." It is, therefore, expected that homogeneous NFs are more likely to exhibit oscillatory behaviour. These are specifically the type of NFs considered in this study, which obey the DPL non-Fourier constitutive equation (2.3.12). Although the bistable mode observed by [1] is clearly a nonlinear phenomenon, it can, to some extent, be captured in the current linear stability analysis by examining the post-critical convection near criticality, particularly when C approaches C_H, allowing the critical Rayleigh number to experience a second minimum, as apparent from Figures 2-4a and 2-5a (see next).

Consequently, the quantity of prime interest is C_H, the value of C at which the minimum Rayleigh number for oscillatory convection coincides with the minimum of the Fourier curve for stationary convection. At $C = C_H$, the minimum Rayleigh number, Ra_m, coincides with the Fourier value $Ra_{mF} = \frac{27\pi^4}{4}$. It is helpful to refer to the curve corresponding to $C = C_H = 0.0655$ in Figure 2-4a for a SPL fluid. A similar curve exists for a DPL fluid ($\gamma > 0$). This would be the curve corresponding to $C = C_H = 0.1415$ for $\gamma = 0.5$. At around $C = C_H$, the neutral curve possesses two minima in Ra_c, which suggests the existence of the bistable mode observed by [1]. Thus, depending on the initial NP concentration or even possibly the imposed cell size, as the curve in Figure 2-4a suggests, conduction can be lost to stationary or oscillatory convection.

For $C > C_H$, linear stability predicts that oscillatory, and not stationary, convection is bound to be observed in reality, with a Hopf bifurcation expected to emerge at Ra_m. Figure 2-9 displays the dependence of the critical Cattaneo number C_H (Figure 2-9a), corresponding wavenumber k_H (Figure 2-9b) and oscillation frequency ω_H (Figure 2-9c) on the Prandtl number for different levels of the thermal conductivity ratio. Both the low and high ranges of Pr values are examined to cover a wide range of non-Fourier fluids and NFs. In this regard, low-temperature liquids ($Pr < 1$) display a strong non-

Fourier character (see [46] and references therein). For most NFs of practical interest, Pr >> 1. In this case, Figure 2-9 suggests that the conditions for onset of oscillatory convection are independent of the Prandtl number. Consequently, it is helpful to examine the critical conditions for large Pr. In this case, recalling the critical Rayleigh number from (4.8) and setting to Ra_{mF}:

$$\lim_{Pr\to\infty} Ra_c = \left(\frac{1+\gamma\beta_H C_H}{C_H}\right)\frac{\beta_H^2}{k_H^2} = Ra_{mF} = \frac{27\pi^4}{4} \tag{2.5.5}$$

Seeking the minimum gives $C_H = \dfrac{2\pi^2 - \beta_H}{\gamma\left(2\beta_H - 3\pi^2\right)\beta_H}$, which, upon substitution into(5.5), leads to the following cubic equation for the wavenumber:

$$\gamma\beta_H^3 + Ra_{mF}\left(\beta_H - 2\pi^2\right) = 0 \tag{2.5.6}$$

Interestingly, the presence of retardation leads to a cubic equation in β, as opposed to the linear equation for γ = 0. However, there seems to be only one positive real root for any γ.

Figure 2-9a indicates that NFs with higher thermometric conductivity (smaller Pr) are less likely to exhibit oscillatory convection, which sets in only at a relatively high NP concentration, and is difficult to detect in practice given the low oscillation frequency (especially for γ > 0 as Figure 2-9c suggests). However, for typical NF solutions (Pr >> 1), the influence of fluid conductivity is less significant as indicated by the flattening of the curves at larger value of Pr, especially for strong retardation. Thus, it is the thermal conductivity ratio of the NF that determines the likelihood for steady or oscillatory convective motion. It is observed that k_H is always larger than, but decreases

asymptotically to, the Fourier limit, $k_{mF} = \frac{\pi}{\sqrt{2}}$, as $\gamma \to 1$ for any Pr (as illustrated here by the curve $\gamma = 0.75$ in Figure 2-9b). The critical C decreases monotonically with Pr for any level of the thermal conductivity ratio, at a steeper rate in the small Pr range (Figure 2-9a). Thus, a more viscous NF tends to exhibit oscillatory convection more easily. Consequently, the choice of the base fluid (viscosity) is crucial if oscillatory convection is desired. However, there is a limit to the influence of the Prandtl number. Indeed, C_H remains essentially unchanged for $Pr > 3$, for any γ. In this case, only the NP concentration becomes the controlling parameter as it influences both the thermal conductivity ratio and the relaxation time (for a given layer gap).

In contrast to the threshold in Cattaneo number (Figure 2-9a), both the wavenumber (Figure 2-9b) and frequency (Figure 2-9c) exhibit an inconsistent response against both the Prandtl number and thermal conductivity ratio. For a NF with small conductivity ratio, both the wavenumber and frequency generally decrease monotonically with Prandtl number, except that the frequency exhibits a weak maximum at small Pr. It appears that this maximum weakens further as γ increases from zero for a fluid with retardation, and eventually disappears to give way to a monotonic increase in frequency with Pr (see Figure 2-9c). A similar trend is predicted for the wavenumber, which also exhibits a maximum that weakens with retardation. Figure 2-9c also reflects the difficulty to observe oscillatory convection as $\gamma \to 1$ (see the ω_H curve for $\gamma = 0.75$).

(a)

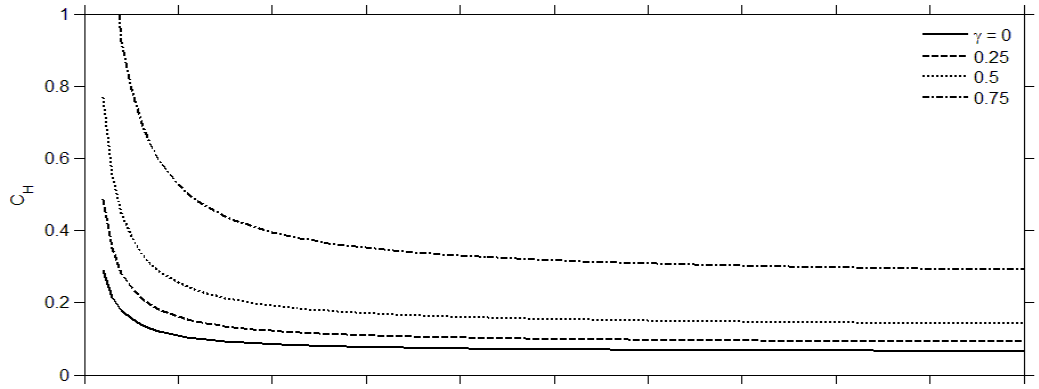

(b)

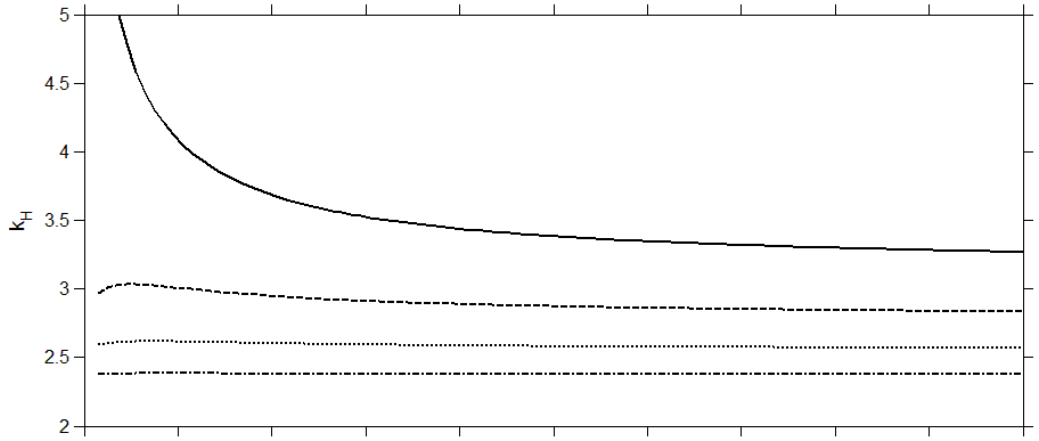

(c)

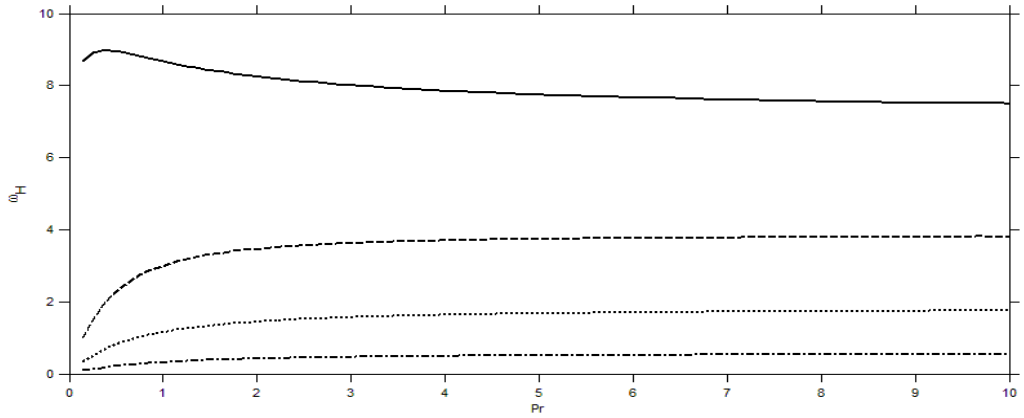

Figure 2-9: *Influence of the Prandtl number on (a) the critical Cattaneo number, CH, (b) the corresponding wavenumber, kH, and (c) the oscillation frequency, ωH, for a dual-phase-lagging fluid with* $\gamma \in [0, 1)$.

2.5.4 Overstability for strongly non-Fourier fluids $(C > C_H)$

The onset of overstability coincides with the emergence of a pair of imaginary eigenvalues in the characteristic equation (2.4.3). Oscillatory convection (overstability) always emerges for strongly non-Fourier DPL fluids (C > C_H) at a critical Rayleigh number $Ra_m < Ra_{mF}$ (see curve C = 0.3 in Figure 2-5a). The conductive state remains unconditionally stable for $Ra < Ra_m$, and becomes overstable for $Ra > Ra_m$. The influence of the thermal conductivity ratio on the onset of overstability is shown in Figure 2-10 for Pr = 10, where the critical Rayleigh number, Ra_m, the corresponding wavenumber, k_m, and frequency, ω_m, for the onset of overstability are plotted against C for $\in [0, 1)$. Both Ra_m (Figure 2-10a) and k_m (Figure 2-10b) generally decrease with C. The jump in wavenumber coincides with the sudden shift from $k_{mF} = \frac{\pi}{\sqrt{2}}$ to $k_m > k_{mF}$ when C exceeds C_H. The corresponding frequency, ω_m (Figure 2-10c) generally displays a maximum that occurs at larger C as increases. The overall frequency decreases with thermal conductivity ratio. The frequency increases sharply (from zero) at C = C_H, reaching the maximum and drops at a rate that decreases with thermal conductivity ratio. Indeed, the maximum weakens significantly with increasing (see the = 0.75 curve in Figure 2-10c), but eventually vanishes. The large C behaviour inferred from (4.8) clearly suggests that this is always the case. The minimum Rayleigh number and corresponding frequency reduce to

$$\lim_{C\to\infty} Ra_m = \gamma Ra_{mF}, \quad \lim_{C\to\infty} \omega_m = \sqrt{\frac{Pr\,\beta_m(1-\gamma)}{C(\gamma+Pr)}} \tag{2.5.7}$$

Interestingly, Figures 2-10a and 2-10c reflect a smooth dependence of the minimum critical Rayleigh number and corresponding frequency on the thermal conductivity ratio or retardation time. Figure 2-10b depicts a discontinuity for the wavenumber, which is

(a)

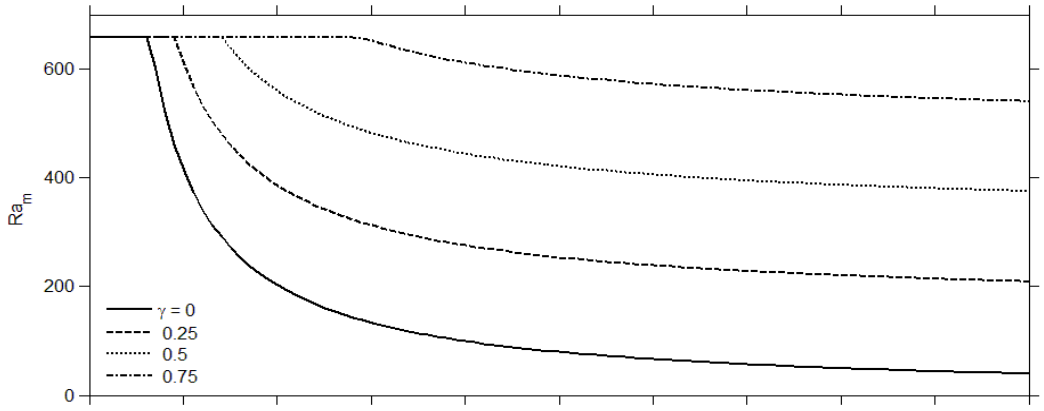

(b)

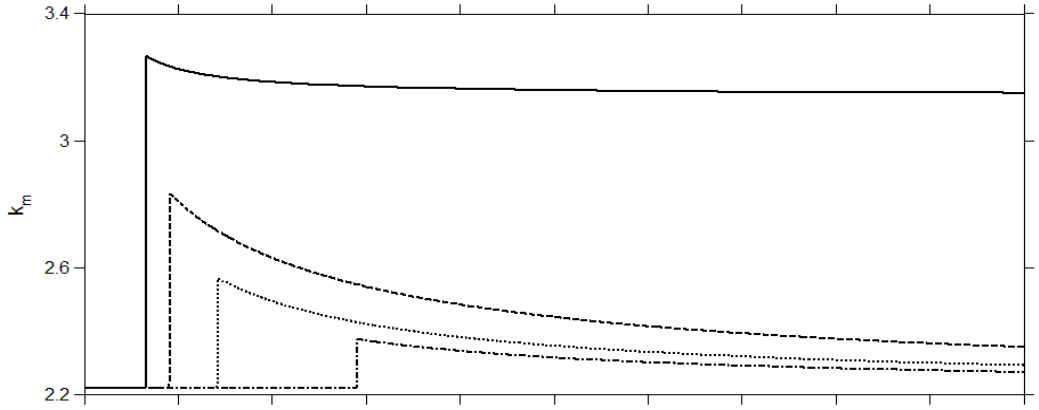

(c)

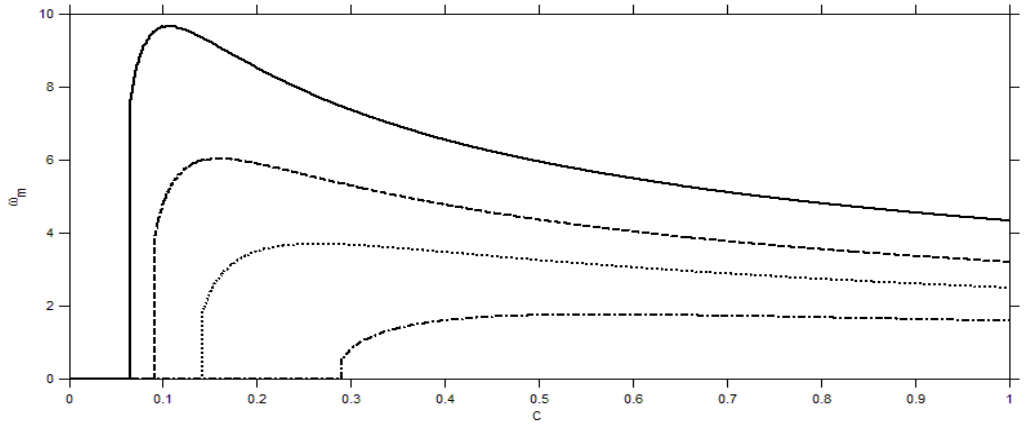

Figure 2-10: *Influence of retardation and relaxation on (a) the critical Rayleigh number, RaH, (b) the corresponding wavenumber, kH, and (c) the oscillation frequency, ωH, for a dual-phase-lagging fluid with* $\gamma \in [0, 1)$ *and Pr = 10.*

easily established for large C. Indeed, (2.5.7) shows that $\lim_{C\to\infty} k_m = k_{mF} = \frac{\pi}{\sqrt{2}}$ for $\gamma > 0$. Recalling the expression for the wavenumber in section 2.5.1, then $\lim_{C\to\infty} k_m = \pi$ for $\gamma = 0$.

An important question regarding oscillatory behaviour is the prediction that various models provide, and the connection with experiment. As mentioned earlier, oscillatory behaviour predicted by the two-phase model is heavily dependent on the type and value of boundary conditions used for the concentration. By accounted for Brownian motion and thermophoretic effects, and generalizing Tzou's work [26], Nield & Kuznetsov's linear stability analysis[23] predicts the existence of oscillatory convection for a relatively narrow range of Rayleigh numbers, starting with twice the value of the minimum critical Rayleigh of the base fluid ($Ra_m > 2Ra_{mF}$). For any oscillatory convection to exist, the concentration at the top boundary must be maintained lower than that at the lower boundary. Understandably, this causes a density gradient to oppose that caused by the temperature differential, leading to oscillatory convection. However, aside from the difficulty in realistically maintaining fixed NP concentrations at the boundaries, the theoretical predictions based on the two-phase model do not agree with experiment. [1] observed that oscillatory behaviour sets in whenever the initial concentration of NP is homogeneous, while in the presence of a fully developed concentration profile, only stationary convection is observed. The current DPL analysis does, indeed, suggest the possibility of oscillatory behaviour for homogeneous NP distribution. In particular, the onset of overstability appears to be enhanced for a more non-Fourier fluid, and is more difficult to achieve for a fluid with significant retardation time or that is highly (heat) conductive. It is important to note that oscillatory convection is not predicted by the two-phase formulation, often adopted in the literature, when the concentrations are taken equal at the two boundaries [23].

Comparison of the theoretical and measured critical oscillation frequencies led to no agreement. This discrepancy was earlier noted by [47] who attributed it to the inadequacy of existing constitutive models, which do not account for the transport of DNA molecules by the flow and their accumulation in stagnation points. These issues are

also bound to plague existing models for the heat transfer in NFs, given the tendency, *albeit* small, of NPs to accumulate. However, on the one hand, in such cases, the cause of the onset of oscillatory convection is still the elasticity of the polymeric solution, or the non-Fourier effect of a NF. On the other hand, for both solution types, the time scale of the oscillation may also be dictated by solute diffusion [1], [47].

The temperature perturbation of a non-Fourier fluid is an important characteristic which represents the thermal behaviour of the fluid close to criticality. Some nonlinear methods, such as amplitude equations, use the temperature perturbation at the critical point (and other eigenfunctions) to obtain the convection state of the fluid. Figure 2-11 shows the influence of the Cattaneo and Rayleigh numbers on the temperature perturbation, Θ_c, at the critical wave number for a single-phase-lagging fluid relative to a Fourier fluid with Pr = 10 and γ=0. At the boundaries, since the temperature is fixed, the corresponding temperature perturbation is zero. So the temperature perturbation is evaluated at a point between the two boundaries (in this case, z=1/2) at the critical wave number $k_c = \frac{\pi}{\sqrt{2}}$ relative to the temperature perturbation, Θ_{cF}, of a Fourier fluid (C=0), which is considered as reference value. Recall that here n=1 and $\Theta_{cF} = \frac{1}{s_o + \beta_n}$ is dependent on Ra since s_o depends on Ra as given by equation (2.4.11). Recall that s_o increases with Ra as illustrated in Figure 2-8 and sharply decreases with wave number. The relative temperature perturbation increases form 1 (when C=0) with Cattaneo number (or relaxation time). As Figure 2-11 shows, the Cattaneo number affects significantly the temperature perturbation. Note that Θ_{cF} and Θ_c both decrease with Ra but the ratio of $\frac{\Theta_c}{\Theta_{cF}}$ increases. The Figure shows that the effect of Cattaneo number is not linear and higher Cattaneo numbers causes more rapid increase. Finally, Figure 2-11 suggests a higher heat transfer due for higher relaxation time in the SPL fluids. Figure 2-12 displays the influence of retardation time on the temperature perturbation at the critical wave number for a dual-phase-lagging fluid with constant Cattaneo number (C=0.06). As expected, the presence of retardation time (or $\gamma > 0$) leads to a decrease in

the non-Fourier character of DPL fluids. The Figure includes five curves for different γ values from 0 to 1. Interestingly, γ diminishes the effect of the Cattaneo number on the temperature perturbation, and finally at γ=1, curve collapses back to the Fourier level $\left(\frac{\Theta}{\Theta_{cF}}=1\right)$.

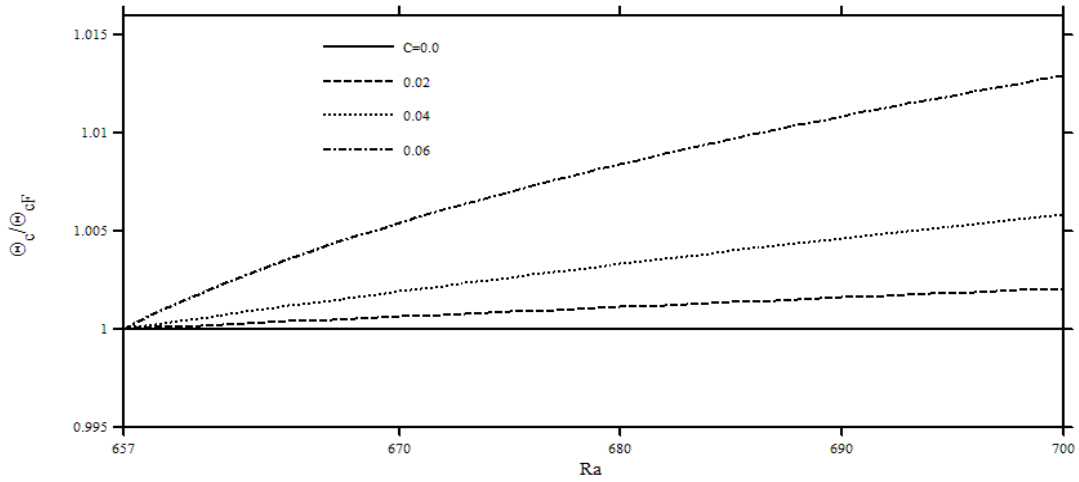

Figure 2-11: *Influence of relaxation time on the temperature perturbation of the critical point for a single-phase-lagging fluid with Pr = 10 and γ=0. Here* Θ_{cF} *is the temperature perturbation at z=1/2, when C=0,* $k=\frac{\pi}{\sqrt{2}}$. ($\Theta_{cF}=\frac{1}{s+\beta}$)

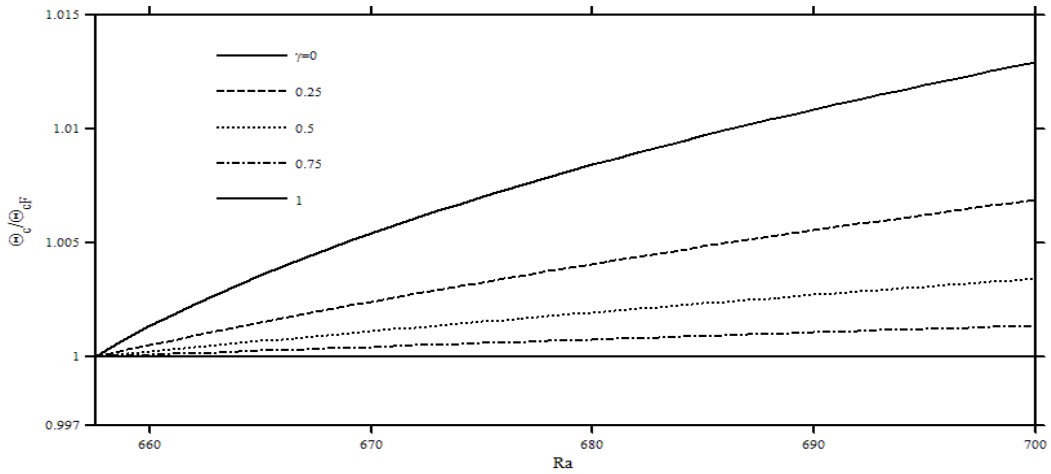

Figure 2-12: *Influence of retardation time on the temperature perturbation of the critical point for a dual-phase-lagging fluid with and Pr = 10. Here C=0.06 and* Θ_{cF} *is the temperature perturbation when, Z=1/2, C=0,* $k = \frac{\pi}{\sqrt{2}}$. ($\Theta_{cF} = \frac{1}{s+\beta}$)

2.6 Conclusions

This study examines the natural convection of non-Fourier fluids of the dual-phase-lagging (DPL) type. These fluids possess a relaxation time and a retardation time, reflecting the delay in the response of the heat flux and the temperature gradient with respect to one another. The limit of a single-phase-lagging (SPL) fluid is recovered upon setting the retardation time to zero. The SPL model is particularly relevant to low-temperature liquids or to fast heat transfer processes. The relevance of the DPL model to nanofluids (NFs) has recently been recognized in the literature, and is emphasized here. The equivalence between the two-phase and DPL models allows the expression of the relaxation time in terms of the nanoparticle (NP) concentration [29]. The retardation-to-relaxation time ratio is then found to be equal to the NF solution-to-solvent thermal conductivity ratio, γ (see section 2.2). The parallels between NFs and polymeric solutions of the Boger type, obeying the Oldroyd-B constitutive equation for stress are established throughout the paper. Similar to viscoelastic fluids, the constitutive equation for heat flux used in the present analysis is frame invariant.

Linear stability analysis indicates that, in contrast to ordinary fluids, a DPL fluid can lose its conductive mode to stationary or oscillatory convection. For small relaxation

time (small Cattaneo number, C), the neutral stability curve comprises a Fourier branch ($k < k_i$) and an oscillatory branch ($k > k_i$). As C increases and reaches a critical value, $C_H(\gamma)$, both stationary and oscillatory convection become equally probable, confirming the existence of the bistable mode observed in experiment [1]. For $C > C_H$, only oscillatory convection is predicted, at a Rayleigh number decreasing with C (see Figures 2-4a and 2-5a). Thus, oscillatory convection increasingly becomes the mode of preference, compared to both conduction and stationary convection. In fact, it is found that, for strongly non-Fourier fluids, oscillatory convection becomes spontaneously observed with no prior conduction. The oscillatory roll size grows with both relaxation and retardation. There is a discontinuity in roll size with respect to retardation, which is clearly reflected in the limit of large C (see Figure 2-10b). Although the oscillation frequency decreases monotonically with roll size (Figures 2-3b and 2-5b), it exhibits a non-monotonic response with respect to relaxation time (emergence of a maximum with respect to C). As expected, retardation tends to attenuate oscillation (see Figures 2-4c and 2-10c).

2.7 References

[1] G. Donzelli, R. Cerbino, and A. Vailati, “Bistable Heat Transfer in a Nanofluid,” *Phys. Rev. Lett.*, vol. 102, no. 10, p. 104503, Mar. 2009.

[2] D. Joseph and L. Preziosi, “Heat waves,” *Rev. Mod. Phys.*, vol. 61, no. 1, pp. 41–73, Jan. 1989.

[3] C. Cattaneo, “A form of heat conduction equation which eliminates the paradox of instantaneous propagation,” *Comptes Rendus*, no. 247, pp. 431–433, 1958.

[4] P. Vernotte, “Some possible complication in the phenomena of thermal conduction,” *Compte Rendus*, no. 252, pp. 2190–2191, 1961.

[5] J. Ordóñez-Miranda and J. J. Alvarado-Gil, “Thermal wave oscillations and thermal relaxation time determination in a hyperbolic heat transport model,” *Int. J. Therm. Sci.*, vol. 48, no. 11, pp. 2053–2062, Nov. 2009.

[6] S. Galović and D. Kostoski, “Photothermal wave propagation in media with thermal memory,” *J. Appl. Phys.*, vol. 93, no. 5, p. 3063, Mar. 2003.

[7] A. Saha, S. Basu, and R. Kumar, “Effects of acoustic-streaming-induced flow in evaporating nanofluid droplets,” *J. Fluid Mech.*, vol. 692, pp. 207–219, Feb. 2012.

[8] A. Vedavarz, S. Kumar, and M. K. Moallemi, “Significance of Non-Fourier Heat Waves in Conduction,” *J. Heat Transfer*, vol. 116, no. 1, p. 221, Feb. 1994.

[9] M. N. O□zis□ik and D. Y. Tzou, “On the Wave Theory in Heat Conduction,” *J. Heat Transfer*, vol. 116, no. 3, p. 526, Aug. 1994.

[10] D. Y. Tzou, *Macro- To Micro-Scale Heat Transfer: The Lagging Behavior*, vol. 1996. CRC Press, 1996, p. 304.

[11] R. R. Letfullin, T. F. George, G. C. Duree, and B. M. Bollinger, “Ultrashort Laser Pulse Heating of Nanoparticles: Comparison of Theoretical Approaches,” *Adv. Opt. Technol.*, vol. 2008, pp. 1–8, 2008.

[12] M. N. and G. L. Daubyy, P.C., “Generalized Fourier equations and thermoconvective instabilities,” *Rev. Mex. F´ISICA*, vol. 48, pp. 57–62, 2002.

[13] G. Lebon and A. Cloot, “Benard-Marangoni instability in a Maxwell-Cattaneo fluid,” *Phys. Lett. A*, vol. 105, no. 7, pp. 361–364, Oct. 1984.

[14] B. Straughan, “Thermal convection with the Cattaneo–Christov model,” *Int. J. Heat Mass Transf.*, vol. 53, no. 1–3, pp. 95–98, Jan. 2010.

[15] D. F. Stranges, R. E. Khayat, and B. Albaalbaki, “Thermal convection of non-Fourier fluids. Linear stability,” *Int. J. Therm. Sci.*, vol. 74, pp. 14–23, Dec. 2013.

[16] M. Niknami and R. E.khayat, “Energy growth of disturbances in a non-Fourier fluid,” *Int. J. Heat Mass Transf.*, vol. 67, pp. 613–626, Dec. 2013.

[17] P. J. Antaki, “Analysis of hyperbolic heat conduction in a semi-infinite slab with surface convection,” *Int. J. Heat Mass Transf.*, vol. 40, no. 13, pp. 3247–3250, Sep. 1997.

[18] P. Vadasz, “Heat Conduction in Nanofluid Suspensions,” *J. Heat Transfer*, vol. 128, no. 5, p. 465, May 2006.

[19] D. Y. Tzou and Y. Zhang, “An analytical study on the fast-transient process in small scales,” *Int. J. Eng. Sci.*, vol. 33, no. 10, pp. 1449–1463, Aug. 1995.

[20] J. Buongiorno, “Convective Transport in Nanofluids,” *J. Heat Transfer*, vol. 128, no. 3, p. 240, Mar. 2006.

[21] S. Samouhos and G. McKinley, “Carbon Nanotube–Magnetite Composites, With Applications to Developing Unique Magnetorheological Fluids,” *J. Fluids Eng.*, vol. 129, no. 4, p. 429, Apr. 2007.

[22] J. A. Eastman, S. R. Phillpot, S. U. S. Choi, and P. Keblinski, “Thermal transport in nanofluids 1,” *Annu. Rev. Mater. Res.*, vol. 34, no. 1, pp. 219–246, Aug. 2004.

[23] D. A. Nield and A. V. Kuznetsov, “The onset of convection in a horizontal nanofluid layer of finite depth,” *Eur. J. Mech. - B/Fluids*, vol. 29, no. 3, pp. 217–223, May 2010.

[24] B. C. Pak and Y. I. Cho, “Hydrodynamic and heat transfer study of dispersed fluids with submicron metallic oxide particles,” *Exp. Heat Transf.*, vol. 11, no. 2, pp. 151–170, Apr. 1998.

[25] B. Kolade, K. E. Goodson, and J. K. Eaton, “Convective Performance of Nanofluids in a Laminar Thermally Developing Tube Flow,” *J. Heat Transfer*, vol. 131, no. 5, p. 052402, May 2009.

[26] D. Y. Tzou, “Instability of Nanofluids in Natural Convection,” *J. Heat Transfer*, vol. 130, no. 7, p. 072401, Jul. 2008.

[27] J. Kim, Y. T. Kang, and C. K. Choi, “Analysis of convective instability and heat transfer characteristics of nanofluids,” *Phys. Fluids*, vol. 16, no. 7, p. 2395, May 2004.

[28] R. C. A. Robert Byron Bird, “Dynamics of Polymeric Liquids : Fluid Mechanics / R.B. Bird, R.C. Armstrong, O. Hassager.,” *John Wiley Sons, New York*, vol. 1, 2nd Ed., 1987.

[29] L. Wang and X. Wei, “Equivalence between dual-phase-lagging and two-phase-system heat conduction processes,” *Int. J. Heat Mass Transf.*, vol. 51, no. 7–8, pp. 1751–1756, Apr. 2008.

[30] J. J. Vadasz and S. Govender, “Thermal wave effects on heat transfer enhancement in nanofluids suspensions,” *Int. J. Therm. Sci.*, vol. 49, no. 2, pp. 235–242, Feb. 2010.

[31] J. N. N. Quaresma, E. N. Macêdo, H. M. da Fonseca, H. R. B. Orlande, and R. M. Cotta, “An Analysis of Heat Conduction Models for Nanofluids,” *Heat Transf. Eng.*, vol. 31, no. 14, pp. 1125–1136, Dec. 2010.

[32] R. J. Donnelly, “The two-fluid theory and second sound in liquid helium,” *Phys. Today*, vol. 62, no. 10, p. 34, Oct. 2009.

[33] C. I. Christov, “On frame indifferent formulation of the Maxwell–Cattaneo model of finite-speed heat conduction,” *Mech. Res. Commun.*, vol. 36, no. 4, pp. 481–486, Jun. 2009.

[34] Roger E. Khayat & Ostoja Starzewski, “On the objective rate of heat and stress fluxes. Connection with micro/nano-scale heat convection,” *Discr. Contin. Dyn.*, 2011. .

[35] D. Y. Tzou and K. S. Chiu, “Temperature-dependent thermal lagging in ultrafast laser heating,” *Int. J. Heat Mass Transf.*, vol. 44, no. 9, pp. 1725–1734, May 2001.

[36] R. Quintanilla and R. Racke, “A note on stability in dual-phase-lag heat conduction,” *Int. J. Heat Mass Transf.*, vol. 49, no. 7–8, pp. 1209–1213, Apr. 2006.

[37] P. Vadasz, “Heat transfer augmentation in nanofluids via nanofins.,” *Nanoscale Res. Lett.*, vol. 6, no. 1, p. 154, Jan. 2011.

[38] M. Quintard and S. Whitaker, *Advances in Heat Transfer Volume 23*, vol. 23, no. C. Elsevier, 1993, pp. 369–464.

[39] D. Joseph and L. Preziosi, “Heat waves,” *Rev. Mod. Phys.*, vol. 61, no. 1, pp. 41–73, Jan. 1989.

[40] H. M. Park and H. S. Lee, “Hopf bifurcations of viscoelastic fluids heated from below,” *J. Nonnewton. Fluid Mech.*, vol. 66, no. 1, pp. 1–34, Sep. 1996.

[41] L. A. Girifalco, *Statistical Mechanics of Solids*. Oxford University Press, 2000, p. 544.

[42] S. M. Fotukian and M. Nasr Esfahany, “Experimental study of turbulent convective heat transfer and pressure drop of dilute CuO/water nanofluid inside a

circular tube," *Int. Commun. Heat Mass Transf.*, vol. 37, no. 2, pp. 214–219, Feb. 2010.

[43] A. V. Getling, "Rayleigh-Bénard convection□: structures and dynamics," *World Scientific, Singapore.*, 1998. [Online]. Available: http://search.library.wisc.edu/catalog/ocm38130717. [Accessed: 14-May-2014].

[44] R. E. Khayat, "Finite-amplitude Taylor-vortex flow of viscoelastic fluids," *J. Fluid Mech.*, vol. 400, pp. 33–58, Dec. 1999.

[45] Z. LI and R. E. KHAYAT, "Finite-amplitude Rayleigh–Bénard convection and pattern selection for viscoelastic fluids," *J. Fluid Mech.*, vol. 529, pp. 221–251, Apr. 2005.

[46] R. Khayat and B. Eu, "Generalized hydrodynamics and Reynolds-number dependence of steady-flow properties in the cylindrical Couette flow of Lennard-Jones fluids," *Phys. Rev. A*, vol. 40, no. 2, pp. 946–958, Jul. 1989.

[47] P. Kolodner, "Oscillatory convection in viscoelastic DNA suspensions," *J. Nonnewton. Fluid Mech.*, vol. 75, no. 2–3, pp. 167–192, Mar. 1998.

Chapter 3

3 Thermal convection of non-Fourier fluids with spectral-perturbation approach

3.1 Introduction

In general, when a thermal disturbance applies to an object, the perturbation felt immediately at all points of the object and the temperature diffusion is described by Fourier's law which gives a parabolic equation. By Fourier's law, the flow rate of heat energy through a surface is proportional to the negative temperature gradient across the surface. Unlimited speed of heat propagation is assumed in Fourier's law as a result Fourier's law is not accurate enough and sometimes another equation is needed to study heat transfer [1]. Cattaneo [2] and Vernotte [3] proposed Cattaneo-Vernotte (C-V) equation including a transient term multiplied by the thermal relaxation time of the subject. [4]

$$\tau \frac{\partial \mathrm{q}}{\partial t} + \mathrm{q} = -k \nabla T \tag{3.1.1}$$

where q is heat flux, k is the thermal conductivity,τ is relaxation time and T is temperature. Thermal relaxation time is related with the average communication time among the collisions of electrons and phonons [5], and theoretically has been estimated for metals, semiconductors and superconductors to be in the order of microseconds (10^{-6} s) to picoseconds (10^{-12} s)[6]–[8]. In most of materials, thermal relaxation time is negligible and Cattaneo equation returns back to the Fourier model. In the other hand, there are some states which the relaxation time is significant and should be considered like non-homogeneous medium [9]–[11], high speed electronic devices [11], ultrashort laser pulses [11], [12] processed meat [13], skin burns[14], heat transfer in stars[15], heat transport in a nuclear fuel rod in a light water reactor [16], drying sand [17] and microscale" applications[10]. It is important to realize that not only relaxation times but also the rate of heating could make the transient term considerable. For example laser pulse heating makes a significant amount of energy over a small time. There are some

applications which the duration of the laser pulse can be measured on the scale of femto- or 10^{-15} seconds [18].

Non-Fourier heat conduction is described with different models. In the Single-Phase-Lag model (SPL), materials have only a relaxation time which exposing the delay in the response of the heat flux [19]. But Dual-Phase-Lag (DPL) model offers existing of a relaxation time and a retardation time in materials exposing the delay in the response of the heat flux and the temperature gradient with respect to one another. Xu et al. [20] used the Dual-Phase-Lag model to analyze the non-Fourier heat transfer process in skin tissue.

Vadasz [21] proved that the problem formulated by the energy equation with Fourier law of conduction in the solid and liquid phases, set up for a particular case of transient hot wire experiments, subject to suitable initial and boundary conditions represents a specific case of Dual-Phase-Lagging heat conduction as

$$\mathrm{q}\left(\mathrm{r}, t+\tau_q\right) = -k\,\nabla T\left(\mathrm{r}, t+\tau_T\right) \tag{3.1.2}$$

where τ_q is relaxation time of heat flux and τ_T is the relaxation time of temperature gradient. According to this relation, the temperature gradient at a point r of the material at time $t+\tau_T$ corresponds to the heat flux density vector at r at time $t+\tau_q$. The delay time τ_T is interpreted as being caused by the micro-structural interactions (smallscale heat transport mechanisms occurring in the micro-scale, or small-scale effects of heat transport in space) such as phonon-electron interaction or phonon scattering, and is called the phase-lag of the temperature gradient. Peshkov [22] was the first one who found the second sound wave in superfluid helium (He II) at low temperatures (T < 2.2 K) experimentally. Non-Fourier effects have been studied in various geometries such as spherical [23], cylindrical [24], slabs [25], crack tip [26] and fins geometry [27], Using numerical [9], [28]–[38] and analytical [39], [40] methods.

Antaki [10] proposed that non-homogeneous structures apparently induce waves by delaying the response between heat flux and temperature gradient. Vadasz [21] suggested that Fourier's law is not valid at the macro-system level when nano-elements are

suspended in the fluid. As a non-homogeneous material with nano-elements, nanofluids have been studied widely as a non-Fourier substance.

Nanofluids are a base fluid, such as water or ethylene glycol, consisting of solid nanoparticles, with sizes normally in the order of 1–100 nm. The NPs could be the oxides of aluminum and silicon, as well as metals such as Titanium, copper and gold [41]–[43]. In recent years nanofluids are very popular topic because of significant enhancement in their thermal properties. In presence of a small percents of nanoparticles, a major increase of the effective thermal conductivity of nanofluids has been stated. For example, a small amount of nanoparticles dispersed in water, ethylene glycol or oil can increase their inherently poor thermal conductivity by 40% [41], [44]–[46].

Different approaches have been used in order to study heat transfer in nanofluids. Buongiorno [44] obtained that thermophoresis and Brownian motion seem to be the only significant factors that could suitably describe the surprising heat transfer capabilities of nanofluids. It should be noted that the Brownian motion is the induced random drifting caused by the collisions of NPs with the molecules in the base fluid, whereas thermophoresis is a diffusive effect that causes particles to move as a result of a temperature gradient within the fluid. Xuan [47] developed the dispersion model of nanofluids and supposed two increases the heat transfer in nanofluids, the enhanced thermal conductivity of nanofluids, and the irregular movement of nanoparticles.

Natural convection has broad applications in different fields such as thermal insulations for earth's mantle [48], solar collectors [49], [50], cooling systems for nuclear reactors [51], atmosphere [52], ocean's circulation [53], [54], heat exchangers [55], double pane windows, micro-electromechanical systems (MEMS) and electronics cooling.

The natural convection of a fluid confined between to horizontal plates and heated from below, under the action of gravity, is called Rayleigh-Bénard convection (RBC). Because of thermal expansion the fluid close to lower plate is lighter than the upper fluid close to the upper plate. A lot of investigations have been done about RBC in before, experimentally [56]–[62] and theoretically[63]–[70]. Due to RBC Cellular flow patterns occurs and these patterns have been seen in many industrial processes, such as in micro-

processing [71], [72], in polymer processing [73]–[75]. In the RBC, fluid is motionless before criticality and the only parameter which could change the flow type, is fluid properties so the best way to study the fluid properties is using RBC [76]. In the other hand, experiment studies of RBC are convenient so the onset of convection, pattern formation and turbulence could be studied by using RBC [77]. The linear stability analysis of Rayleigh-Bénard convection for free-free, rigid-rigid or rigid-free boundary conditions is available in many textbooks [78], [79]. Note that presuming slip condition at both (free-free) boundaries considerably shortens the solution process. Additionally, in RBC problem, the free-free and rigid-rigid conditions have the same flow and heat transfer attributes qualitatively [80].

Conduction of a non-Fourier fluid is lost to convection once a critical value of the Rayleigh number, Rac is exceeded and finally leads to a variety of pattern formations in which the fluid goes up in some areas and goes down in others with a finite [81]. When Rayleigh number is close to Rac, convective flow carries part of heat applied then diminishing the temperature gradient and subsequently the buoyancy force, accordingly the gain of this pattern is restricted. Finally at a point temperature gradient and the reduction due to convective motion are equal and stability achieved. In this situation, any convective pattern like rolls, squares or hexagons have been seen but the most probable pattern is convective rolls [80].

In the linear stability analysis nonlinear terms are omitted and it can only determine the critical threshold for loss of steady conduction or steady convection but to get the convective flow behavior, the interaction among all linear and nonlinear terms should be considered and more nonlinear analysis is needed. Many nonlinear approaches have been used to foresee the convective flow patterns in the slightly supercritical convection and they expand the solution to the nonlinear governing equations on the basis of solution to the linearized problem. Perturbation approach near criticality [69], [82], the method of amplitude equations [83]–[85], and the extended Lorenz model [68] are some of these nonlinear approaches.

Lorenz [63] proposed a low-order dynamical system approach named the Lorenz model. Following the Lorenz model some low-dimensional dynamical systems have been progressed, including intense truncation [65]–[67], [86].Also finite amplitude convection has been considered with the perturbation expansion approach. Malkus and Veronis [69] created evolution equations by taking care of the nonlinear inertial and thermal convection terms as perturbations of the linear convection problem. In this approach, the temperature and velocity, with insignificant disturbances from the post-critical range, have a spatial dependence which strongly simulates the critical mode.

Most of the Presented nonlinear approaches of natural convection are restricted to the weakly nonlinear convection and arbitrary mode selection [70], [87], [88]. In this paper a spectral approach has been used, which is spectral in character and applicable for wider range of the post-critical regime, to study nonlinear convection of a non-Fourier fluid.

As mentioned before, superfluid helium (He II) at low temperatures ($T < 2.2$ K) has non-Fourier behavior. Nusselt number of low-temperature gaseous helium in free convection obeys the relation $Nu = 0.173Ra^{0.28}$ [89] which is higher compare with a regular fluid like Nitrogen [90]. Regarding the non-Fourier behavior of nanofluids, enhancement of heat transfer has been seen in many studies such as vertical enclosure [91]–[93], CNTs [94] and forced convection [95]–[97]. Few studies have been carried out for natural convection heat transfer characteristics of nanofluids. Khanafer et al. [91] simulated natural convection of nanofluids in a vertical rectangular enclosure numerically. They used copper nanoparticles in water and found that heat transfer increases with the volumetric fraction at any Grashof number. However, Putra et al. [98] detected conflicting findings in the experimental research that in natural convection heat transfer in enclosures, presence of nanoparticles in base fluid may result in noticeable diminution, instead of gain. Ding [99] reported systematic decrease in the natural convective heat transfer coefficient with increasing particle concentration and mentioned that possible reasons could be the convection made by concentration difference, particle–surface and particle–particle interactions, and modifications of the dispersion properties.

3.2 Problem formulation

Consider a thin layer of a Newtonian non-Fourier liquid confined between the (X, Y) planes at $Z = 0$ and the plane $Z = D$, maintained at fixed temperatures $T_0 + \delta T$ and T_0, respectively. The fluid layer is assumed to be of infinite horizontal extent. Convection sets in whenever viscous effects are overcome by buoyancy. Here **g** = - g$\mathbf{e}_z$, where g is the acceleration due to gravity. Boussinesq's approximation, which express that the effect of compressibility is insignificant everywhere in the conservation equations except in the buoyancy term, is supposed to hold so the density ρ depends on the temperature T, following:

$$\rho = \rho_0\left[1 - \alpha_T\left(T - T_0\right)\right] \tag{3.2.1}$$

Here α_T is the coefficient of volume expansion and ρ_0 is the mass density of the fluid at T_0. The fluid is assumed to be incompressible, of specific heat at constant pressure C_p, thermal conductivity K and viscosity μ. In this case, the temperature and pressure gradient for a stationary fluid are given by $T_s = -\left(Z/D\right)\delta T + T_0 + \delta T$ and $dP_s / dZ = -\rho_0\left[1 - \alpha_T \delta T\left(1 - Z/D\right)\right]g$, respectively α_T and is the thermal expansion coefficient. The main governing equations two-dimensional flow patterns are as following,

$$\nabla \cdot \mathbf{V} = 0 \tag{3.2.2}$$

$$\rho_0\left(\mathbf{V}_t + \mathbf{V}\cdot\nabla\mathbf{V}\right) = -\nabla P - \rho g\mathbf{e_z} + \mu\Delta\mathbf{V} \tag{3.2.3}$$

$$\rho_0 c_p\left(T_t + \mathbf{V}\cdot\nabla T\right) = -\nabla\cdot\mathbf{Q} \tag{3.2.4}$$

In this work, the heat flux is assumed to be governed by the generalized Cattaneo-Vernotte equation (Christov [19]), namely,

$$\tau_Q\left(\mathbf{Q}_t + \mathbf{V}\cdot\nabla\mathbf{Q} - \mathbf{Q}\cdot\nabla\mathbf{V} + \mathbf{Q}\nabla\cdot\mathbf{V}\right) = -\mathbf{Q} - K\nabla T \tag{3.2.5}$$

where τ is a relaxation coefficient. Note that the term $\mathbf{Q}\nabla\cdot\mathbf{V}$ is zero. Here **V =** (U, V, W) is the velocity vector and **Q** being the dimensional heat flux. It is also feasible to produce a generalized energy equation. In fact, upon taking the divergence of (3.2.5), noting the identity $\nabla\cdot(\mathbf{a}\cdot\nabla\mathbf{b}) = \nabla\mathbf{a}:\nabla\mathbf{b} + \mathbf{a}\cdot\nabla(\nabla\cdot\mathbf{b})$, **a** and **b** being two general vectors, and using (3.2.5), one attains

$$\begin{aligned}&\tau_Q\left[T_{tt} + 2\mathbf{V}\cdot\nabla T_t + \mathbf{V}_t\cdot\nabla T + \mathbf{V}\cdot\nabla(\mathbf{V}\cdot\nabla T)\right]\\&\quad + T_t + \mathbf{V}\cdot\nabla T = \kappa\nabla^2 T,\end{aligned} \tag{3.2.6}$$

The related boundary conditions at the lower and upper plates are taken to correspond to free-free conditions. In this case:

$$\begin{aligned}&\mathbf{V}(X,Y,Z=0,t)\cdot\mathbf{e}_z = \mathbf{V}(X,Y,Z=1,t)\cdot\mathbf{e}_z = 0,\\&\mathbf{V}_{zz}(X,Y,Z=0,t)\cdot\mathbf{e}_z = \mathbf{V}_{zz}(X,Y,Z=0,t)\cdot\mathbf{e}_z = 0,\\&\theta(X,Y,Z=0,t) = \theta(X,Y,Z=0,t) = 0.\end{aligned} \tag{3.2.7}$$

We introduce perturbations ($\mathbf{V}, \theta, \pi, q_i$) and put them into equations (3.2.2) to (3.2.5), respectively and obtain a set of equations as

$$\nabla\cdot\mathbf{V} = 0 \tag{3.2.8}$$

$$\mathbf{V}_t + \mathbf{V}\cdot\nabla\mathbf{V} = -\frac{1}{\rho_0}\nabla\pi + \alpha_T g\theta\mathbf{e}_z + \upsilon\Delta\mathbf{V} \tag{3.2.9}$$

$$\begin{aligned}&\tau_Q\left[T_{tt} + 2\mathbf{V}\cdot\nabla T_t + \mathbf{V}_t\cdot\nabla T - W_t + \mathbf{V}\cdot\nabla(\mathbf{V}\cdot\nabla T - W)\right]\\&\quad + T_t + \mathbf{V}\cdot\nabla T - W = \kappa\nabla^2 T,\end{aligned} \tag{3.2.10}$$

Equations (3.2.8)- (3.2.10)is non-dimensionalized with the length, time and velocity scales L, Γ and U given by $L = D, \Gamma = \frac{D^2}{\kappa}, U = \frac{\kappa}{D}$, then we introduce temperature,

pressure, and heat flux scales as, $\left[T^{\#}\right]=\delta T$, $[P]=\frac{\mu\kappa}{D^2}$, $[q^*]=K\frac{\delta T}{D}$, where $\kappa=\frac{K}{\rho c_p}$.

The following non-dimensional groups have been stated, namely the Rayleigh number, the Prandtl number and the Cattaneo number, given by

$$\mathrm{Pr}=\frac{\nu}{\kappa} \quad , \quad C=\frac{\tau\kappa}{D^2} \quad , \quad \mathrm{Ra}=\frac{\delta T\alpha_T g D^3}{\nu\kappa} . \tag{3.2.11}$$

To get non-dimensional state, all non-dimensional variables with their scales are put in equations (3.2.8) - (3.2.10)

$$\nabla\cdot\mathbf{v}=0 \tag{3.2.12}$$

$$\mathrm{Pr}^{-1}\left(\mathbf{v}_t+\mathbf{v}\cdot\nabla\mathbf{v}\right)=-\nabla p+\mathrm{Ra}\theta\mathbf{e}_z+\Delta\mathbf{v} \tag{3.2.13}$$

$$C\left[\theta_{tt}+2\mathbf{v}\cdot\nabla\theta_{\mathbf{t}}+\mathbf{v_t}\cdot\nabla\theta-w_t+\mathbf{v}\cdot\nabla\left(\mathbf{v}\cdot\nabla\theta-w\right)\right] +\theta_{\mathbf{t}}+\mathbf{v}\cdot\nabla\theta-w=\nabla^2\theta \tag{3.2.14}$$

The influence of the Cattaneo number on the overall marginal stability picture is typically illustrated in Figure 3-1, where the marginal stability curves are plotted against the wavenumber for Pr = 10. Note that Ra_c corresponds to critical Rayleigh number. For a Fourier fluid, the marginal stability curve is independent of Pr and there is an exchange of stability between the pure conduction state and stationary convection for any wavenumber. For relatively small C > 0, each non-Fourier curve includes a stationary branch, also part of the Fourier curve and an oscillatory convective branch (overstability).

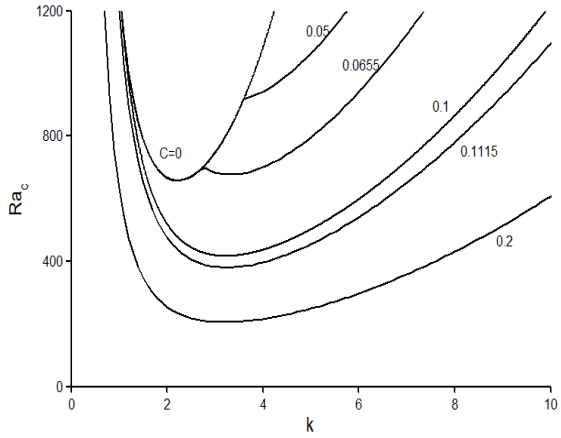

Figure 3-1: *Influence of the Cattaneo number on the marginal stability curves in the Rac-k plane for a single-phase-lagging fluid (Pr = 10).*

3.3 Spectral solution for steady convection

Only steady convection is examined in this paper. A spectral approach has been used to obtain the flow and temperature fields in the post-critical range of Rayleigh number. The presented approach is valid for strongly nonlinear convection. In the spectral method the flow and temperature fields expand periodically in the streamwise direction using orthonormal shape function in the transverse direction.

The flow and temperature fields are periodic in the x direction with wavelength 2π/k and of the general form

$$\psi(x,z)=\sum_{a=-L}^{L}\sum_{m=1}^{M}\psi_{am}e^{iakx}f_m(z),\qquad \theta(x,z)=\sum_{a=-L}^{L}\sum_{m=1}^{M}\theta_{am}e^{iakx}g_m(z) \tag{3.3.1}$$

where ψ_{am} and θ_{am} are invariable coefficients, and f_m and g_m are properly selected orthonormal polynomials being suitable for the boundary conditions. Here indices $a,b,c\in[-L,L]$ and $m,n,p\in[0,M]$, where L and M are the number of modes in the x and z

directions, respectively. Because of the homogeneity of conditions under the symmetry transformation

$$x \to -x, \qquad z \to z, \qquad \psi \to -\psi, \qquad \theta \to \theta \tag{3.3.2}$$

solution (3.3.1) shrinks to

$$\psi(x,z) = \sum_{a=1}^{L}\sum_{m=1}^{M} \psi_{am} sin(akx) f_m(z), \tag{3.3.3}$$

$$\theta(x,z) = \sum_{m=1}^{M} \theta_{0m} g_m(z) + \sum_{a=1}^{L}\sum_{m=1}^{M} \theta_{am} cos(akx) g_m(z) \tag{3.3.4}$$

To obtain the governing equation of coefficients, above equations should substitute into the equations (3.2.13) and (3.2.14) and project onto the proper modes. (3.2.13) and (3.2.14) multiply by $sin(ckx) f_p(z)$ and $cos(ckx) f_p(z)$ respectively, and integrate over the intervals $0 \le x \le 2\pi / k;$ and $0 \le z \le 1$, to obtain

$$\sum_{a,b=1}^{L}\sum_{m,n=1}^{M} A1_{abc,mnp}\psi_{am}\psi_{bn} + Pr\sum_{a=1}^{L}\sum_{m=1}^{M}\left(A2_{ac,mp}\psi_{am} + RaA3_{ac,mp}\theta_{am}\right) = 0 \tag{3.3.5}$$

$$\begin{aligned} &C\sum_{a,b=1,d=0}^{L}\sum_{m,n,q=1}^{M} A4_{abdc,mnqp}\psi_{am}\psi_{bn}\theta_{dq} + C\sum_{a=1,b=0}^{L}\sum_{m,n=1}^{M} A5_{abc,mnp}\psi_{am}\psi_{bn} \\ &+ \sum_{a=1,b=0}^{L}\sum_{m,n=1}^{M} A6_{abc,mnp}\psi_{am}\theta_{bn} + \sum_{a=1}^{L}\sum_{m=1}^{M} A7_{ac,mp}\psi_{am} + \sum_{a=0}^{L}\sum_{m=1}^{M} A8_{ac,mp}\theta_{am} = 0 \end{aligned} \tag{3.3.6}$$

where the matrix coefficients are

$$
\begin{aligned}
A1_{abc,mnp}\big|_{c>0} &= bk\left\langle S_a C_b S_c\right\rangle\left\langle f'_m f''_n f_p\right\rangle - b^3k^3\left\langle S_a C_b S_c\right\rangle\left\langle f'_m f_n f_p\right\rangle \\
&\quad + ak\left\langle C_a S_b S_c\right\rangle\left(b^2k^2\left\langle f_m f'_n f_p\right\rangle - \left\langle f_m f'''_n f_p\right\rangle\right) \\
A2_{ac,mp}\big|_{c>0} &= -\left\langle S_a S_c\right\rangle\left(a^4k^4\left\langle f_m f_p\right\rangle - 2a^2k^2\left\langle f''_m f_p\right\rangle + \left\langle f^{iv}_m f_p\right\rangle\right) \\
A3_{ac,mp}\big|_{c>0} &= -\left\langle S_a S_c\right\rangle ak\left\langle g_m f_p\right\rangle
\end{aligned}
\tag{3.3.7}
$$

and

$$
\begin{aligned}
\mathrm{A4_{abdc,mnqp}} &= +\mathrm{bdk^2}\left\langle \mathrm{S_a C_b S_d C_c}\right\rangle\left\langle \mathrm{f'_m f'_n g_q g_p}\right\rangle + \mathrm{d^2k^2}\left\langle \mathrm{S_a S_b C_d C_c}\right\rangle\left\langle \mathrm{f'_m f'_n g_q g_p}\right\rangle \\
&\quad - \mathrm{b^2k^2}\left\langle \mathrm{S_a S_b C_d C_c}\right\rangle\left\langle \mathrm{f'_m f_n g'_q g_p}\right\rangle - \mathrm{bdk^2}\left\langle \mathrm{S_a C_b S_d C_c}\right\rangle\left\langle \mathrm{f'_m f_n g'_q g_p}\right\rangle \\
&\quad - \mathrm{adk^2}\left\langle \mathrm{C_a S_b S_d C_c}\right\rangle\left\langle \mathrm{f_m f''_n g_q g_p}\right\rangle - \mathrm{adk^2}\left\langle \mathrm{C_a S_b S_d C_c}\right\rangle\left\langle \mathrm{f_m f'_n g'_q g_p}\right\rangle \\
&\quad - \mathrm{abk^2}\left\langle \mathrm{C_a C_b C_d C_c}\right\rangle\left\langle \mathrm{f_m f'_n g'_q g_p}\right\rangle - \mathrm{abk^2}\left\langle \mathrm{C_a C_b C_d C_c}\right\rangle\left\langle \mathrm{f_m f_n g''_q g_p}\right\rangle \\
\mathrm{A5_{abc,mnp}} &= +\mathrm{b^2k^2}\left\langle \mathrm{S_a S_b C_c}\right\rangle\left\langle \mathrm{f'_m f_n g_p}\right\rangle + \mathrm{abk^2}\left\langle \mathrm{C_a C_b C_c}\right\rangle\left\langle \mathrm{f_m f'_n g_p}\right\rangle \\
\mathrm{A6_{abc,mnp}} &= \mathrm{bk}\left\langle \mathrm{S_a S_b C_c}\right\rangle\left\langle \mathrm{f'_m g_n g_p}\right\rangle + \mathrm{ak}\left\langle \mathrm{C_a C_b C_c}\right\rangle\left\langle \mathrm{f_m g'_n g_p}\right\rangle \\
\mathrm{A7_{ac,mp}} &= -\mathrm{ak}\left\langle \mathrm{C_a C_c}\right\rangle\left\langle \mathrm{f_m g_p}\right\rangle \\
\mathrm{A8_{ac,mp}} &= -\left\langle \mathrm{C_a C_c}\right\rangle\left[\mathrm{a^2k^2}\left\langle \mathrm{g_m g_p}\right\rangle - \left\langle \mathrm{g''_m g_p}\right\rangle\right]
\end{aligned}
\tag{3.3.8}
$$

where $S_a \equiv sin(akx), C_a \equiv cos(akx)$, $a,b,c \in [0,L]$ (unless otherwise specified) and the brackets < > denote integration over *x* or *z*. It is convenient to extrude one equation from equations (3.3.5) and (3.3.6) and rewrite them as

$$cRa\pi\theta_{cp} = Pr^{-1} \sum_{a,b=1}^{L} \sum_{m,n=1}^{M} A1_{abc,mnp}\psi_{am}\psi_{bn} + \sum_{a=1}^{L} \sum_{m=1}^{M} A2_{ac,mp}\psi_{am} \tag{3.3.9}$$

$$\begin{aligned} &C \sum_{a,b=1}^{L} \sum_{m,n,q=1}^{M} A4_{ab0c,mnqp}\psi_{am}\psi_{bn}\theta_{0q} + C \sum_{a,b,d=1}^{L} \sum_{m,n,q=1}^{M} A4_{abdc,mnqp}\psi_{am}\psi_{bn}\theta_{dq} \\ &+C \sum_{a,b=1}^{L} \sum_{m,n=1}^{M} A5_{abc,mnp}\psi_{am}\psi_{bn} + c\pi \sum_{m,n=1}^{M} \left\langle f_m g'_n g_p \right\rangle \psi_{cm}\theta_{0n} \\ &+ \sum_{a,b=1}^{L} \sum_{m,n=1}^{M} A6_{abc,mnp}\psi_{am}\theta_{bn} + \sum_{a=1}^{L} \sum_{m=1}^{M} A7_{ac,mp}\psi_{am} + \sum_{a=1}^{L} \sum_{m=1}^{M} A8_{ac,mp}\theta_{am} = 0 \end{aligned} \tag{3.3.10}$$

$$\begin{aligned} &C \sum_{a,b=1}^{L} \sum_{m,n,q=1}^{M} A4_{ab00,mnqp}\psi_{am}\psi_{bn}\theta_{0q} + C \sum_{a,b,d=1}^{L} \sum_{m,n,q=1}^{M} A4_{abd0,mnqp}\psi_{am}\psi_{bn}\theta_{dq} \\ &+C \sum_{a,b=1}^{L} \sum_{m,n=1}^{M} A5_{ab0,mnp}\psi_{am}\psi_{bn} + \sum_{a,b=1}^{L} \sum_{m,n=1}^{M} A6_{ab0,mnp}\psi_{am}\theta_{bn} + \sum_{m=1}^{M} A8_{00,mp}\theta_{0m} = 0 \end{aligned} \tag{3.3.11}$$

Note that indices now $a,b,c \in [1,L]$. This general system of equations (3.3.9-3.3.11) is valid for any boundary conditions. At this stage, functions $f_m(z)$ and $g_m(z)$ need be specified which satisfy the boundary conditions at z = 0 and z = 1. This study considers the free-free conditions, one chooses the *z*-dependent functions as

$$f_m(z) = g_m(z) = \sqrt{2}\sin(m\pi z) \tag{3.3.12}$$

Thus, the equations (3.3.9) to (3.3.11) simplify to:

$$\frac{\pi}{k}\beta_{cp}^2\psi_{cp} + cRa\pi\theta_{cp} = Pr^{-1} \sum_{a,b=1}^{L} \sum_{m,n=1}^{M} C1_{abc,mnp}\psi_{am}\psi_{bn} \tag{3.3.13}$$

$$C\sum_{a,b=1}^{L}\sum_{m,n,q=1}^{M} A4_{ab0c,mnqp}\psi_{am}\psi_{bn}\theta_{0q} + C\sum_{a,b,d=1}^{L}\sum_{m,n,q=1}^{M} A4_{abdc,mnqp}\psi_{am}\psi_{bn}\theta_{dq}$$
$$+C\sum_{a,b=1}^{L}\sum_{m,n=1}^{M} A5_{abc,mnp}\psi_{am}\psi_{bn} + c\pi\sum_{m,n=1}^{M} B1_{mnp}\psi_{cm}\theta_{0n} + \sum_{a,b=1}^{L}\sum_{m,n=1}^{M} C2_{abc,mnp}\psi_{am}\theta_{bn} = \quad (3.3.14)$$
$$c\pi\psi_{cp} + \frac{\pi}{k}\beta_{cp}\theta_{cp}$$

$$C\sum_{a,b=1}^{L}\sum_{m,n,q=1}^{M} A4_{ab00,mnqp}\psi_{am}\psi_{bn}\theta_{0q} + C\sum_{a,b,d=1}^{L}\sum_{m,n,q=1}^{M} A4_{abd0,mnqp}\psi_{am}\psi_{bn}\theta_{dq}$$
$$+C\sum_{a,b=1}^{L}\sum_{m,n=1}^{M} A5_{ab0,mnp}\psi_{am}\psi_{bn} + \sum_{a,b=1}^{L}\sum_{m,n=1}^{M} A6_{ab0,mnp}\psi_{am}\theta_{bn} \quad (3.3.15)$$
$$-\frac{2\pi}{k}\beta_{0p}\theta_{0p} = 0$$

where $\beta_{cp} = c^2k^2 + p^2\pi^2$. The most important benefit of these equations is reliability over any range of the parameters, specifically the post-critical range of the Rayleigh number. The only problem is the possible existence of multiple solution branches. These nonlinear equations must be solved numerically. In this study, a perturbation approach, as a weakly nonlinear approach, is employed.

3.4 Convection close to criticality

To treat nonlinear convection, a spectral approach is presented in this section which is not based on arbitrary mode selection. The spectral methodology consists of expanding the flow and temperature fields periodically along the layer, and using orthonormal shape functions in the transverse direction. The Galerkin projection is then implemented to generate the equations for the expansion coefficients. Since most of the interesting bifurcation picture is close to criticality, a perturbation approach is developed to solve the nonlinear spectral system in the weakly post-critical range. To leading order, the Lorenz model is recovered. Spectral approach reveals the number and type required modes. Here, the perturbation parameter in the problem defines a small deviation from the critical Rayleigh number for the onset of convection, and is given by

$$\varepsilon = \frac{Ra - Ra_{cr}}{Ra_{cr}} < 1, \tag{3.4.1}$$

where $Ra_{cr} = \beta^3 \big/ k^2$ is critical Rayleigh number. Experimentally has been shown taht the amplitude of motion is proportional to $\sqrt{\varepsilon}$ [80], [100].In this case, the unknown stream function and temperature coefficients could expand as

$$\begin{aligned} \psi_{am} &= \sqrt{\varepsilon}\psi 1_{am} + \varepsilon\psi 2_{am} + \ldots \\ \theta_{am} &= \sqrt{\varepsilon}\theta 1_{am} + \varepsilon\theta 2_{am} + \ldots \\ \theta_{0m} &= \varepsilon\theta 2_{0m} + \varepsilon^{3/2}\theta 3_{0m} + \ldots \end{aligned} \tag{3.4.2}$$

After substituting (3.4.2) into (3.3.13)-(3.3.15), terms will be sorted in order of ε. To $\mathrm{O}\left(\sqrt{\varepsilon}\right)$ which is leading order, one has

$$Ra_{cr}\theta 1_{cp} + \frac{\beta_{cp}^2}{ck}\psi 1_{cp} = 0 \qquad , \qquad c\psi 1_{cp} + \frac{1}{k}\beta_{cp}\theta 1_{cp} = 0 \tag{3.4.3}$$

and to the next order, that is to $\mathrm{O}(\varepsilon)$,

$$\frac{\pi}{k}\beta_{cp}^2\psi 2_{cp} + c\pi Ra_{cr}\theta 2_{cp} = Pr^{-1}C1_{11c,11p}\psi 1_{11}^2 = 0 \tag{3.4.4a}$$

$$c\pi\psi 2_{cp} + \frac{\pi}{k}\beta_{cp}\theta 2_{cp} = C2_{11c,11p}\psi 1_{11}\theta 1_{11} = 0. \tag{3.4.4b}$$

$\theta 1_{cp} = \psi 1_{cp} = \theta 2_{cp} = \psi 2_{cp} = 0$ can be exclude from equations (3.4.3) and (3.4.4) except for $\theta 1_{11} = -\frac{k}{\beta}\psi 1_{11}$ and $\theta 2_{11} = -\frac{k}{\beta}\psi 2_{11}$, which by solving the higher order solution will be found. In this case, from equation (3.3.15),

$$\theta 2_{02} = \frac{\sqrt{2}k^2}{8\pi}\left(C - \frac{1}{\beta}\right)\psi 1_{11}\psi 1_{11}. \tag{3.4.5}$$

Also, to $O\left(\varepsilon^{3/2}\right)$, one has

$$\frac{\beta_{cp}^2}{k}\psi 3_{cp} + cRa_{cr}\theta 3_{cp} = -cRa_{cr}\theta 1_{cp} \tag{3.4.6a}$$

$$\begin{aligned} c\pi\psi 3_{cp} + \frac{\pi}{k}\beta_{cp}\theta 3_{cp} &= C\sum_{a,b,d=1}^{L}\sum_{m,n,q=1}^{M} A4_{abdc,mnqp}\psi 1_{am}\psi 1_{bn}\theta 1_{dq} \\ &+ C\sum_{a,b=1}^{L}\sum_{m,n=1}^{M} A5_{abc,mnp}\left(\psi 1_{am}\psi 2_{bn} + \psi 2_{am}\psi 1_{bn}\right) + \sum_{m,n=1}^{M} c\pi\left\langle f_m g'_n g_p\right\rangle \psi 1_{cm}\theta 2_{0n} \end{aligned} \tag{3.4.6b}$$

by setting $c = p = 1$,

$$\psi 1_{11} = \theta 1_{11} = 0,$$

$$\psi 1_{11} = \pm\frac{1}{k\sqrt{\left(C\left(-\frac{\pi^2}{\beta} - \frac{1}{4}\right) + \frac{1}{4\beta}\right)}}, \qquad \theta 1_{11} = \pm\frac{1}{\beta\sqrt{\left(C\left(-\frac{\pi^2}{\beta} - \frac{1}{4}\right) + \frac{1}{4\beta}\right)}} \tag{3.4.7}$$

which is the same as Lorenz flow and consists of the conduction state and the supercritical bifurcation convective branches. If $c = p = 1$, $\theta 3_{11} = -\frac{k}{\beta}\psi 3_{11} - \theta 1_{11}$, with $\theta 3_{11}$ and $\psi 3_{11}$ are yet to be obtained. If $c = 1 and\ p = 3$ one has

$$\psi 3_{13} = \left(-\frac{\beta^3}{\beta^3 - \beta_{13}^3} \right) \psi 1_{11}, \qquad \theta 3_{13} = -\frac{k\beta_{13}^2}{\beta^3}\psi 3_{13} = \frac{k}{\beta}\left(\frac{\beta_{13}^2}{\beta^3 - \beta_{13}^3} \right) \psi 1_{11} \tag{3.4.8}$$

Also, to this order,

$$\theta 3_{02} = \frac{\sqrt{2}k}{\beta_{02}}\left(Ck\pi\psi 1_{11}\psi 2_{11} + \frac{\pi}{2}\psi 1_{11}\theta 2_{11} + \frac{\pi}{2}\psi 2_{11}\theta 1_{11} \right) \tag{3.4.9}$$

To $O\left(\varepsilon^2\right)$ and $O\left(\varepsilon^{5/2}\right)$,

$$\psi 2_{am} = \theta 2_{am} = \theta 3_{0m} = 0, \qquad \forall a > 0, \forall m \tag{3.4.10}$$

and

$$\theta 3_{11}=\frac{\left(\begin{array}{l}\frac{\beta}{k}\sqrt{2}\pi\theta 2_{02}\theta 1_{11}-\beta C\pi^2\psi 1_{11}\theta 1_{11}\theta 1_{11}-\beta C\pi^2\psi 1_{11}\theta 1_{11}\theta 1_{11}\\ +\frac{1}{2}Ck\psi 1_{11}\beta\psi 1_{11}\theta 1_{11}+\psi 1_{11}\frac{\beta}{4}\theta 1_{11}\theta 1_{11}-Ck\pi^2\psi 1_{11}\psi 1_{11}\theta 3_{13}\\ -Ck\pi^2\psi 1_{11}\psi 3_{13}\theta 1_{11}-Ck\pi^2\psi 3_{13}\psi 1_{11}\theta 1_{11}\\ -\frac{1}{\sqrt{2}}Ck^2\pi\psi 1_{11}\psi 1_{11}\psi 1_{11}\theta 2_{02}+\frac{1}{2}Ck^2\psi 3_{13}\psi 1_{11}\psi 1_{11}\\ +\frac{k}{4}\psi 1_{11}\theta 3_{13}\psi 1_{11}+\frac{k}{4}\psi 3_{13}\theta 1_{11}\psi 1_{11}+\sqrt{2}\pi\psi 3_{13}\theta 2_{02}\end{array}\right)}{\left(\begin{array}{l}-\frac{k}{\beta^2}Ra_{cr}-\frac{\beta}{k}\sqrt{2}\pi\theta 2_{02}-Ck\pi^2\psi 1_{11}\psi 1_{11}+\beta C\pi^2\psi 1_{11}\theta 1_{11}\\ +\beta C\pi^2\psi 1_{11}\theta 1_{11}-\frac{1}{2}Ck\psi 1_{11}\beta\psi 1_{11}+\frac{k}{4}\psi 1_{11}\psi 1_{11}-\psi 1_{11}\frac{\beta}{4}\theta 1_{11}\end{array}\right)} \tag{3.4.11}$$

$$\psi 3_{11}=-\frac{\beta}{k}\left(\theta 3_{11}+\theta 1_{11}\right),$$

Note, all coefficients are found in this relation. At this stage, it is helpful to give the expressions for the stream function and temperature to:

$$\begin{aligned}\psi(x,z)=&\sqrt{2}\left(\sqrt{\varepsilon}\psi 1_{11}+\varepsilon^{3/2}\psi 3_{11}\right)\sin(kx)\sin(\pi z)\\ &+\varepsilon^{3/2}\sqrt{2}\psi 3_{13}\sin(kx)\sin(3\pi z),\end{aligned} \tag{3.4.12}$$

$$\begin{aligned}\theta(x,z)=&\sqrt{2}\cos(kx)\left[\left(\sqrt{\varepsilon}\theta 1_{11}+\varepsilon^{3/2}\theta 3_{11}\right)\sin(\pi z)+\varepsilon^{3/2}\theta 3_{13}\sin(3\pi z)\right]\\ &+\sqrt{2}\left(\varepsilon\theta 2_{02}+\varepsilon^2\theta 4_{02}\right)\sin(2\pi z)+\sqrt{2}\varepsilon^2\theta 4_{04}\sin(4\pi z).\end{aligned} \tag{3.4.13}$$

Clearly, these expressions show the modes required to each desired order. The corresponding Nusselt number will obtain in the next section.

Figure 3-2 displays the influence of ε on the expansion coefficients in (3.4.12) and (3.4.13) in a Fourier fluid (C=0). The leading- and higher-order contributions for modes $\varphi_{am}, \theta_{am}$ and θ_{0m} are presented in Figures 3-2a, 3-2b and 3-2c, respectively. Figure 3-2a indicates that the leading-order contribution is essentially dominant for φ_{11}. The φ_{31} mode is essentially negligible, suggesting that, for Fourier fluid convective rolls do not exhibit any significant deformation from elliptical geometry which is limited to the stream function and the temperature geometry would change. Figures 3-2b and 3-2c indicate, respectively, that the higher order contributions for modes θ_{11} and θ_{02} are significant. Although the small contributions of modes θ_{13} and θ_{04}, they are not negligible.

(a)

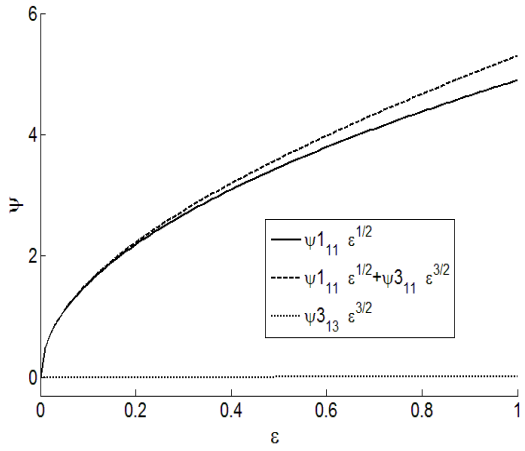

(b)

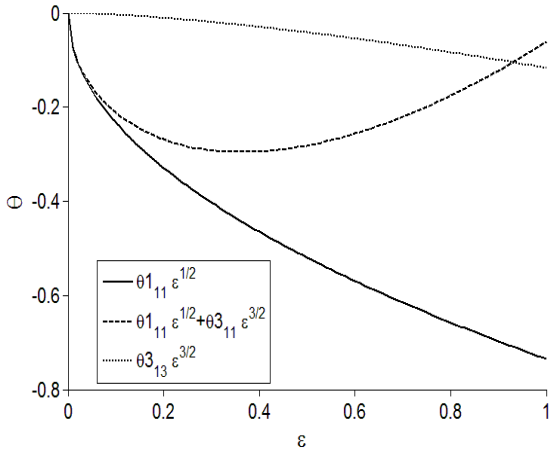

(c)

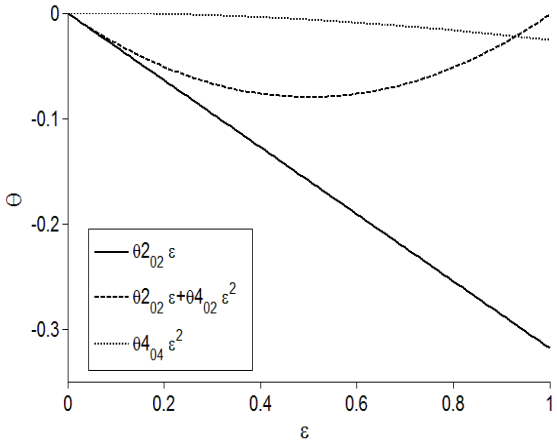

Figure 3-2: *Influence of higher-order terms in the perturbation of the stream function (a), the x-dependent (b) and x-independent (c) temperature deviation for a Fourier fluid. Here* $k = \frac{\pi}{\sqrt{2}}$ *and C=0. In this Figure dashed line corresponds to the leading-order term (of Spectral solution) and solid lines correspond to Spectral solution including leading and higher order terms.*

These modes, lead to the deformation of the temperature field which, are shown more precisely in the Figure 3-3. Figures 3-3a, 3-3b and 3-3c illustrate the influence of ε on the temperature and stream function for a Fourier fluid (C=0) in ε=0.1, 0.5 and 1.0 respectively. Generally, by increasing the ε, higher order terms have more effect which is more obvious for temperature field shown in Figure 3-3. Deformation of the temperature fields are shown in Figure 3-4a to 4c for ε=0.1, 0.5 and 1.0 respectively. Obviously, when ε=1, the high order term of θ_{13} is governing and the dominant mode.

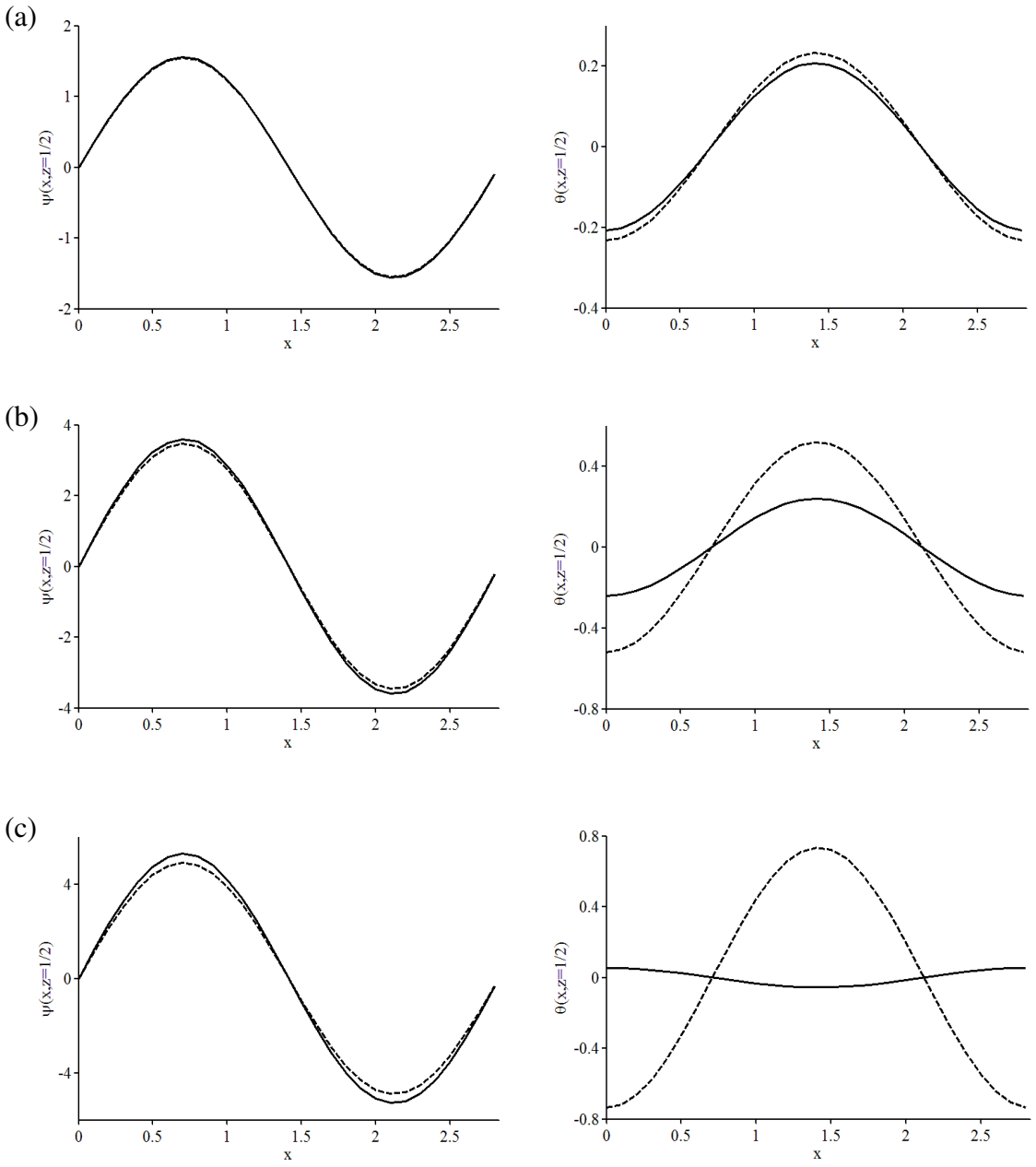

Figure 3-3: *Distributions of the leading-order and higher-order terms on the stream function and temperature deviation at (a) ε = 0.1, (b) ε = 0.5 and (c)ε = 1 for a Fourier fluid. Here C=0,* $k = \frac{\pi}{\sqrt{2}}$ *and z = ½.In this Figure dashed line corresponds to the leading-order term (of Spectral solution) and solid lines correspond to Spectral solution including leading and higher order terms.*

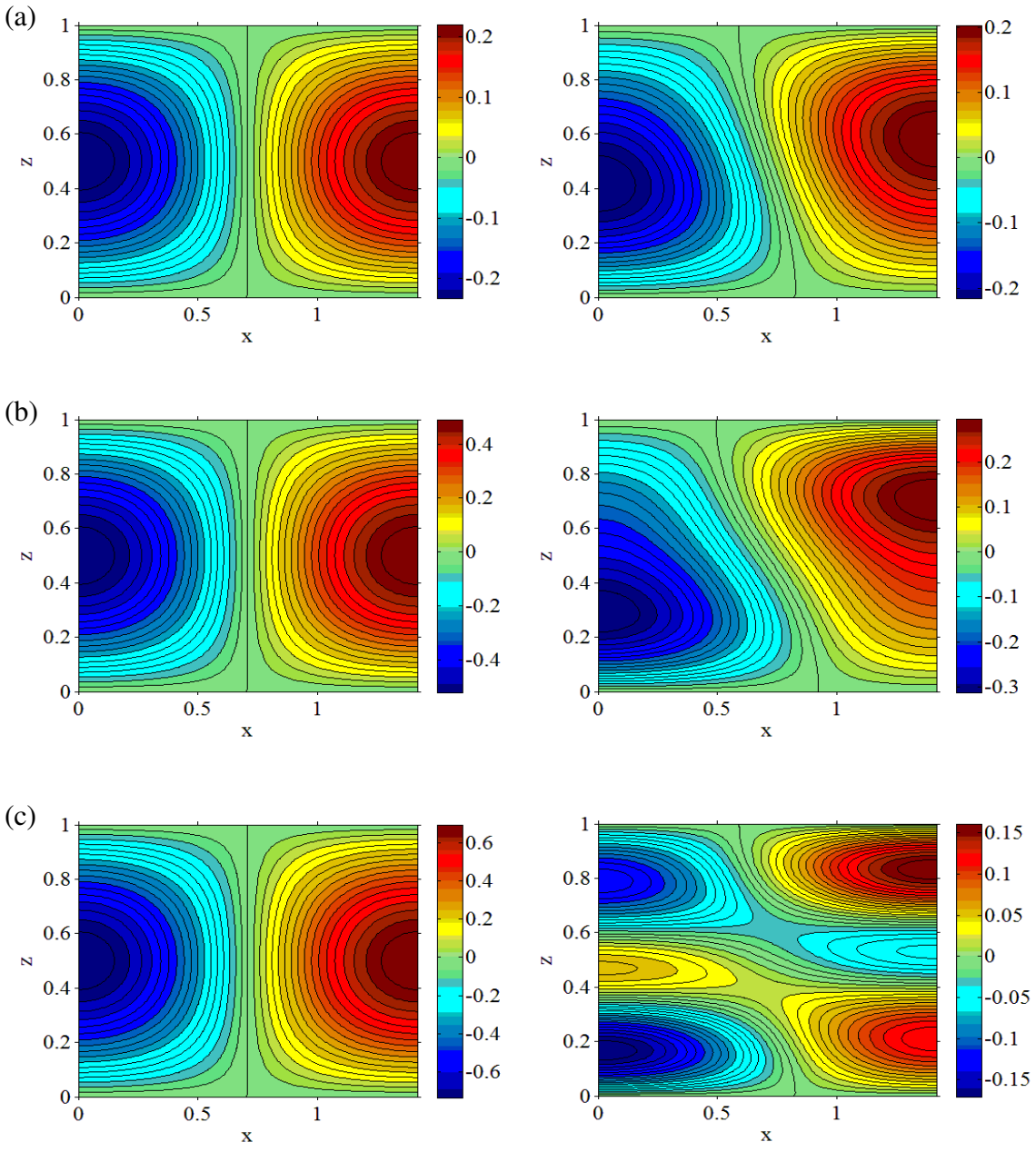
(a)
(b)
(c)
z
x
0
0.2
0.4
0.5
0.6
0.8
1
-0.1
-0.2
-0.3
-0.4
-0.6
0.05
0.1
0.15

Figure 3-4: *Distributions of the leading-order and higher-order temperature deviation at (a) ε = 0.1, (b) ε = 0.5 and (c) ε = 1 for a Fourier fluid. Here C=0,* $k = \frac{\pi}{\sqrt{2}}$ *and z = ½. In this Figure the left columns corresponds to the leading-order term (of Spectral solution) and right columns correspond to Spectral solution including leading and higher order terms.*

Figure 3-5 depicts the influence of the higher-order correction as function of the Rayleigh number (Figure 3-5a) and wave number (Figure 3-5b) in a Fourier fluid. As predicted, the discrepancy between the leading- and higher-order corrections in Figure 3-5a is the same as for the temperature deviation in Figure 3-3 and higher-order contributions diminish both temperature deviation and Nusselt number. In high Rayleigh numbers, the high-order terms overcome the leading-order terms finally. Figure 3-5b reveals that the influence of higher-order terms depends significantly on the wave number. Interestingly, in Fourier fluids, *NuLO* is independent of wave number although leading-order terms of theta are dependent.

(a)

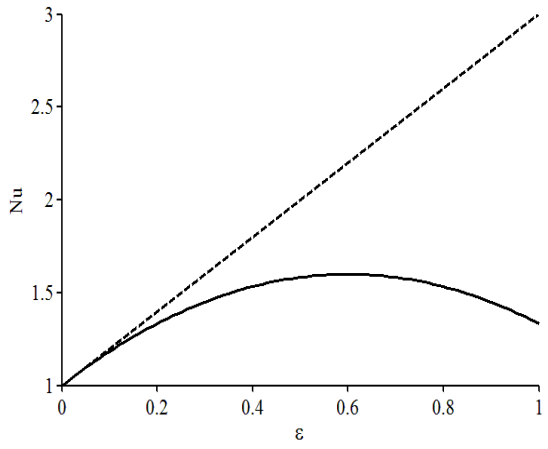

(b)

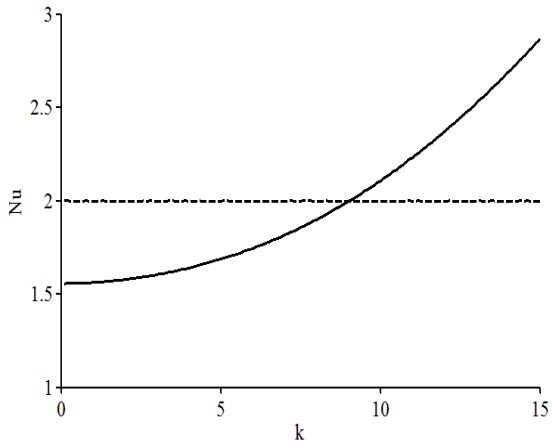

Figure 3-5: *Influence of higher-order terms in the perturbation of the Nusselt number as function of ε (a) and the wavenumber (b). Here C=0 and in (b) ε=0.5. In this Figure dashed line corresponds to the leading-order term (of Spectral solution) and solid lines correspond to Spectral solution including leading and higher order terms.*

For any wave number, there is one specific Cattaneo number which directs $\psi 1_{11}$ and $\theta 1_{11}$ to infinity namely maximum feasible Cattaneo number. Figure 3-6 illustrates the typical dependence of the maximum feasible Cattaneo number on wave number. Figure 3-6 expresses that the higher value of Cattaneo number, the less range of applicable wave number. In Fourier fluids (C=0), there is no restriction for wave number and non-Fourier fluids could not have Cattaneo number more than $\frac{1}{5\pi^2}$. Ordinary value of relaxation time is low, as is shown in Figure 2-1, which makes Cattaneo number very small even for small dimensions and having high value of Cattaneo number is impractical. In the other hand, equation (2.2.10) confirms that for any concentration of nano-particles, relaxation time is limited and as a result, Cattaneo number is limited too.

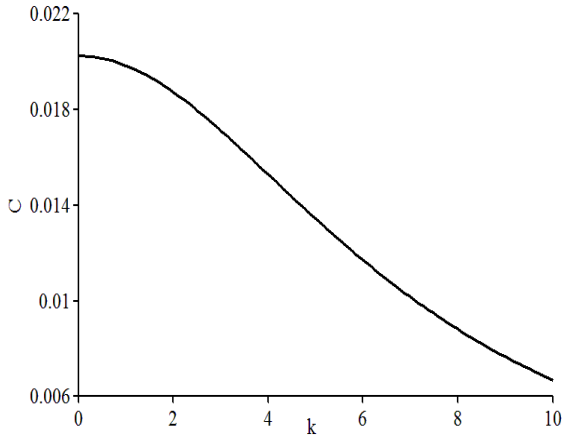

Figure 3-6: *Influence of the wave number on maximum acceptable Cattaneo number.*

The influence of the Cattaneo number on the perturbation of the stream function, the x-dependent and x-independent temperature deviation for two non-Fourier fluids with C = 0.005 (left column) and C = 0.01(right column) is typically illustrated in Figure 3-7, where the stream function curves (first row), the x-dependent (second row) and x-independent temperature deviation (third row) are plotted against the ε (deviation from the critical Rayleigh number) for Pr = 10. At the first row, are the stream function curves of leading and higher order terms for two non-Fourier fluids which show that Canttaneo number increases both leading term in the stream function, as the 11 mode, which comprises leading($\psi 1_{11}$) and higher order($\psi 3_{11}$) terms, increases generally. In the other hand, for C=0.005, magnitude of $\psi 3_{11}$ decreases compare to Fourier case (Figure 3-2a). At a value of Cattaneo number $\psi 3_{11}$ becomes zero and finally for relatively high Cattaneo number, it turns to negative value with higher magnitude as diminishes the 11 mode curve for high Cattaneo numbers. The same results arise from the x-dependent and x-independent temperature deviation curves which show relatively high Cattaneo numbers improve the effect of high order modes.

(a)

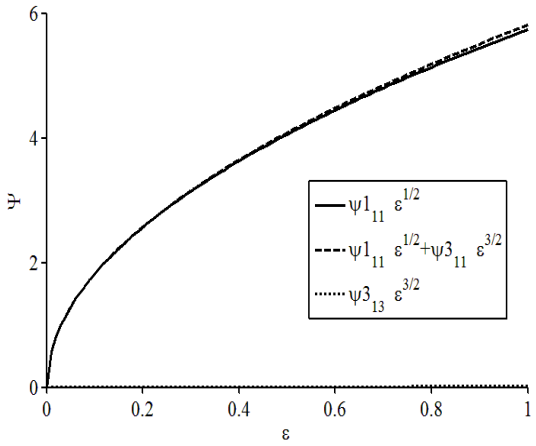
Ψ
ε
ψ1$_{11}$ ε$^{1/2}$
ψ1$_{11}$ ε$^{1/2}$+ψ3$_{11}$ ε$^{3/2}$
ψ3$_{13}$ ε$^{3/2}$

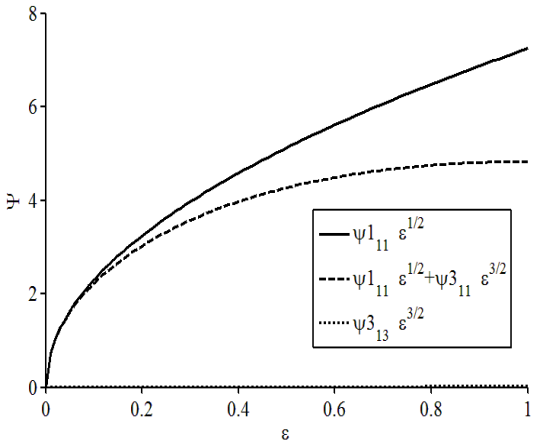
Ψ
ε
ψ1$_{11}$ ε$^{1/2}$
ψ1$_{11}$ ε$^{1/2}$+ψ3$_{11}$ ε$^{3/2}$
ψ3$_{13}$ ε$^{3/2}$

(b)

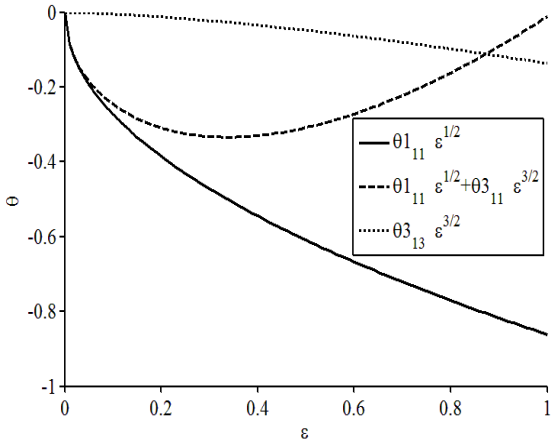
θ
ε
θ1$_{11}$ ε$^{1/2}$
θ1$_{11}$ ε$^{1/2}$+θ3$_{11}$ ε$^{3/2}$
θ3$_{13}$ ε$^{3/2}$

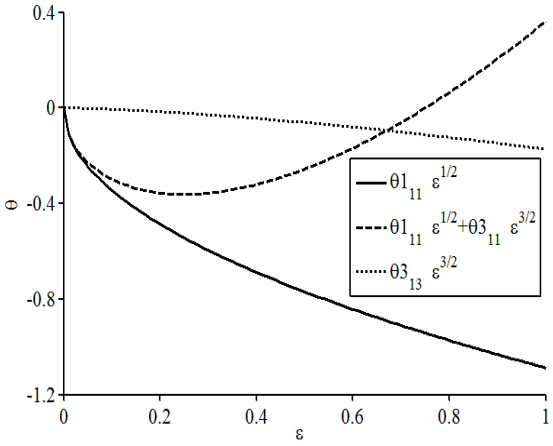
θ
ε
θ1$_{11}$ ε$^{1/2}$
θ1$_{11}$ ε$^{1/2}$+θ3$_{11}$ ε$^{3/2}$
θ3$_{13}$ ε$^{3/2}$

(c)

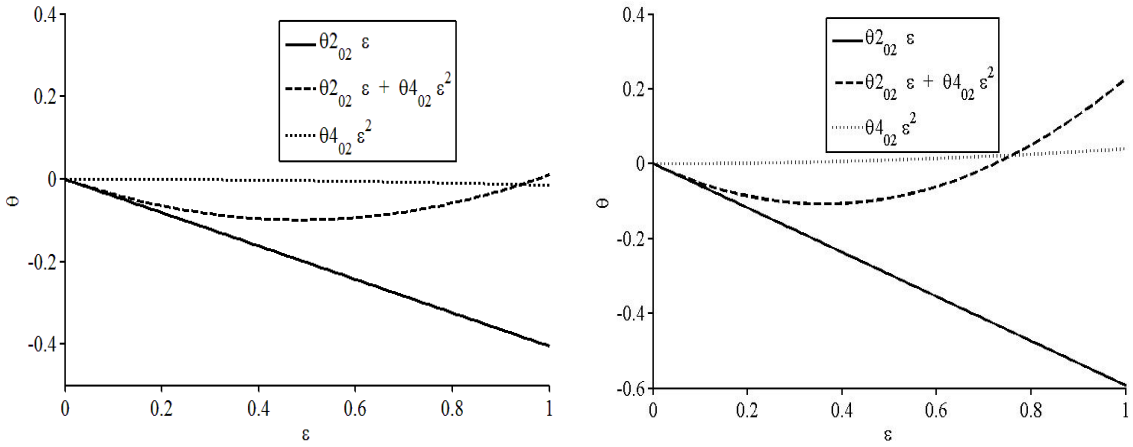

Figure 3-7: *Influence of Cattaneo number on the perturbation of (a) the stream function, (b) the x-dependent and (c) x-independent temperature deviation for two non-Fourier fluids with C = 0.005 (left column) and C = 0.01(right column). Here* $\mathrm{k} = \frac{\pi}{\sqrt{2}}$ *.In this Figure dashed line corresponds to the leading-order term (of Spectral solution) and solid lines correspond to Spectral solution including leading and higher order terms.*

Figure 3-8 illustrates the influence of Cattaneo number on the temperature and stream function for two non-Fourier fluids (C=0.005 and C=0.01) in ε=0.1, 0.5 and 1.0 respectively. Comparing Figure 3-8 with left column of Figure 3-3 shows that in the relatively small/high Cattaneo numbers, the higher order terms have additive/decreasing role in the stream function. For Cattaneo numbers close to 0.005, the higher order terms have no effect in the stream function.

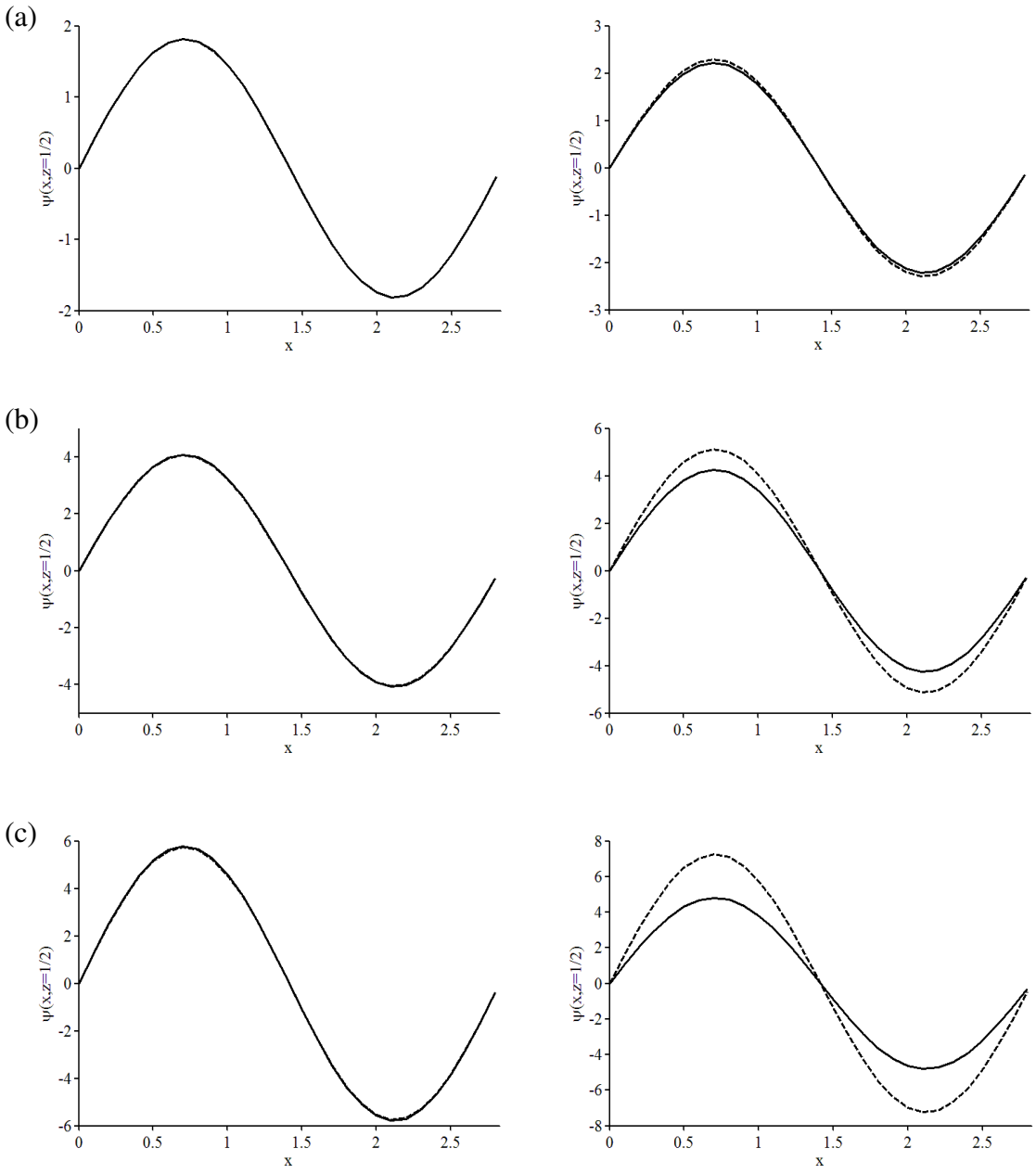

Figure 3-8: *Distributions of the leading-order and higher-order terms on the stream function at (a) ε = 0.1, (b) ε = 0.5 and (c) ε = 1 for two non-Fourier fluids with C = 0.005(left column) and C = 0.01(right column). Here* $\mathrm{k} = \frac{\pi}{\sqrt{2}}$ *and z = ½.In this Figure dashed line corresponds to the leading-order term (of Spectral solution) and solid lines correspond to Spectral solution including leading and higher order terms.*

Figure 3-9 illustrates the influence of Cattaneo number on the leading-order and higher-order terms of the temperature deviation at ε = 0.1, ε = 0.5 and ε = 1 for two non-Fourier fluids with C = 0.005 and C = 0.01. As expected, the difference between the leading- and higher-order corrections in Figure 3-9 agrees with the temperature deviation in Figure 3-7. Generally Cattaneo number increases the discrepancy which means higher magnitude of higher order terms. Distributions of the leading-order and higher-order temperature deviation in the x-z domain are illustrated in Figures 3-10 and 3-11. The left columns contribute to the leading-order terms and the right columns include the higher order corrections. Generally increasing ε (or Rayleigh number) amplifies the effect of higher order terms which the dominant term changes with Cattaneo number. When ε=1 , Figure 3-10 shows that 13 mode is the dominant mode for C=0.005 but for C=0.01, 02 mode is the dominant mode. Note the temperature profiles are horizontal for 02 mode. Despite the obvious changes in the temperature profiles with Cattaneo number, there is no noticeable change as shown in Figure 3-12.

(a)

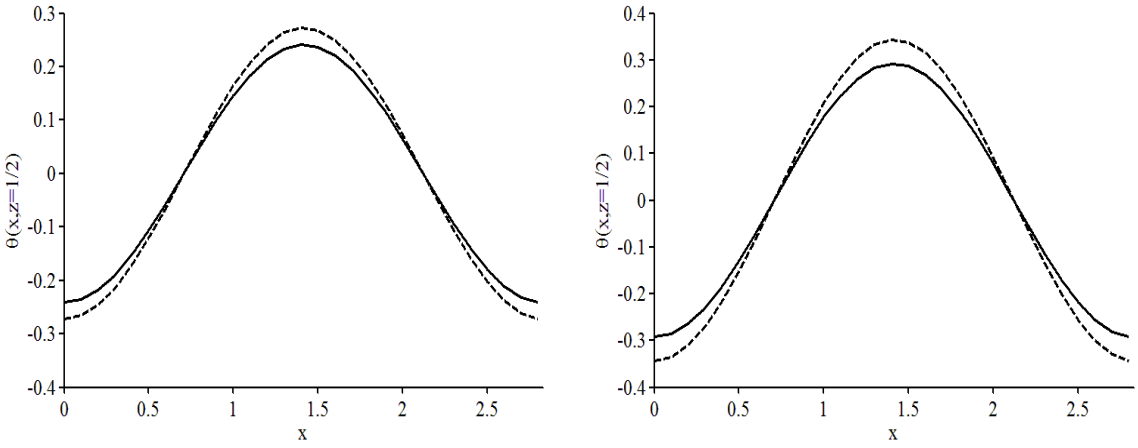

(b)

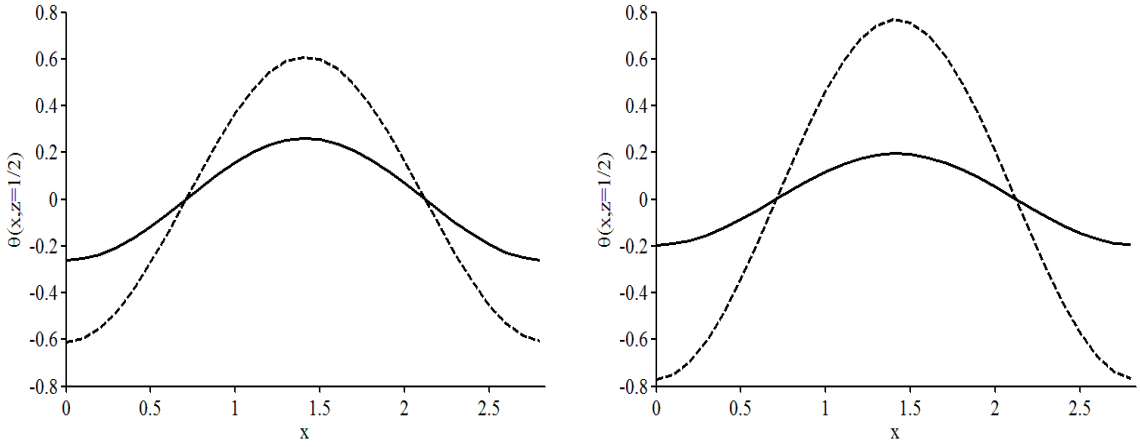
θ(x,z=1/2)
x
0.8
0.6
0.4
0.2
0
-0.2
-0.4
-0.6
-0.8
0
0.5
1
1.5
2
2.5

(c)

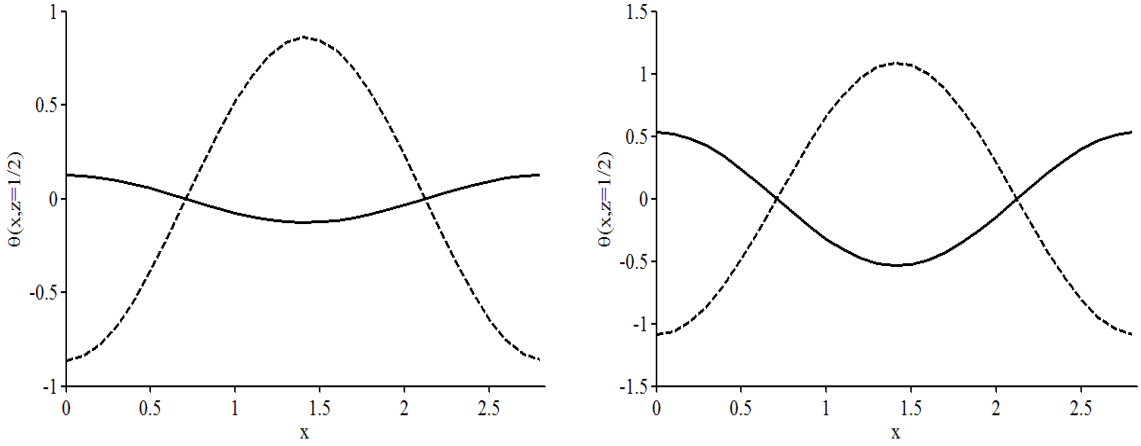
θ(x,z=1/2)
x
1
0.5
0
-0.5
-1
1.5
-1.5
0
0.5
1
1.5
2
2.5

Figure 3-9: *Distributions of the leading-order and higher-order terms on the temperature deviation at (a) ε = 0.1, (b) ε = 0.5 and (c) ε = 1 for two non-Fourier fluids with C = 0.005(left column) and C = 0.01(right column). Here* $\mathrm{k} = \frac{\pi}{\sqrt{2}}$ *and z = ½.In this Figure dashed line corresponds to the leading-order term (of Spectral solution) and solid lines correspond to Spectral solution including leading and higher order terms.*

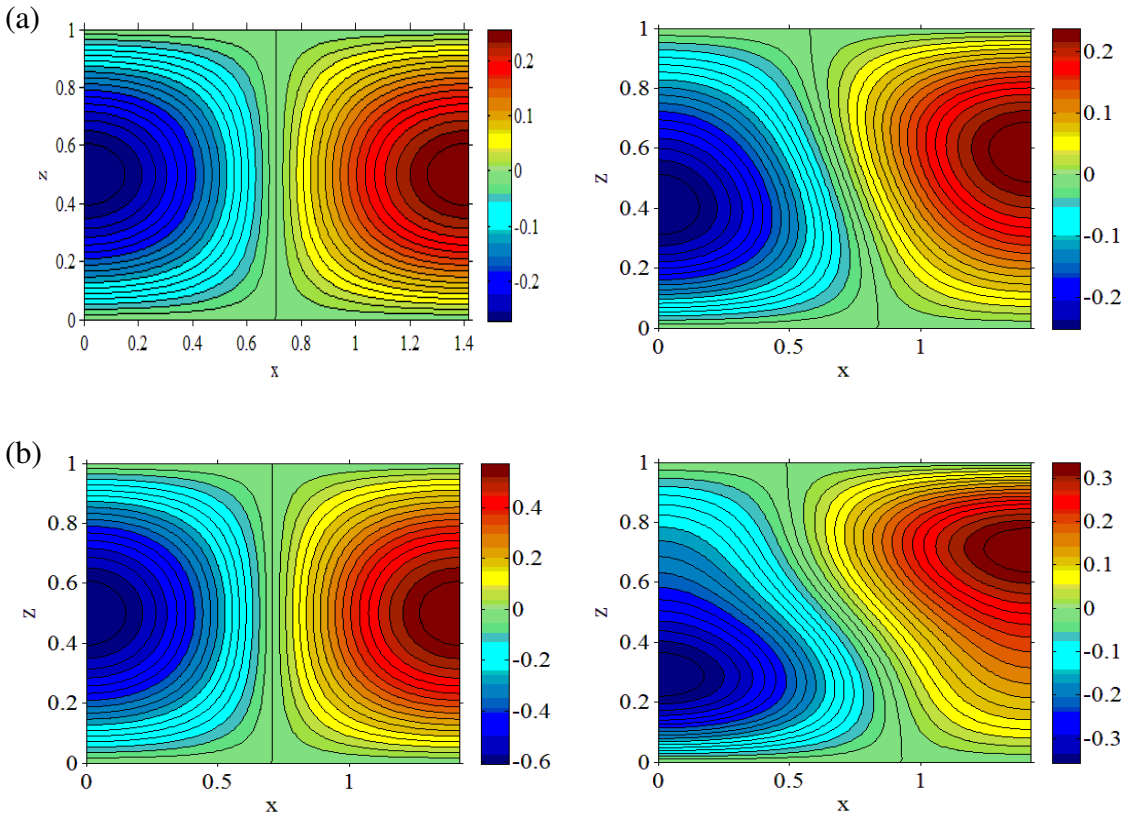

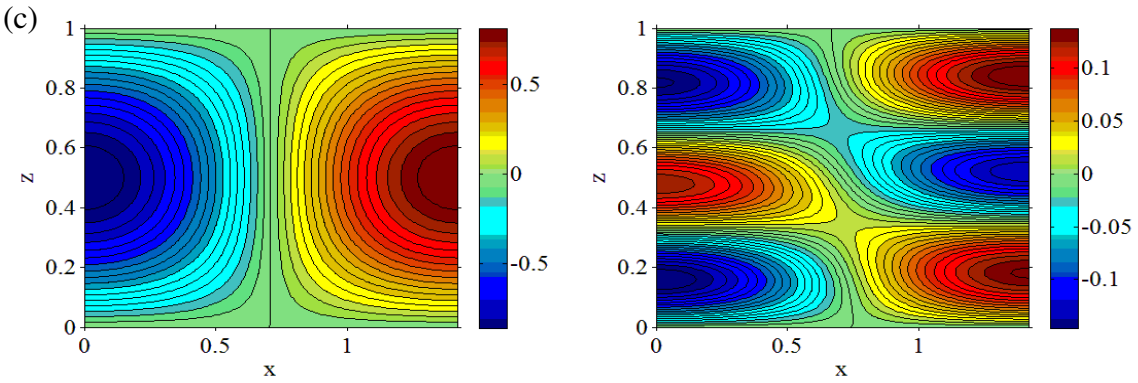

Figure 3-10: *Distributions of the leading-order and higher-order temperature deviation at (a) ε = 0.1(b), ε = 0.5 and (c) ε = 1 for a non-Fourier fluid. Here C=0.005,* $\mathrm{k} = \frac{\pi}{\sqrt{2}}$ *and z = ½. In this Figure the left columns corresponds to the leading-order term (of Spectral solution) and right columns correspond to Spectral solution including leading and higher order terms.*

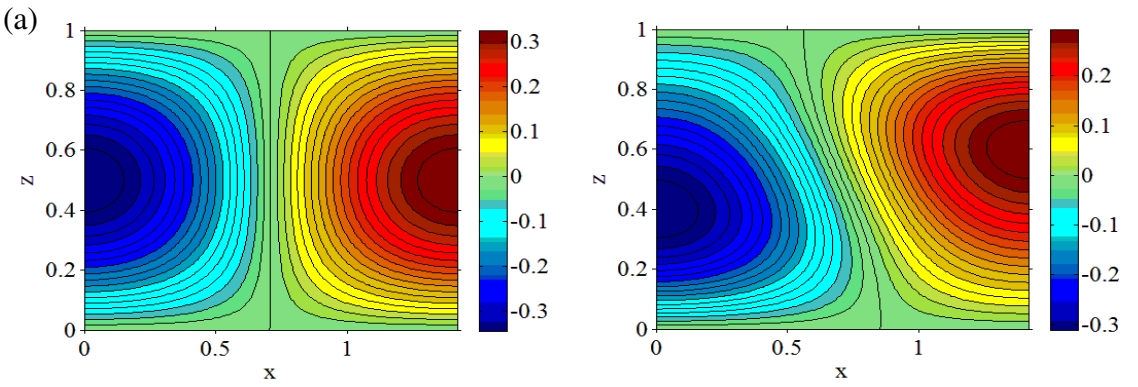

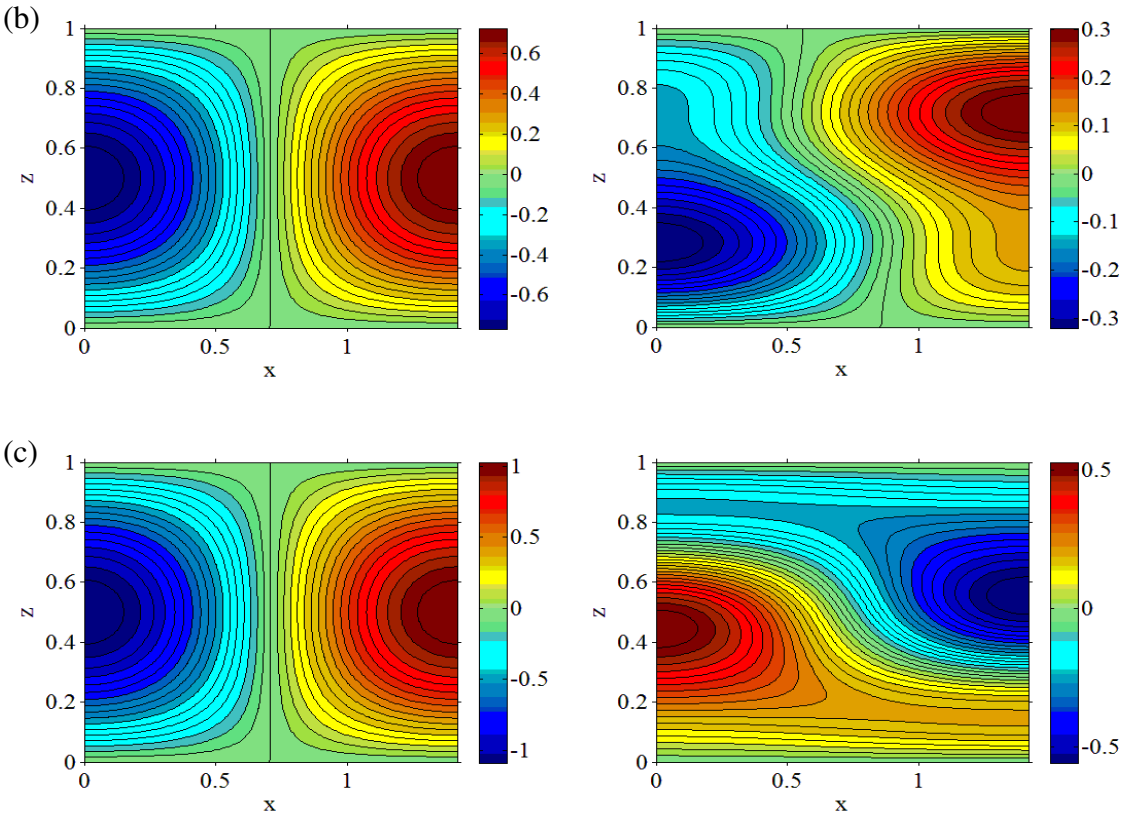

Figure 3-11: *Distributions of the leading-order and higher-order temperature deviation at (a) ε = 0.1, (b) ε = 0.5 and (c) ε = 1 for a non-Fourier fluid. Here C=0.01,* $\mathrm{k} = \frac{\pi}{\sqrt{2}}$ *and z = ½. In this Figure the left columns corresponds to the leading-order term (of Spectral solution) and right columns correspond to Spectral solution including leading and higher order terms..*

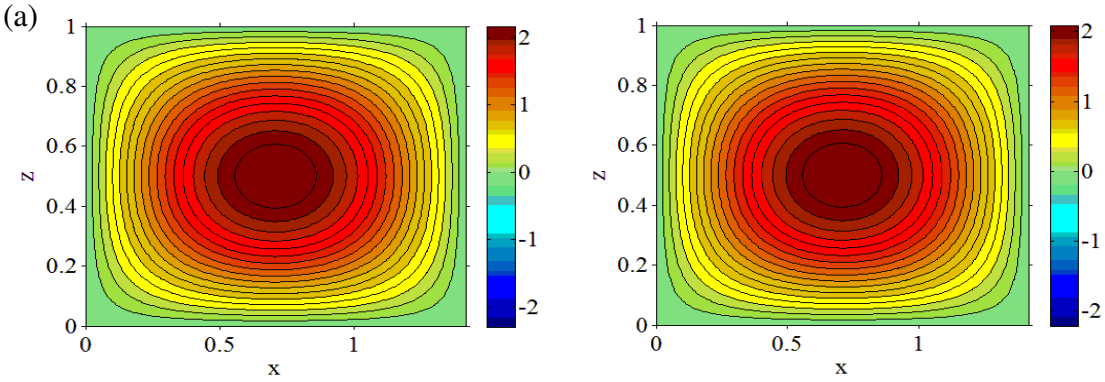

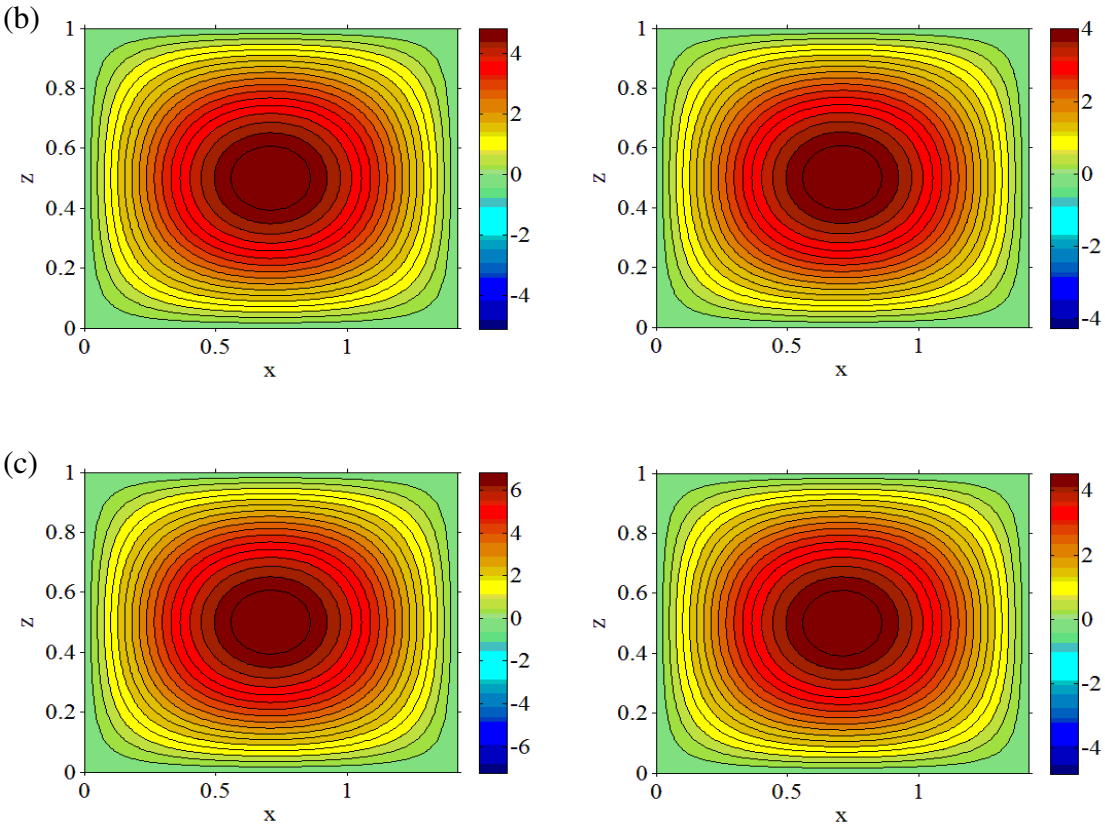

Figure 3-12: *Distributions of the leading-order and higher-order stream function at(a) ε = 0.1, (b) ε = 0.5 and (c) ε = 1 for a non-Fourier fluid. Here C=0.01,* $k = \frac{\pi}{\sqrt{2}}$ *and z = ½. In this Figure the left columns corresponds to the leading-order term (of Spectral solution) and right columns correspond to Spectral solution including leading and higher order terms.*

3.5 Nusselt number

Usually the most interesting parameter for description convective heat transport is a non-dimensional term, Nusselt number *Nu*, which is characterized as the ratio of the heat transports with and without convection. To be more convenient, Nusselt number is defined as the average over the whole horizontal extent at the lower or upper plane as,

$$Nu = 1 + \overline{qz}\Big|_{z=0} \tag{3.5.1}$$

where qz is heat flux in z direction. In Fourier case, heat flux could obtain from the Fourier's law but in non-Fourier case, qz is engaged in a set of coupled equations. Here, equation (3.2.14) for steady state is as,

$$C\left(-w_z + uqz_x + wqz_z - w_x qx - w_z qz\right) = -qz - \theta_z \tag{3.5.2}$$

Since the Nusselt number is defined in the lower or upper plate, the boundary condition of $w\left(x, z=0, t\right)=0$ could be implemented to equation (3.5.2) as following,

$$\left(Cu\right)qz_x + \left(1 - Cw_z\right)qz = +Cw_z - \theta_z \tag{3.5.3}$$

where velocities and temperature are determined in the previous section. Thus, the most general steady state solutions of equation (3.5.3), presuming periodicity in the x direction with wavelength $2\pi/k$, is of the form

$$qz = qz_0 + \sum_{a=1}\left[qz_a^1 C_{akx} + qz_a^2 S_{akx}\right],\ qz_x = \sum_{a=1}\left[-akqz_a^1 S_{akx} + akqz_a^2 C_{akx}\right] \tag{3.5.4}$$

After substituting equation (3.5.4) into equation (3.5.3) and keeping terms in the same factor of S_{akx} or C_{akx}, all coefficients of equation (3.5.4) are determined. Because of periodicity in the x direction, the only term which plays role in Nusselt number is

$$qz_0 = \frac{A_2\left(1 + A_7A_4 - A_4A_6\right) - \left(1 + A_7A_4\right)A_1A_5}{1 + A_7A_4 - A_4A_6 - \left(1 + A_7A_4\right)A_3} \tag{3.5.5}$$

Where A_1 to A_7 are given in appendix A. Thus, the final Nusselt number equation becomes:

$$Nu = 1 + qz_0 \tag{3.5.6}$$

Figure 3-13 illustrates the influence of Cattaneo number on the Nusselt number, including the leading-order (left column) and higher-order terms correction (right column) as a function of ε and wavenumber for non-Fourier fluids.

(a)

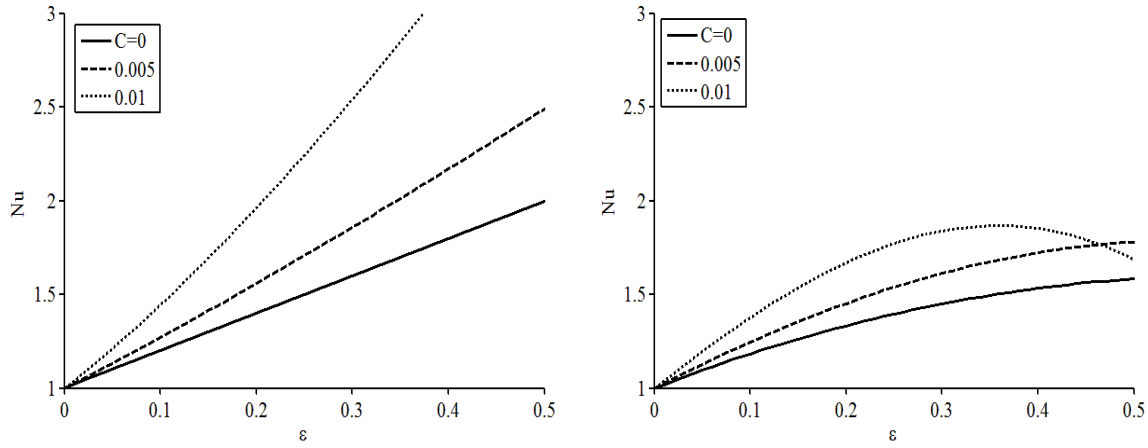

(b)

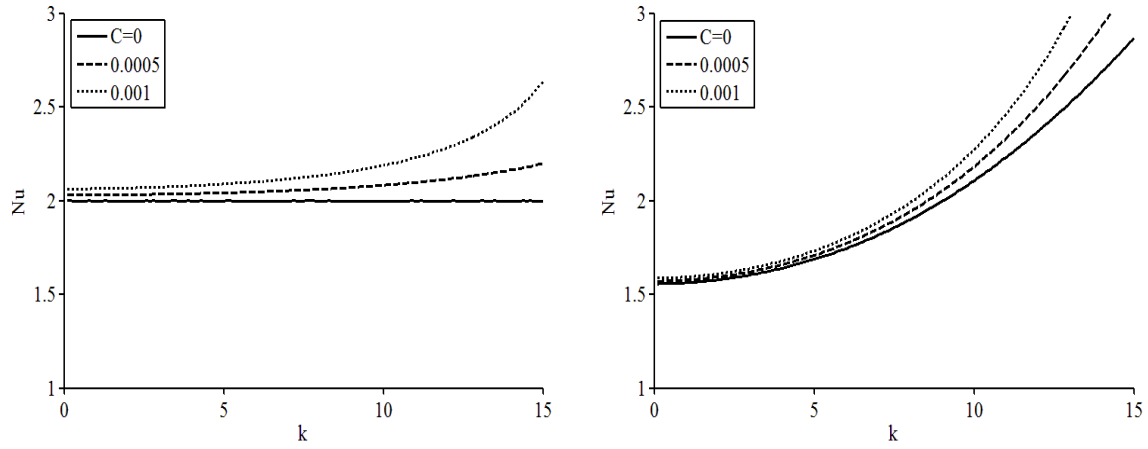

Figure 3-13: *Dependence of the Nusselt number, including the leading-order and higher-order terms on (a) ε and (b) wavenumber. In this Figure dashed line corresponds to the leading-order term (of Spectral solution) and solid lines correspond to Spectral solution including leading and higher order terms.*

The discrepancy between the leading- and higher-order corrections in non-Fourier cases is more than in a Fourier case which increases by the perturbation of Rayleigh number. The Cattaneo number increases the Nusselt number which decreases for higher ε, because

ε increases the influence of higher-order terms. In non-Fourier fluids the leading order terms are dependent on wave number and increase significantly for higher wane numbers. Interestingly, unlike $\theta 1_{11}$ (equation (3.4.7)), Nusselt number increases with wave number in non-Fourier fluid. Generally, Nusselt number increases with Cattaneo number or, by taking a nanofluid as the non-Fourier fluid, adding nano particles to the base fluid, increases the heat transfer as it was expected before. Buyuk [101] has studied natural convection heat transfer of water-based nanofluids in an inclined square enclosure with effective properties of nanofluids and found Nusselt number increases by increasing nanoparticle concentration (or non-Fourier characteristic) when enclosure is heated from below. Also, Wen and Ding [102] found that existence of Al_2O_3 nanoparticles in water can result in considerable increment of convective heat transfer even more than the enhancement of the effective thermal conductivity of nanofluids.

3.6 Conclusion

A nonlinear spectral approach is used to model the post-critical convective state for thermo-gravitational instability in a non-Fourier fluid of the single-phase-lagging (SPL) type heated from below. To treat nonlinear convection, a spectral approach is presented in this section which is not based on arbitrary mode selection. Non-Fourier heat conduction has been described with different models. Single-Phase-Lag model (SPL) has been considered comprising relaxation time which exposes the delay in the response of the heat flux. Spectral approach reveals the number and type required modes. Finally the effect of relaxation time on the heat transfer has been studied a compared with the Fourier fluid. It has been shown that the leading-order contribution is essentially dominant for temperature field and stream function. Although modes θ_{13} and θ_{04} have small contributions, but they are not negligible and lead to the deformation of the temperature field especially in higher Rayleigh numbers. At the end, it has been shown that the Cattaneo number increases the Nusselt number.

3.7 References

[1] D. Joseph and L. Preziosi, “Heat waves,” *Rev. Mod. Phys.*, vol. 61, no. 1, pp. 41–73, Jan. 1989.

[2] C. Cattaneo, “A form of heat conduction equation which eliminates the paradox of instantaneous propagation,” *Comptes Rendus*, no. 247, pp. 431–433, 1958.

[3] P. Vernotte, “Some possible complication in the phenomena of thermal conduction,” *Compte Rendus*, no. 252, pp. 2190–2191, 1961.

[4] G. Donzelli, R. Cerbino, and A. Vailati, “Bistable Heat Transfer in a Nanofluid,” *Phys. Rev. Lett.*, vol. 102, no. 10, p. 104503, Mar. 2009.

[5] J. Ordóñez-Miranda and J. J. Alvarado-Gil, “Thermal wave oscillations and thermal relaxation time determination in a hyperbolic heat transport model,” *Int. J. Therm. Sci.*, vol. 48, no. 11, pp. 2053–2062, Nov. 2009.

[6] S. Galović and D. Kostoski, “Photothermal wave propagation in media with thermal memory,” *J. Appl. Phys.*, vol. 93, no. 5, p. 3063, Mar. 2003.

[7] A. Vedavarz, S. Kumar, and M. K. Moallemi, “Significance of Non-Fourier Heat Waves in Conduction,” *J. Heat Transfer*, vol. 116, no. 1, p. 221, Feb. 1994.

[8] M. N. O□zis□ik and D. Y. Tzou, “On the Wave Theory in Heat Conduction,” *J. Heat Transfer*, vol. 116, no. 3, p. 526, Aug. 1994.

[9] P. Duhamel, “A new finite integral transform pair for hyperbolic conduction problems in heterogeneous media,” *Int. J. Heat Mass Transf.*, vol. 44, no. 17, pp. 3307–3320, Sep. 2001.

[10] P. J. Antaki, “Analysis of hyperbolic heat conduction in a semi-infinite slab with surface convection,” *Int. J. Heat Mass Transf.*, vol. 40, no. 13, pp. 3247–3250, Sep. 1997.

[11] P.-T. Hsu and Y.-H. Chu, “An inverse non-Fourier heat conduction problem approach for estimating the boundary condition in electronic device,” *Appl. Math. Model.*, vol. 28, no. 7, pp. 639–652, Jul. 2004.

[12] F. Jiang, “Non-Fourier heat conduction phenomena in porous material heated by microsecond laser pulse,” *Microscale Thermophys. Eng.*, vol. 6, no. 4, pp. 331–346, Jan. 2003.

[13] K. Mitra, S. Kumar, A. Vedevarz, and M. K. Moallemi, “Experimental Evidence of Hyperbolic Heat Conduction in Processed Meat,” *J. Heat Transfer*, vol. 117, no. 3, p. 568, Aug. 1995.

[14] W. Dai, H. Wang, P. M. Jordan, R. E. Mickens, and A. Bejan, “A mathematical model for skin burn injury induced by radiation heating,” *Int. J. Heat Mass Transf.*, vol. 51, no. 23–24, pp. 5497–5510, Nov. 2008.

[15] L. Herrera and N. Falcón, “Heat waves and thermohaline instability in a fluid,” *Phys. Lett. A*, vol. 201, no. 1, pp. 33–37, May 1995.

[16] G. Espinosa-Paredes and E.-G. Espinosa-Martínez, “Fuel rod model based on Non-Fourier heat conduction equation,” *Ann. Nucl. Energy*, vol. 36, no. 5, pp. 680–693, May 2009.

[17] R. J. Meyer, “Ultrasonic drying of saturated porous solids via second sound.” 30-Oct-2002.

[18] R. R. Letfullin, T. F. George, G. C. Duree, and B. M. Bollinger, “Ultrashort Laser Pulse Heating of Nanoparticles: Comparison of Theoretical Approaches,” *Adv. Opt. Technol.*, vol. 2008, pp. 1–8, 2008.

[19] C. I. Christov, “On frame indifferent formulation of the Maxwell–Cattaneo model of finite-speed heat conduction,” *Mech. Res. Commun.*, vol. 36, no. 4, pp. 481–486, Jun. 2009.

[20] F. Xu, T. Lu, and K. A. Seffen, “Dual-Phase-Lag Model of Skin Bioheat Transfer,” in *2008 International Conference on BioMedical Engineering and Informatics*, 2008, vol. 1, pp. 505–511.

[21] P. Vadasz, “Heat Conduction in Nanofluid Suspensions,” *J. Heat Transfer*, vol. 128, no. 5, p. 465, May 2006.

[22] V. Peshkov, “Second sound in helium II,” *J. Phys. 8*, p. 381, 1944.

[23] S. C. Mishra and A. Stephen, “Combined mode conduction and radiation heat transfer in a spherical geometry with non-Fourier effect,” *Int. J. Heat Mass Transf.*, vol. 54, no. 13–14, pp. 2975–2989, Jun. 2011.

[24] S. C. Mishra and H. Sahai, “Analyses of non-Fourier heat conduction in 1-D cylindrical and spherical geometry – An application of the lattice Boltzmann method,” *Int. J. Heat Mass Transf.*, vol. 55, no. 23–24, pp. 7015–7023, Nov. 2012.

[25] P. J. Antaki, “Solution for non-Fourier dual phase lag heat conduction in a semiinfinite slab with surface heat flux,” *Int. J. Heat Mass Transf.*, vol. 41, no. 14, pp. 2253–2258, Jul. 1998.

[26] B. L. Wang and J. C. Han, “A crack in a finite medium under transient non-Fourier heat conduction,” *Int. J. Heat Mass Transf.*, vol. 55, no. 17–18, pp. 4631–4637, Aug. 2012.

[27] C.-H. Huang and H.-H. Wu, “An iterative regularization method in estimating the base temperature for non-Fourier fins,” *Int. J. Heat Mass Transf.*, vol. 49, no. 25–26, pp. 4893–4902, Dec. 2006.

[28] K.-C. Liu and H.-T. Chen, “Analysis for the dual-phase-lag bio-heat transfer during magnetic hyperthermia treatment,” *Int. J. Heat Mass Transf.*, vol. 52, no. 5–6, pp. 1185–1192, Feb. 2009.

[29] H. Zhang, S. Zhang, X. Guo, and J. Bi, “Multiple spatial and temporal scales method for numerical simulation of non-classical heat conduction problems: one dimensional case,” *Int. J. Solids Struct.*, vol. 42, no. 3–4, pp. 877–899, Feb. 2005.

[30] C.-C. Wang, “Direct and inverse solutions with non-Fourier effect on the irregular shape,” *Int. J. Heat Mass Transf.*, vol. 53, no. 13–14, pp. 2685–2693, Jun. 2010.

[31] Y. Chou and R.-J. Yang, “Application of CESE method to simulate non-Fourier heat conduction in finite medium with pulse surface heating,” *Int. J. Heat Mass Transf.*, vol. 51, no. 13–14, pp. 3525–3534, Jul. 2008.

[32] W. Wu and X. Li, “Application of the time discontinuous Galerkin finite element method to heat wave simulation,” *Int. J. Heat Mass Transf.*, vol. 49, no. 9–10, pp. 1679–1684, May 2006.

[33] T.-M. Chen, “A hybrid Green’s function method for the hyperbolic heat conduction problems,” *Int. J. Heat Mass Transf.*, vol. 52, no. 19–20, pp. 4273–4278, Sep. 2009.

[34] C. Han-Taw and L. Jae-Yuh, “Analysis of two-dimensional hyperbolic heat conduction problems,” *Int. J. Heat Mass Transf.*, vol. 37, no. 1, pp. 153–164, Jan. 1994.

[35] C. Han-Taw and L. Jae-Yuh, “Numerical analysis for hyperbolic heat conduction,” *Int. J. Heat Mass Transf.*, vol. 36, no. 11, pp. 2891–2898, Jul. 1993.

[36] Q.-M. Fan and W.-Q. Lu, “A new numerical method to simulate the non-Fourier heat conduction in a single-phase medium,” *Int. J. Heat Mass Transf.*, vol. 45, no. 13, pp. 2815–2821, Jun. 2002.

[37] J. Ghazanfarian and Z. Shomali, “Investigation of dual-phase-lag heat conduction model in a nanoscale metal-oxide-semiconductor field-effect transistor,” *Int. J. Heat Mass Transf.*, vol. 55, no. 21–22, pp. 6231–6237, Oct. 2012.

[38] Y. Chou and R.-J. Yang, “Two-dimensional Dual-Phase-Lag thermal behavior in single-/multi-layer structures using CESE method,” *Int. J. Heat Mass Transf.*, vol. 52, no. 1–2, pp. 239–249, Jan. 2009.

[39] T. T. Lam and E. Fong, “Application of solution structure theorem to non-Fourier heat conduction problems: Analytical approach,” *Int. J. Heat Mass Transf.*, vol. 54, no. 23–24, pp. 4796–4806, Nov. 2011.

[40] D. W. Tang and N. Araki, “Non-fourier heat conduction in a finite medium under periodic surface thermal disturbance,” *Int. J. Heat Mass Transf.*, vol. 39, no. 8, pp. 1585–1590, May 1996.

[41] L. W. et al. Y. Ding, H. Chen, “Heat Transfer Intensification Using Nanofluids,” *J. Part. Powder*, vol. 25, pp. 23–36, 2007.

[42] J. Buongiorno, “Convective Transport in Nanofluids,” *J. Heat Transfer*, vol. 128, no. 3, p. 240, Mar. 2006.

[43] S. Samouhos and G. McKinley, “Carbon Nanotube–Magnetite Composites, With Applications to Developing Unique Magnetorheological Fluids,” *J. Fluids Eng.*, vol. 129, no. 4, p. 429, Apr. 2007.

[44] J. Buongiorno, “Convective Transport in Nanofluids,” *J. Heat Transfer*, vol. 128, no. 3, pp. 240–250, 2006.

[45] J. Garg, B. Poudel, M. Chiesa, J. B. Gordon, J. J. Ma, J. B. Wang, Z. F. Ren, Y. T. Kang, H. Ohtani, J. Nanda, G. H. McKinley, and G. Chen, “Enhanced thermal conductivity and viscosity of copper nanoparticles in ethylene glycol nanofluid,” *J. Appl. Phys.*, vol. 103, no. 7, p. 074301, Apr. 2008.

[46] P. Vadasz, “Heat transfer augmentation in nanofluids via nanofins.,” *Nanoscale Res. Lett.*, vol. 6, no. 1, p. 154, Jan. 2011.

[47] Y. Xuan and W. Roetzel, “Conceptions for heat transfer correlation of nanofluids,” *Int. J. Heat Mass Transf.*, vol. 43, no. 19, pp. 3701–3707, Oct. 2000.

[48] *Mantle Convection: Plate Tectonics and Global Dynamics*. CRC Press, 1989, p. 881.

[49] Y. Varol and H. F. Oztop, "A comparative numerical study on natural convection in inclined wavy and flat-plate solar collectors," *Build. Environ.*, vol. 43, no. 9, pp. 1535–1544, Sep. 2008.

[50] I. Haraksingh, I. A. Mc Doom, and O. S. C. Headley, "A natural convection flat-plate collector solar cooker with short term storage," *Renew. Energy*, vol. 9, no. 1–4, pp. 729–732, Sep. 1996.

[51] D. Jo, S. Park, J. Park, H. Chae, and B. Lee, "Cooling capacity of plate type research reactors during the natural convective cooling mode," *Prog. Nucl. Energy*, vol. 56, pp. 37–42, Apr. 2012.

[52] D. L. Hartmann, L. A. Moy, and Q. Fu, "Tropical Convection and the Energy Balance at the Top of the Atmosphere," *J. Clim.*, vol. 14, no. 24, pp. 4495–4511, Dec. 2001.

[53] J. Marshall and F. Schott, "Open-ocean convection: Observations, theory, and models," *Rev. Geophys.*, vol. 37, no. 1, pp. 1–64, 1999.

[54] S. Rahmstorf, "The Thermohaline Ocean Circulation: A System with Dangerous Thresholds?," *Clim. Change*, vol. 46, no. 3, pp. 247–256, Aug. 2000.

[55] A.-M. Gustafsson, L. Westerlund, and G. Hellström, "CFD-modelling of natural convection in a groundwater-filled borehole heat exchanger," *Appl. Therm. Eng.*, vol. 30, no. 6–7, pp. 683–691, May 2010.

[56] H. Bénard, "Les Tourbillons Cellulaires dans une Nappe Liquide Transportant de la Chaleur par Convection en Régime Permanent," *Ann. Chem. Phys.*, vol. 23.

[57] A. Chiffaudel, S. Fauve, and B. Perrin, "Viscous and Inertial Convection at Low Prandtl Number: Experimental Study," *Europhys. Lett.*, vol. 4, no. 5, pp. 555–560, Sep. 1987.

[58] S. Cioni, S. Ciliberto, and J. Sommeria, “Experimental study of high-Rayleigh-number convection in mercury and water,” *Dyn. Atmos. Ocean.*, vol. 24, no. 1–4, pp. 117–127, Jan. 1996.

[59] M. Dubois and P. Bergé, “Experimental study of the velocity field in Rayleigh-Bénard convection,” *J. Fluid Mech.*, vol. 85, no. 04, p. 641, Apr. 2006.

[60] V. Kek and U. Müller, “Low Prandtl number convection in layers heated from below,” *Int. J. Heat Mass Transf.*, vol. 36, no. 11, pp. 2795–2804, Jul. 1993.

[61] F. H. Busse and R. M. Clever, “Instabilities of convection rolls in a fluid of moderate Prandtl number,” *J. Fluid Mech.*, vol. 91, no. 02, p. 319, Apr. 2006.

[62] J. M. AURNOU and P. L. OLSON, “Experiments on Rayleigh–Bénard convection, magnetoconvection and rotating magnetoconvection in liquid gallium,” *J. Fluid Mech.*, vol. 430, pp. 283–307, Mar. 2001.

[63] E. N. Lorenz, “Deterministic Nonperiodic Flow.,” *J. Atmos. Sci.*, vol. 20, no. 2, pp. 130–141, 1963.

[64] L. R. (J W. Strutt, “On Convection Currents in a Horizontal Layer of Fluid, when the Higher Temperature is on the Under Side,” *Phil. Mag.*, vol. 32, no. 192, pp. 529–546, 1916.

[65] R. E. Khayat, “Chaos and overstability in the thermal convection of viscoelastic fluids,” *J. Nonnewton. Fluid Mech.*, vol. 53, pp. 227–255, Jul. 1994.

[66] R. E. Khayat, “Non-linear overstability in the thermal convection of viscoelastic fluids,” *J. Nonnewton. Fluid Mech.*, vol. 58, no. 2–3, pp. 331–356, Jul. 1995.

[67] R. E. Khayat, “Chaos in the thermal convection of weakly shear-thinning fluids,” *J. Nonnewton. Fluid Mech.*, vol. 63, no. 2–3, pp. 153–178, Apr. 1996.

[68] P. Hohenberg and J. Swift, “Hexagons and rolls in periodically modulated Rayleigh-Bénard convection,” *Phys. Rev. A*, vol. 35, no. 9, pp. 3855–3873, May 1987.

[69] W. V. R. Malkus and G. Veronis, “Finite amplitude cellular convection,” *J. Fluid Mech.*, vol. 4, no. 03, pp. 225–260, Mar. 2006.

[70] J. H. Curry, “A generalized Lorenz system,” *Commun. Math. Phys.*, vol. 60, no. 3, pp. 193–204, 1978.

[71] M. Krishnan, V. M. Ugaz, and M. A. Burns, “PCR in a Rayleigh-Bénard convection cell.,” *Science*, vol. 298, no. 5594, p. 793, Oct. 2002.

[72] N.-T. Nguyen and S. T. Wereley, *Fundamentals and Applications of Microfluidics*. Boston, MA, USA: Artech House, 2006, p. 471.

[73] L. Li, S. Sosnowski, E. Kumacheva, M. A. Winnik, S. Rajaram, S. T. Balke, and C. E. Chaffey, “Coalescence at the Surface of a Polymer Blend As Studied by Laser Confocal Fluorescence Microscopy,” *Langmuir*, vol. 12, no. 9, pp. 2141–2144, Jan. 1996.

[74] H. SUNKARA, “Lattice dynamics of colloidal crystals during photopolymerization of acrylic monomer matrix,” vol. 33, no. 4, pp. 887 – 894, 1998.

[75] T. W. Pojman, J. A., and McCardle, “Functionally gradient polymeric materials,” 6,057,406, 2000.

[76] F. H. Busse, “Transition to turbulence in Rayleigh-Benard convection,” *Hydrodyn. Instab. Transit. to Turbul. (A82-12478 02-34) Berlin*, pp. 97–137, 1981.

[77] D. Lohse and K.-Q. Xia, “Small-Scale Properties of Turbulent Rayleigh-Bénard Convection,” *Annu. Rev. Fluid Mech.*, vol. 42, no. 1, pp. 335–364, Jan. 2010.

[78] *Hydrodynamic Stability*. Cambridge UK: Cambridge University Press, 1981, p. 628.

[79] S. Chandrasekhar, *Hydrodynamic and Hydromagnetic Stability*. New York, NY, USA: Dover Publications IVC, 1961, p. 652.

[80] A. V. Getling, "Rayleigh-Bénard convection : structures and dynamics," *World Scientific, Singapore.*, 1998. [Online]. Available: http://search.library.wisc.edu/catalog/ocm38130717. [Accessed: 14-May-2014].

[81] M. Cross and P. Hohenberg, "Pattern formation outside of equilibrium," *Rev. Mod. Phys.*, vol. 65, no. 3, pp. 851–1112, Jul. 1993.

[82] A. Schlüter, D. Lortz, and F. Busse, "On the stability of steady finite amplitude convection," *J. Fluid Mech.*, vol. 23, no. 01, p. 129, Mar. 2006.

[83] A. C. Newell and J. A. Whitehead, "Finite bandwidth, finite amplitude convection," *J. Fluid Mech.*, vol. 38, no. 02, p. 279, Mar. 2006.

[84] G. Parmentier, P. M., Reginer, V. C., and Lebon, "Nonlinear analysis of coupled gravitational and capillary thermoconvection in thin fluid layers," *Phys. Rev. E*, vol. 54, no. 1, pp. 411–423, 1996.

[85] P. Parmentier, G. Lebona, and V. Regnier, "Weakly nonlinear analysis of Bénard–Marangoni instability in viscoelastic fluids," *J. Nonnewton. Fluid Mech.*, vol. 89, no. 1–2, pp. 63–95, Feb. 2000.

[86] A. Vikhansky, "Thermal convection of a viscoplastic liquid with high Rayleigh and Bingham numbers," *Phys. Fluids*, vol. 21, no. 10, pp. 1–7, 2009.

[87] J. McLaughlin, "Successive bifurcations leading to stochastic behavior," *J. Stat. Phys.*, vol. 15, no. 4, pp. 307–326, Oct. 1976.

[88] A. Aceves, H. Adachihara, C. Jones, J. C. Lerman, D. W. McLaughlin, J. V. Moloney, and A. C. Newell, "Chaos and coherent structures in partial differential equations," *Phys. D Nonlinear Phenom.*, vol. 18, no. 1–3, pp. 85–112, Jan. 1986.

[89] D. C. Threlfall, "Free convection in low-temperature gaseous helium," *J. Fluid Mech.*, vol. 67, no. 01, p. 17, Mar. 2006.

[90] J. Ekin, *Experimental Techniques for Low-Temperature Measurements*. Oxford University Press, 2006, p. 704.

[91] K. Khanafer, K. Vafai, and M. Lightstone, "Buoyancy-driven heat transfer enhancement in a two-dimensional enclosure utilizing nanofluids," *Int. J. Heat Mass Transf.*, vol. 46, no. 19, pp. 3639–3653, Sep. 2003.

[92] A. B. Kasaeian, "Convection Heat Transfer Modeling of Ag Nanofluid Using Different Viscosity Theories," *IIUM Engineering Journal*, vol. 13, no. 1. 20-Apr-2012.

[93] A. G. A. Nnanna, "Experimental Model of Temperature-Driven Nanofluid," *J. Heat Transfer*, vol. 129, no. 6, p. 697, 2007.

[94] "Experimental Investigation of Convective Heat Transfer Coefficient of CNTs Nanofluid under Constant Heat Flux," *Proc. World Congr. Eng.*, p. 6, 2011.

[95] L. G. Asirvatham, N. Vishal, S. K. Gangatharan, and D. M. Lal, "Experimental Study on Forced Convective Heat Transfer with Low Volume Fraction of CuO/Water Nanofluid," *Energies*, vol. 2, no. 1, pp. 97–110, Mar. 2009.

[96] B. C. Pak and Y. I. Cho, "Hydrodynamic and heat transfer study of dispersed fluids with submicron metallic oxide particles," *Exp. Heat Transf.*, vol. 11, no. 2, pp. 151–170, Apr. 1998.

[97] Y. Xuan and Q. Li, "Investigation on Convective Heat Transfer and Flow Features of Nanofluids," *J. Heat Transfer*, vol. 125, no. 1, p. 151, Feb. 2003.

[98] N. Putra, W. Roetzel, and S. K. Das, “Natural convection of nano-fluids,” *Heat Mass Transf.*, vol. 39, no. 8–9, pp. 775–784, Dec. 2002.

[99] D. Wen and Y. Ding, “Formulation of nanofluids for natural convective heat transfer applications,” *Int. J. Heat Fluid Flow*, vol. 26, no. 6, pp. 855–864, Dec. 2005.

[100] *Bénard Cells and Taylor Vortices*. Cambridge: Cambridge University Press, 1993, p. 350.

[101] E. Büyük Öğüt, “Natural convection of water-based nanofluids in an inclined enclosure with a heat source,” *Int. J. Therm. Sci.*, vol. 48, no. 11, pp. 2063–2073, Nov. 2009.

[102] D. Wen and Y. Ding, “Experimental investigation into convective heat transfer of nanofluids at the entrance region under laminar flow conditions,” *Int. J. Heat Mass Transf.*, vol. 47, no. 24, pp. 5181–5188, Nov. 2004.

[103] L. Wang and X. Wei, “Equivalence between dual-phase-lagging and two-phase-system heat conduction processes,” *Int. J. Heat Mass Transf.*, vol. 51, no. 7–8, pp. 1751–1756, Apr. 2008.

Chapter 4

4 Conclusions and Recommendations

4.1 Conclusions

This study examines the natural convection of non-Fourier fluids of the dual-phase-lagging (DPL) type. These fluids possess a relaxation time and a retardation time, reflecting the delay in the response of the heat flux and the temperature gradient with respect to one another. The limit of a single-phase-lagging (SPL) fluid is recovered upon setting the retardation time to zero. The SPL model is particularly relevant to low-temperature liquids or to fast heat transfer processes. The relevance of the DPL model to nanofluids (NFs) has recently been recognized in the literature, and is emphasized here. The equivalence between the two-phase and DPL models allows the expression of the relaxation time in terms of the nanoparticle (NP) concentration [1]. The retardation-to-relaxation time ratio is then found to be equal to the NF solution-to-solvent thermal conductivity ratio, γ (see section 2.2). The parallels between NFs and polymeric solutions of the Boger type, obeying the Oldroyd-B constitutive equation for stress are established throughout the paper. Similar to viscoelastic fluids, the constitutive equation for heat flux used in the present analysis is frame invariant.

Linear stability analysis indicates that, in contrast to ordinary fluids, a DPL fluid can lose its conductive mode to stationary or oscillatory convection. For small relaxation time (small Cattaneo number, C), the neutral stability curve comprises a Fourier branch ($k < k_i$) and an oscillatory branch ($k > k_i$). As C increases and reaches a critical value, $C_H(\gamma)$, both stationary and oscillatory convection become equally probable, confirming the existence of the bistable mode observed in experiment [2]. For $C > C_H$, only oscillatory convection is predicted, at a Rayleigh number decreasing with C (see Figures 2-4a and 2-5a). Thus, oscillatory convection increasingly becomes the mode of preference, compared to both conduction and stationary convection. In fact, it is found that, for strongly non-Fourier fluids, oscillatory convection becomes spontaneously observed with no prior conduction. The oscillatory roll size grows with both relaxation and retardation. There is a discontinuity in roll size with respect to retardation, which is

clearly reflected in the limit of large C (see Figure 2-10b). Although the oscillation frequency decreases monotonically with roll size (Figures 2-3b and 2-5b), it exhibits a non-monotonic response with respect to relaxation time (emergence of a maximum with respect to C). As expected, retardation tends to attenuate oscillation (see Figures 2-4c and 2-10c).

A nonlinear spectral approach is used to model the post-critical convective state for thermo-gravitational instability in a non-Fourier fluid of the single-phase-lagging (SPL) type heated from below. To treat nonlinear convection, a spectral approach is presented in this section which is not based on arbitrary mode selection. Non-Fourier heat conduction has been described with different models. Single-Phase-Lag model (SPL) has been considered comprising relaxation time which exposes the delay in the response of the heat flux. Spectral approach reveals the number and type required modes. Finally the effect of relaxation time on the heat transfer has been studied a compared with the Fourier fluid. It has been shown that the leading-order contribution is essentially dominant for temperature field and stream function. Although modes θ_{13} and θ_{04} have small contributions, but they are not negligible and lead to the deformation of the temperature field especially in higher Rayleigh numbers. At the end, it has been shown that the Cattaneo number increases the Nusselt number.

4.2 Recommendations for future work

Some assumptions have been made in this study to develop the mathematical formulations, which generate some limitations for the direct use of the current work in practical applications. For instance, the results are acceptable for Rayleigh numbers close to the critical Rayleigh number. The non-Fourier fluid is confined between two horizontal planes and it is assumed that there is no friction between fluid and the planes (free- free boundary condition).

The current study focuses on the linear stability analyses of DPL fluids and thermal convection of SPL fluids and the current work can be expanded in the following ways:

a) In the current study, liquid is confined between two infinite horizontal plates. Linear stability analysis and thermal convection can be performed to examine the stability of DPL and SPL fluids in other geometries like vertical and inclined infinite plates.

b) A spectral approach has been employed to attain the flow and temperature fields in the post-critical range of Rayleigh number. Other mathematical approaches could be used to verify the results, for instance amplitude equations and Lorenz models.

c) Perturbation from the critical Rayleigh number has been defined as $\varepsilon = \frac{Ra - Ra_{cr}}{Ra_{cr}}$ which limits the accuracy for small Rayleigh numbers. A change in this definition could help to have accurate results in a wide span of Rayleigh numbers. The proposed perturbation is $\varepsilon = \frac{Ra - Ra_{cr}}{Ra}$ which always is smaller than one.

4.3 References

[1] L. Wang and X. Wei, “Equivalence between dual-phase-lagging and two-phase-system heat conduction processes,” *Int. J. Heat Mass Transf.*, vol. 51, no. 7–8, pp. 1751–1756, Apr. 2008.

[2] G. Donzelli, R. Cerbino, and A. Vailati, “Bistable Heat Transfer in a Nanofluid,” *Phys. Rev. Lett.*, vol. 102, no. 10, p. 104503, Mar. 2009.

Appendices

Appendix A

$$A_1 = -\frac{1}{2}C\pi\left(k\left(U_{11}+3U_{13}\right)+\left(W_{11}+3W_{13}\right)\right)\approx 0 \quad \text{(A-1)}$$

$$A_2 = -2\pi\Theta_{02}-4\pi\Theta_{04} \quad \text{(A-2)}$$

$$A_3 = -C\pi\left(W_{11}+3W_{13}\right) \quad \text{(A-3)}$$

$$A_4 = -C\pi\left(k\left(U_{11}+3U_{13}\right)-\frac{1}{4}\left(W_{11}+3W_{13}\right)\right) \quad \text{(A-4)}$$

$$A_5 = \pi\left(CW_{11}+3CW_{13}-\Theta_{11}-3\Theta_{13}\right) \quad \text{(A-5)}$$

$$A_6 = \frac{1}{2}C\pi\left(k\left(U_{11}+3U_{13}\right)-\left(W_{11}+3W_{13}\right)\right) \quad \text{(A-6)}$$

$$A_7 = -\frac{1}{2}C\pi\left(3k\left(U_{11}+3U_{13}\right)+\left(W_{11}+3W_{13}\right)\right) \quad \text{(A-7)}$$

.

Curriculum Vitae

Name: Rahim Mohammadhasani Khorasany

Post-secondary Education and Degrees:

Amir Kabir University of Technology (Tehran Polytechnic)
Tehran, Iran
2000-2004 B.A.

Sharif University of Technology
Tehran, Iran
2004-2006 MSc.

The University of Western Ontario
London, Ontario, Canada
2010-2014 MSc.

Related Work Experience

Teaching Assistant
The University of Western Ontario
2010-2014

Publications:

R. Mohammadhasani Khorasany, M. Fesanghary, A Novel Approach for Synthesis of Cost-Optimal Heat Exchanger Networks, Computers & Chemical Engineering (2008)

Rahim M. Khorsany, Seyednasrollah S.M., Manzari M.T., Hannani S.K., Three Dimensional Simulation of Oil Reservoir Using Black–Oil Model, Sharif Scientific Journal, Iran (2008)

Rahim M. Khorasany, Daniel F. Stranges, KHAYAT, R. E. 2011, Thermal Convection of Non-Fourier Fluids. Part I. Linear and Weakly Nonlinear Analyses, 61stCanadian Chemical Engineering Conference (CSChE 2011), London, Ontario, Canada (2011)

Daniel F. Stranges, Rahim M. Khorasany, KHAYAT, R. E. 2011, Rayleigh-Bernard Convection of Nanofluids, Part II- Nonlinear Analyses, 61stCanadian Chemical Engineering Conference (CSChE 2011), London, Ontario, Canada (2011)

Roger E. Khayat, Daniel Stranges, Rahim Khorasany, Mohammd Niknami, Bashar Albaalbaki, Thermal Convection of Nanofluids: A NonFourier Perspective and Linear Stability Analysis, World Congress on Engineering (2012)